Transient Metabolic Alterations Induced by Chemotherapeutics in Cancer Persisters

By

Prashant Karki

A Dissertation submitted to the Department of Chemical & Biomolecular Engineering

Cullen College of Engineering

in partial fulfillment of the requirements for the degree of

DOCTOR OF PHILOSOPHY in Chemical and Biomolecular Engineering

Chair of Committee: Dr. Mehmet A. Orman

Committee Member: Dr. Richard C. Willson

Committee Member: Dr. Navin Varadarajan

Committee Member: Dr. Mehmet Sen

Committee Member: Dr. Muayyad Al-Ubaidi

University of Houston

May 2022

Acknowledgement

I would like to express my sincere gratitude to my advisor Dr. Mehmet A. Orman for his continuous guidance and support during my Ph.D. career. Thank you, Dr. Orman, for believing in me and always motivating me to strive for better. You have been very patient with me and helped me grow into the researcher that I am now. It was a pleasure and an honor to be a member of your research group and I will do my best to make you proud.

I would like to thank my committee members Dr. Richard Willson, Dr. Navin Varadarajan, Dr. Mehmet Sen, Dr. Muayyad Al-Ubaidi, and my adviser Dr. Mehmet A. Orman for taking their time and effort to review my work while providing helpful suggestions. I would like to thank the University of Houston Department of Chemical and Biomolecular Engineering for allowing me to pursue my graduate studies.

I would like to thank Dr. Vahideh Angardi for collaborating in the projects presented on this thesis. Thank you, Dr. Vahideh; it would not have been possible to finish these studies without you. I would like to thank Shayne Sensenbach for conducting experiments for chapter 3. I also extend my thanks to the members of Orman Lab; Sayed G. Mohiuddin, Aslan Massahi, Hanny Ngo, and Shreyashi Gosh for helping me through these five years. Thank you all for helping and motivating me to move forward.

Lastly, I would like to thank my parents and family members for believing in me and allowing me to pursue my goal. Thank you for all your love and support. I hope to make you all proud.

Abstract

Acquired drug tolerance has been a major challenge in cancer therapy. Recent evidence has revealed the existence of slow-cycling persister cells that survive drug treatments and give rise to multi-drug tolerant mutants in cancer. The mechanisms associated with persister phenotypes are highly diverse and complex, and many aspects of persister cell physiology remain to be explored. In this study, we aim to characterize the metabolic profiles of cancer persister cells mediated by cancer therapeutics, as epigenetic changes induced by drugs can lead to a transient metabolic rewiring of persister cells that can be associated with the phenotypic switch between normal and persister cell state. Determining the metabolic mechanisms underlying persister cell survival and maintenance will facilitate the development of novel treatment strategies that target persisters and enhance cancer therapy.

In our first project, we treated melanoma cells with various conventional chemotherapeutic agents and showed that melanoma persister cells are not necessarily preexisting dormant cells. In fact, our data indicate they may be induced by cancer chemotherapeutics. Furthermore, with the use of untargeted metabolomics and phenotype microarrays, we demonstrated a transient upregulation in Krebs cycle metabolism in persister cells. We verified that targeting mitochondrial activity can significantly reduce melanoma persister levels. The reported metabolic remodeling feature seems to be a conserved characteristic of melanoma persistence, as it has been observed in various melanoma persister subpopulations derived from a diverse range of chemotherapeutics.

In the next project, we explored metabolic alterations in melanoma cells mediated by Vemurafenib (VEM), a BRAF inhibitor. Co-treatment with BRAF inhibitors is a common treatment strategy for melanoma cancer. However, how a BRAF inhibitor itself alters melanoma cell metabolism and mediates persister survival is not well understood. Our findings demonstrate that metabolites associated with phospholipid synthesis, pyrimidine, one-carbon metabolism, and

branched-chain amino acid metabolism are significantly altered in vemurafenib persister cells when compared to the bulk cancer population. Our data also show that vemurafenib persisters have higher lactic acid consumption rates as well as higher cell viability in a medium with lactate as the primary carbon source compared to control cells, further validating the existence of a unique metabolic reprogramming in these drug-tolerant cells.

In the final project, we aim to elucidate the signaling pathways that link the therapeutic treatments to the observed metabolic reprogramming in melanoma persister cells. Using a high throughput assay with commercially available antibody arrays and western blotting, we identified that the cJUN pathway was transiently upregulated in cultures treated with chemotherapeutic agents. We further show that co-treatment with a cJUN inhibitor, JNK-In-8, resulted in an increased survival rate in cancer cells in the presence of chemotherapeutic agents. Furthermore, we highlighted that the phenomenon associated with cJUN was predominantly active in cultures treated with antimetabolites that act as a nucleoside analog for deoxycytidine. Overall, these results lead us to believe that cJUN, which is at the crossroads for both cell survival and apoptotic pathways, plays a significant role in persister physiology.

Table of Contents

List of Tables

List of Figures

Chapter 1 Cancer and its importance

Cancer is one of the leading causes of death worldwide. American cancer society estimates that approximately 1,898,160 new cancer cases will be diagnosed in the United States in 2021. Additionally, an estimate of 608,570 deaths is caused by cancer in the US.[1] Although the mortality rate associated with cancer has declined over time, these are still staggering numbers that make cancer the 2nd leading cause of death. Despite the medical advances and scientific research that has allowed us to characterize and understand the disease better, finding a cure for cancer still poses a big challenge. As cancer occurs by a series of successive genetic mutations leading to the overall change in cell functions and proliferation, there are many factors such as chemical exposure, radiation, age, lifestyle habits that contribute to the development of cancer.[3–5] To get a complete picture of the disease, research focusing on each cancer type is necessary. For the projects presented in this study, we primarily focused on melanoma, a common type of skin cancer.

1.1 Melanoma

Melanoma is the most aggressive and lethal type of skin cancer. It is caused by genetic mutations in melanocytes, which are pigment-producing cells found in the skin.[6] Metastatic melanoma makes up roughly 1% of skin cancer cases in the US, and yet, it is responsible for more deaths per year than all other skin cancer types combined [7]. According to data collected between 2014 and 2018 in the United States, the yearly incidence rate for melanoma was 22.8 per 100,000[8] with an estimated recurrence rate of 8.8%[9]. Davies *et al*. reported BRAF (rapidly accelerated fibrosarcoma B-type kinase) mutations in 59% of melanomas from a library of cancer cell lines, with the V600E substitution being the most common[10]. The MAPK (mitogen-activated protein kinase)/ERK (extracellular signal-regulated kinase) signaling pathway is a kinase cascade pathway involved in cell proliferation, in which the BRAF protein activates MEK (mitogen-activated protein

kinase kinase, or MAPKK) [11]. Therefore, a mutation in the BRAF protein can lead to uncontrolled cell proliferation and the spread of tumor cells.

1.2 Treatment of melanoma

Over the years, several treatment/therapeutic approaches have been established for melanoma. Depending on the various feature of melanoma (including the genetic profile, location, and stage), treatment options include surgical removal, administering chemotherapeutics, immunotherapy, radiotherapy, bio chemotherapy, targeted therapy, or photodynamic therapy.[6] Although the most recommended form of melanoma treatment is the administration of adjuvant therapies such as targeted therapy and immunotherapy,[12,13] in some cases of metastatic melanoma chemotherapy is administered. Although chemotherapy is one of the earliest forms of treatment for melanoma, it still remains to be significant in the palliative treatment of refractory, progressive, and relapsed cases of melanoma.[14] Since tumor cells are associated with rapid and uncontrolled proliferation, chemotherapy compromises cytotoxic drugs that target various mechanisms that are associated with cell proliferation such as DNA replication, RNA synthesis, protein synthesis, or inhibiting specific functions such as microtubule formation, cell differentiation, and more.[15,16] Based on the mechanism of their actions, chemotherapeutic agents are typically classified into the following types: alkylating agents, antimetabolites, antimicrotubular agents, antibiotics, topoisomerase inhibitors, and others (including agents that do have a variety of mechanisms such as protease inhibitors).[16] Among the various chemotherapeutics available, dacarbazine and temozolomide have been used as standard care for cases related to metastatic melanoma.[17,18] Both of these cancer drugs fall under the category of alkylating agents. Dacarbazine is one of the first chemotherapeutic agents administered for malignant melanoma either as a single treatment or as a combination treatment.[19–21] The first trial of temozolomide for melanoma, on the other hand, was first conducted by Middleton *et al.* which compared the overall survival, progression-free survival, objective response, safety, and pharmacokinetics of temozolomide with those of dacarbazine.[18]

Conventional chemotherapy however poses various challenges. One of the major setbacks is the development of resistance against the administered chemotherapeutic agents. The problem of drug resistance in cancer is multifaceted. There are many factors including, but not limited to, growth kinetics, tumor heterogeneity, micro-tumor environment, immune system, and physical barriers.[22] Hence it has been a limiting factor to cure and a driving force in the relapse of cancer. The initial solution to drug resistance was switching from single-agent chemotherapy to combination therapy. This approach found success in various forms of cancer including testicular, breast, and lymphoma cancer.[23–25] However over time, treatment of cancer with combination chemotherapy had now reached a plateau. Additionally, the emergence of stem cells and other cancer subpopulations acquired drug tolerance and multi-drug resistance has posed a challenge in the complete treatment of cancer.[26]

1.3 Persisters and drug tolerance

Tumor heterogeneity is driven by various factors including genetic instability due to mutation,[27] microtumor environments,[28] epigenetic modifications,[29] and cancer stem cells (CSCs).[30] Recent studies have shown the existence of small sub-populations of cancer cells that are capable of avoiding therapeutic pressure by entering a dormant/slow-cycling phase. These cells termed "drug tolerant persister cells" are observed in cancer originating from various tissue types.[31–33] Since, conventional cancer therapies target the mechanisms underlying the rapid growth of tumor cells, the existence of persisters has posed to be a significant challenge in achieving the complete eradication of cancer. This phenomenon resembles bacterial persistence, which is characterized by slow growth coupled with the ability to tolerate unusually high levels of drugs and has been documented across multiple tumor cell lines and in response to a variety of therapeutic challenges [32]. The molecular mechanisms underlying the observed tolerance of persister cells are highly complex and are still limited. However, recent evidence has brought some mechanistic insight on survival as well as the formation of persister cells (Figure 1.1). Unlike drug resistant

mutant cells, persisters are not genetically different from the bulk cancer population. Hence, the drug tolerance exhibited by these cells is transient and the progenies of persisters still show sensitivity to the cancer drugs.[31,32,34] There is two proposed hypothesis regarding the source of persister cells. The first hypothesis suggests that persister cells are pre-existing cells in the cancer bulk population that can selectively survive the therapeutic pressure. While another hypothesis is that the therapeutic pressure induces a phenotypic switch to/from the persistence state.[35–38] For drug induced persister research, cells are treated with a high concentration of cancer drugs, and the samples are collected post-treatment for characterization.

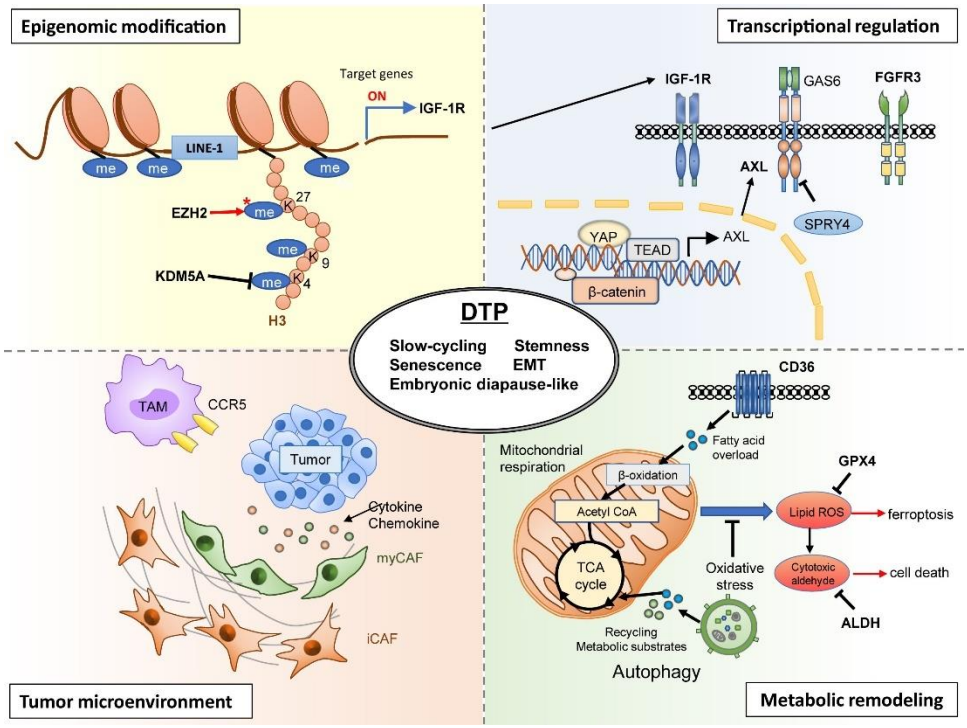

Figure 1.1 Mechanisms that regulate the persister phenotype.[39]

One of the key studies in persister was conducted by Sharma *et al.*, where they treated PC-9 lung cancer cells with chemotherapeutic agents for 9 days and showed the existence of small fraction of persister cells. They further demonstrated that the emergence of drug tolerant persisters is mediated by a transient chromatin state which is dependent on insulin like growth factor (IGF-1R) and engagement of chromatin modifying gene KDM5A/RBP2/Jarid1A, a rentinoblastoma-

binding protein that exhibits H3K4-demethylating activity).[31] Raha *et al.* sorted a small fraction of untreated cells (~ 5% of the bulk population) that expressed high aldehyde dehydrogenase (ALDH) activity, which has been associated with stem cell like characteristics, that were enriched in the persister population.[40] In addition to ALDH, various other stem cell markers such as CD133, CD24, SOX2, OLIG2, NFIA, JARID1B and CD271 are highly expressed in persister cells from various cell lines.[31,41–43] Still, whether persister cells are a sub-population within stem cell phenotype has yet to be confirmed by robust functional studies. Additional evidences of cells expressing high histone H3K4 demethylase JARID1B, as well as resistant genes such as AXL, EGFR, JUN and more before therapeutic pressure supports the existence of persister sub-population.[37,41] Recent study published by Kurppa *et al.* reported that different drug treatment can drive persister formation either by clonal selection or stochastic drug induction.[44] This further highlights the complexity of understanding the specific mechanism pertaining to the persister phenotype.

1.4 Significance of studying persisters

Cancer recurrence and development of multi-drug resistance have been a challenge for cancer treatment. The existence of persister cells can be one of the leading factors in the generation of resistant mutants. Since these cells can survive multiple rounds of chemotherapy, prolonged exposure to specific cancer drugs will eventually lead persisters to act as a reservoir for resistant mutant cells. Recent evidence has shown that diverse drug resistance mechanisms can arise from drug tolerant persister cells[45]. In their study, by treating P-9 cells with lethal concentration of erlotinib for a long period while frequently allowing periods of resuscitation in between, Ramirez *e.t. al* showed that the generated erlotinib resistant persister cells showed decrease in the sensitivity to the drug. Over time, the genomic screening of the cells resulted in the progenies of the persister cells that have harbored mutations such as T790M and MET amplification, which led to an overall increased resistance to EGFR inhibitors. In fact, some of the colonies showed decreased sensitivity to multiple drug classes.

On the bright side, research that can elucidate the mechanism of persister regulation provides key targets that can be aimed to eradicate persister cells. Sharma *et al.*, using transcriptomics analysis, showed that persister cells from non-small cell lung cancer have an altered chromatin state that requires the histone demethylase RBP2/KDM5A/Jarid1.[46] These persister cells maintain their viability through IGF-1 receptor signaling. The group showed that the inhibition of histone deacetylase (H3K9/K14) with tricostatin led to the elimination of persisters. In addition to tricostatin while screening for HDAC inhibitors, they found AEW541, a selective inhibitor of IGF-1R kinase, that eliminates the emergence of persisters.[31] Similarly Hanguer *et al.* showed that persister cells were selectively dependent on GPX4, a lipid hydroperoxidase, to survive oxidative stress and upon inhibition of the enzyme persisters were vulnerable to ferroptosis.[32] Furthermore, they conducted screening experiments and identified GPX4 inhibitorRSL3 and ML210 to be selectively lethal to persisters. Additionally, persister cells are reported to have active fatty acid β-oxidation as a significant pathway for energy production.[47] These studies further emphasize the need to conduct persister research to identify vital metabolic targets that can lead to more effective treatment of cancer cells. Targeting persister cells can be a promising strategy in cancer therapy, and it can essentially be categorized into two different approaches. The first approach is to prevent cells to enter the persister cell state while the other is to design anti-persister therapies that directly target mechanisms that are active and needed for the maintenance of the persister cell state. In our study, we focused on the latter approach by studying metabolic mechanisms that are active in persister cells and essential for their survival.

Chapter 2 A Transient Metabolic State in Melanoma Persister Cells Mediated by Chemotherapeutic Treatments

Conventional chemotherapy is one of the most common treatment strategies used to rapidly kill proliferating cancer cells. Unlike targeted therapeutics, chemotherapeutics may not be cancer type specific. However, according to American Cancer Society, chemotherapy is not often used for melanoma patients due to the reported high relapse rates [48]. Chemotherapeutics may stimulate a persistence state in melanoma cells, which remains to be characterized. Most chemotherapeutics cause DNA damage, which induces the phosphorylation of Ataxia Telangiectasia Mutated (ATM) and Ataxia Telangiectasia and Rad3-related protein (ATR) kinases [49]. ATM-mediated growth arrest can be facilitated by the transcription factor p53, which activates the cyclin-dependent kinase (CDK) inhibitor p21 [50,51]. In the absence of functional p53, ATM and ATR can still induce cell cycle arrest, as these regulators, together with Checkpoint Kinases 1 and 2 (CHK1 and CHK2), reduce CDK activity, thus resulting in cell dormancy via the inactivation of cell proliferation-related signaling pathways [52].

As we think chemotherapy can induce persistence state in melanoma cells, the metabolic alteration associated with growth arrest is inevitable during drug treatment. Metabolic reprogramming, including rapid ATP generation, increased biosynthesis of macromolecules, and maintenance of cellular redox balance under nutrient-depleted conditions and other stresses, is one of the hallmarks of cancer [53] and occurs to meet the essential needs of cancer cells. Aerobic glycolysis, known as the Warburg effect, is the most common feature of metabolic reprogramming observed in cancer cells. This phenomenon is characterized by the increased consumption of glucose via glycolysis and the downregulation of oxidative phosphorylation irrespective of oxygen availability and mitochondrial activity [54–56]. This shift seems to be essential for supporting the large-scale biosynthetic processes that are required for active cell proliferation [55]. Although aerobic glycolysis appears to occur in many rapidly dividing mammalian cells, this may not necessarily be

the case in persisters, which exist in a slowly proliferating state. Metabolic alteration in persister cells potentially extends beyond glycolysis, and these cells can rely on different metabolic pathways to evade drug effects. Understanding the metabolic state of persisters will provide important insights that are likely to aid the development of novel and broadly effective cancer treatments. In a study conducted by Shen *et al.*, [57] they revealed the existence of a metabolic mechanism, characterized by the upregulation of fatty acid oxidation, in the melanoma persister cell population mediated by BRAF and MEK inhibitors. Although many studies have shown that oxidative stress plays a critical role in persistence [41,58,59], we first need to obtain a comprehensive understanding of the metabolic state of persister cells to explore their metabolism as a therapeutic target. We still need to elucidate (i) whether the metabolic alteration observed in persister cells is a hallmark of cancer persistence, (ii) whether it is a transient state induced by cancer therapeutics and (iii) whether it depends on drug type, concentration and treatment duration. In this study, our characterization of the metabolic mechanisms of melanoma persister cells revealed that (i) metabolic alteration associated with increased mitochondrial activity seems to be a general characteristic of melanoma persisters, (ii) the observed metabolic state in persisters is transient, and (iii) this metabolic state is a result of the inhibition of cell growth, which can be mediated by a wide range of chemotherapeutics.

2.1 Material and Methods

2.1.1 Cell lines and chemicals

The melanoma cell lines (A375 and RPMI-7951) was purchased from American Type Culture Collection (ATCC) (Manassas, VA). Unless otherwise stated, all chemicals and growth media were obtained from Fisher Scientific (Waltham, MA). A375 and RPMI-7951 cells were maintained in Dulbecco's modified Eagle's medium (DMEM) supplemented with 10% fetal bovine serum (FBS), 100 units penicillin and 100 µg streptomycin/mL at 37 °C in a 5% CO2 incubator. MitoPlates, S-1 (catalog# 14105) containing glycolysis and Krebs cycle substrates, and I-1 (catalog

14104) containing ETC inhibitors were obtained from Biolog, Inc. (Hayward, CA). Saponin (catalog# 47036), used as a cell permeabilization reagent, was purchased from Sigma Aldrich (St. Louis, MO). Phycoerythrin (PE) conjugated antibodies were purchased from BD biosciences (San Jose, CA). Stock solutions for all chemotherapeutic agents were prepared with DMSO as the solvent. Phenothiazine drugs [trifluoperazine (TFZ), thioridazine (TDZ), and fluphenazine (FPZ)] were dissolved in sterile deionized (DI) water. The cells were always cultured in DMEM at 37 °C with 5% carbon dioxide (CO2) in a humidified incubator; they were treated with chemotherapeutics when they reached a confluency of ~40-50%.

2.1.2 Persister assays

Persister isolation was performed using a strategy published in a previous study [60]. Approximately 2.5 x 10^6 cells were suspended in 15 ml of DMEM, plated in T-75 flasks and incubated for 24 h to obtain the desired confluency (~40-50%). Then, the medium was removed and replaced with fresh growth medium containing a chemotherapeutic agent at 10x or 100x the half maximal inhibitory concentration (IC_{50}), as listed in Table 1. The control cells were treated with the solvent (i.e., DMSO) only. After 3 days of treatment, the cells were washed with 10 ml of Dulbecco's phosphate-buffered saline (DPBS) twice and detached from the flasks with 2 ml of trypsin-EDTA (0.25% trypsin and 0.9 mM EDTA) for ~1-2 min. After ~1-2 min, 5 ml of DMEM was added, and the cell suspension was transferred to a 10-ml centrifuge tube. The cell suspension was centrifuged at 800 revolutions per minute (rpm) for 5 min, and the supernatants were removed. The cell pellets were resuspended in fresh drug-free media and plated in a T-75 flask. After 24 h of incubation, dead cells floating in the culture medium were removed, and the adherent, live cells were collected for the subsequent assays described below. Of note, when the cells were treated with drugs for 9 days, the medium was changed every 3 days.

To generate kill curves, 3 x 10^5 cells were plated in each well of a 6-well plate with 3 ml of DMEM and incubated as described above. Similarly, the cells were treated with

chemotherapeutics for 3 days and then collected to count the live cells with trypan blue staining [61] using a countess II automated cell counter (catalog# A27977, Thermo Fisher Scientific). The ratio of surviving cells to untreated control cells was plotted to generate a kill curve profile.

2.1.3 Live/dead staining

After chemotherapeutic treatments, cells were collected and transferred to fresh medium in a 12-well plate. After 24 h of incubation, the medium with dead cells was removed and replaced with fresh DMEM. Live/dead st5aining was performed with the ReadyProbes Cell Viability Imaging Kit (Blue/Green) (catalog# R37609, Thermo Fisher Scientific) as described by the protocol provided by the vendor. Fluorescence quantification of stained cells was carried out in standard DAPI (excitation: 360 nm and emission: 460 nm) and GFP (excitation: 470 nm and emission: 525 nm) channels by EVOS M7000 florescence microscopy (catalog# AMF7000, Thermo Fisher). The NucBlue live cell reagent is cell permeant, and the NucGreen dead cell reagent is cell impermeant. Hence, dead cells emit green and blue fluorescence, while live cells only emit blue fluorescence. Live and dead cells were used as controls; dead cells were generated by treatment with 70% ethanol for 30 min.

2.1.4 Apoptosis

We performed apoptosis assays using the annexin-V fluorescein isothiocyanate (FITC)/propidium iodide (PI) kit (catalog# P50-929-7; Thermo Fisher Scientific). One of the early markers of apoptosis is the appearance of phosphatidylserine (PS) on the surface of the cells. PS is usually located in the membrane leaflets that face the cytosol. However, during apoptosis, PS is exposed to the outer leaflet of the cell membrane [62]. Annexin V binds to PS with high specificity in the presence of calcium [63]. Cells treated with chemotherapeutics were resuspended in fresh medium and plated in a T-75 flask at 37 °C for 24 h. After 24 h, the cells were collected and resuspended in PBS to obtain a density of 5 x 10^5 cells per ml. Two hundred microliters of the cell suspension was transferred to a microcentrifuge tube. The cell suspension was centrifuged at 800

rpm for 5 min. The supernatant was removed, and the pellet was resuspended in 195 µl of binding buffer. Five microliters of annexin V-FITC solution was added, and the cell suspension was incubated for 10 min at room temperature in the dark. Following incubation, the washing step was repeated to remove any excess dye. The cell pellet was resuspended in 190 µl of binding buffer and stained with 10 µl of PI for the detection of dead cells. Finally, the cell suspension was transferred to a 5-ml test tube containing PBS to obtain a final volume of 1 ml cell suspension. The sample was analyzed with a flow cytometer. The cells were excited at 488 nm and 561 nm to assess green (annexin V-FITC) and red (PI) fluorescence, respectively. The green fluorescence was detected with a 520 nm emission filter; the red fluorescence was detected with a 615 nm emission filter. Cells that are FITC-positive but PI-negative are in the early phase of apoptosis; cells that are both FITC-positive and PI-positive are in the late phase of apoptosis, and cell that are both FITC-negative and PI-negative are live cells. Untreated live cells, dead cells and cytarabine-treated cells were used to gate the cell subpopulations on flow cytometry diagrams. Dead cells were generated by treatment with 70% ethanol for 30 min. Cytarabine is known to induce apoptosis [64]; cells were treated with 50 µM cytarabine for 3 days before staining the cells with the dyes.

2.1.5 Metabolomics study

After 3 days of gentamicin (GEM) treatment at 10 x IC_{50}, the surviving cells were collected in a 10-ml centrifuge tube, washed with 2 ml PBS by centrifugation (5 min at 800 rpm) and pooled in a microcentrifuge tube to obtain ~100 µl of cell pellet. A dry ice/ethanol bath was used to rapidly cool and freeze the cell pellet. Untreated cells were used as a control. The frozen samples were sent to Metabolon Inc. (Morrisville, NC). Metabolon's protocols were used for the sample extraction, instrument settings, and conditions for the MS platforms (see details in article [65]). Initial data analysis was performed by Metabolon. Briefly, the obtained biochemical data were normalized to the protein concentration (assessed by Bradford assay) of each respective sample. The normalized data were used to form a matrix to perform unsupervised hierarchical clustering with the

Clustergram function in MATLAB. Metabolites in persisters were compared with those in control groups using ANOVA with a significance threshold of $P \leq 0.05$. A Q-value was used to estimate the false discovery rate, and low Q-values ($Q < 0.1$) indicated high confidence in the results.

2.1.6 MitoPlate assay

To assess the mitochondrial function of cells, phenotype microarray plates (S-1, catalog# 14105) were used. Mitoplate assays employ a modified version of tetrazolium dye that can be reduced intracellularly by ETC activity across the membranes of metabolically active mitochondria, resulting in the production of water-soluble formazan. The color change associated with formazan production can be detected by absorbance measurements at 590 nm (OD_{590}) and correlates with cellular ETC activities. The assay employed Biolog Mitochondrial Assay Solution (BMAS, catalog# 72303) together with dye mixture MC (tetrazolium-based dye, catalog# 74353) provided by Biolog, Inc. In a 50-ml sterile reservoir, 2 x BMAS, MC, 960 μg/ml saponin and sterile water were gently mixed in a 6:4:1:1 ratio to obtain the assay mixture. Thirty microliters of the assay mixture was distributed to each well of the 96-well microarray and incubated at 37 °C for 1 h to dissolve the preloaded substrates.

Control or chemotherapeutic-treated cells were collected in a 10-ml centrifuge tube and centrifuged at 800 rpm for 5 min. The supernatant was removed, and the cell pellet was washed with PBS twice to remove any debris. Finally, the cell pellet was resuspended in 1x BMAS to achieve a final cell density of 1×10^6 cells per ml. Thirty microliters of the cell suspension was pipetted into each well of the microarray containing the assay mixture. The final assay mixture was composed of 3×10^4 cells per well. After inoculation, the OD_{590} was measured every 10 min with a Varioskan Lux Microplate Reader (catalog# VLBL00GD0, Thermo Fisher Scientific). These data were then normalized by subtracting the absorbance readings of control (no substrate) wells.

2.1.7 Modified MitoPlate assay

To verify the accuracy of the MitoPlate assay, the same procedure was repeated in a standard half-area 96-well plate with a slight modification. Like the MitoPlate assay described above, the assay mixture consisted of BMAS, dye and saponin. However, sterile water was replaced with a solution consisting of 96 mM Krebs cycle substrates (i.e., sodium malate, sodium fumarate or sodium succinate). 2 x BMAS, MC, saponin and substrate solution were mixed at a 6:4:1:1 ratio to prepare the assay mixture, and 30 µl of the assay mixture was transferred to each well of the 96-well plate. Similarly, 30 µl of the cell suspension in 1x BMAS was added to each well of the plate containing the assay mixture so that each well contained 4 mM substrate and 3 x 10^4 cells. After inoculation, the OD_{590} was measured every 10 min with a microplate reader. For the control conditions, the ETC inhibitors rotenone or antimycin A were added to the assay mixtures. The final concentration of the inhibitors in the culture was 10 µM. These data are then normalized by subtracting the absorbance reading of control wells (no substrate).

For "no substrate" controls, the MitoPlate assays were repeated without adding Krebs cycle substrates. In this case, after mixing 2 x BMAS, MC, saponin and water at 6:4:1:1 ratio, 30 µl of the assay mixture was transferred to each well of the plate. Then, 30 µl of the cell suspension in 1x BMAS was added to each well, and OD_{590} measurements were performed similarly.

2.1.8 Cell growth assay

A375 cells were stained with carboxyfluorescein succinimidyl ester (CFSE) dye using CellTrace proliferation kits (catalog# C34570, Thermo Fisher Scientific). CFSE dye can freely diffuse across the cell membrane and produce a stable fluorescent signal following an enzymatic reaction with cellular esterases [66]. The cells were stained with 5 µM CFSE dye following the protocol in the manual. A total of 3 x 10^5 stained cells were seeded in each well of a 6-well plate and incubated for 24 h. After 24 h, the medium was removed and replaced with fresh DMEM with chemotherapeutic agents at the indicated concentrations. The cells were treated for six days, and

the growth medium was changed every three days. Every 24 h, cells were detached from the wells with trypsin, collected and resuspended in 1 ml PBS for analysis with a flow cytometer. The cells were excited at 488 nm, and green fluorescence was detected with a 520-nm emission filter. The fluorescence half-life for all conditions was calculated using the decay equation below:

$$F = F_o 2^{\frac{-(t-t_O)}{t_d}} \qquad (1)$$

where F_o is the mean fluorescence intensity for cells at time to; td is the half-life time; and F is the mean fluorescence intensity for cells at time t. In this study, to was chosen as day 0. The half-life time was calculated with SOLVER in Excel by minimizing the sum of normalized mean square errors (NMSE) between experimental and predicted model data.

2.1.9 Microscopy analysis for cell growth

Cells were stained with 5 μM CFSE dye following the protocol provided in the CellTrace kit. A total of 3 x 10^5 cells were then seeded in each well of a 6-well plate and incubated for 24 h. After 24 h, the medium was removed from each well and replaced with medium including a chemotherapeutic agent. After 3 days of incubation, cells were washed with 3 ml DPBS, detached with 200 μl of trypsin, resuspended in 1 ml medium, transferred to a 1.5-ml microcentrifuge tube and centrifuged at 800 rpm for 5 min. The supernatant was removed, and the cell pellet was resuspended in 1 ml fresh drug-free growth medium and transferred to each well of a 6-well plate. After 24 h of incubation, the growth medium was replaced with 1 ml DPBS. The cells were then analyzed under an EVOS M7000 fluorescence microscope (excitation: 470 nm and emission: 525 nm).

2.1.10 ALDEFLUOR assay

An ALDEFLUOR assay kit (catalog# NC9610309, Thermo Fisher Scientific) was used to measure the cellular aldehyde dehydrogenase (ALDH) activity. A total of 3 x 10^5 cells were plated in each well of a 6-well plate with 3 ml of DMEM and incubated for 24 h. After 24 h, the growth

medium was removed and replaced with fresh growth medium containing 20 nM GEM. Every 24 h, the cells were washed with 3 ml DPBS, detached with 200 µl trypsin, resuspended in 1 ml growth medium and transferred to a microcentrifuge tube. The cell suspension was centrifuged at 800 rpm for 5 min, and the supernatant was removed. This washing procedure was repeated with DPBS to remove all the residuals. Finally, the cell pellet was resuspended in 1 ml of ALDEFLUOR assay buffer. Five microliters of the activated ALDEFLUOR reagent was added to the cell suspension and mixed. After mixing, 500 µl of the cell suspension was immediately transferred to another microcentrifuge tube containing 5 µl of diethylamino-benzaldehyde (DEAB), which was used as a negative control, as DEAB inhibits ALDH activity. The samples were then incubated at 37 °C for 45 min. After incubation, the cell suspension was centrifuged at 800 rpm for 5 min, and the supernatant was removed. The cell pellet was resuspended in 500 µl of ice-cold ALDEFLUOR assay buffer and transferred to a 5-ml test tube. Each sample was stained with 1.5 µM PI, incubated for 15 min at room temperature and analyzed by flow cytometry. The cells were excited at 488 nm and 561 nm for green and red fluorescence, respectively. The green fluorescence was detected with a 520-nm emission filter; the red fluorescence was detected with a 615-nm emission filter.

2.1.11 Measuring CD271, CD44 and CD34 biomarkers

Approximately, 2.5 x 10^6 cells were seeded in a T-75 flask containing 15 ml of DMEM and incubated for 24 h. After 24 h, cells were either treated with a chemotherapeutic agent or left untreated. At indicated time points, cells were detached, collected in a 15 ml centrifuge tube, centrifuged at 800 rpm for 5 mins and the supernatant was discarded. The cells were then washed with 5 ml of DPBS. Finally, 1 x 10^6 cells were resuspended in 100 µl of cell stain buffer (catalog# 554657) in a microcentrifuge tube. Then, 20 µl of a Phycoerythrin (PE) conjugated antibody [CD271 (catalog# 557196), CD44 (catalog# 555479), or CD34 (555822); BD Biosciences, San Jose, CA] or its respective IgG control was added, and the cell suspension was incubated at room temperature for 30 mins. After incubation, the cells were centrifuged at 800 rpm for 5 mins and the

supernatant was discarded. The cell pellet was resuspended in 500 µl of cell stain buffer, stained with 0.25 µM of SYTOX green and incubated for 15 min at room temperature. The cells were then transferred to a 5 ml test tube and analyzed with a flow cytometer. The cells were excited at 488 nm and 561 nm for green and red fluorescence, respectively. The green fluorescence was detected with a 520-nm emission filter; the red fluorescence was detected with a 586-nm emission filter.

2.1.12 Inhibitor screening

Approximately 1 x 10^4 cells were suspended in 150 µl of DMEM, plated in each well of a 96-well plate and incubated for 24 h. Then, the medium was removed and replaced with 150 µl of DMEM containing GEM (20 nM) and/or the ETC inhibitors obtained from the Biolog I-1 plate (catalog # 14104). Of note, the ETC inhibitors are in their solid forms in the I-1 plate; therefore, 150 µl of DMEM with or without GEM was added to each well of the I-1 plate in advance. After 2 h of incubation, the media were transferred from the I-1 plate to the 96-well plate containing the cells mentioned above. After 3 days of treatment, the medium was removed, and the cells were washed with 100 µl of DPBS twice. Then, 150 µl of drug and inhibitor-free medium was transferred to each well of the 96-well plate. After incubating the cells for 24 h, the growth medium was removed and replaced with 100 µl of fresh medium. Finally, 10 µl of 3-(4,5-dimethylthiazol-2-yl)-2,5-diphenyltetrazolium bromide (MTT, catalog # 97062-376, VWR) (5 mg/ml) was added to each well to measure the cell viability, and the cells were incubated at 37 °C for 3 h. At 3 h, the medium was removed and replaced with 100 µl of MTT solubilization buffer [67]. After 20 min of incubation at 37 °C, the absorbance at 570 nm (OD570) was measured with a microplate reader.

2.1.13 Validation of the inhibitor screening assay results

A total of 3 x 10^5 cells were plated in each well of a 6-well plate with 3 ml of DMEM and incubated for 24 h as described above. The cells were cotreated with GEM and/or phenothiazine for 3 days. After 3 days, the surviving cells were washed with 2 ml DPBS, detached with 200 µl of trypsin for 1-2 min, resuspended in fresh drug-free DMEM and incubated for 24 h. After 24 h, the

cells were collected as described above, transferred to a microcentrifuge tube in PBS, and enumerated with trypan blue solution (0.4%) and the automated cell counter. If the surviving cell levels were under the limit of detection, we used a flow cytometer. To do this, the cell suspension was centrifuged at 800 rpm for 5 min, and the supernatant was removed. The cell pellet was resuspended in 500 µl of 0.85% sodium chloride (NaCl) solution. Then, the cells were stained with 0.25 µM SYTOX green (catalog # S7020, Thermo Fisher Scientific) and SYTO60 red (catalog # S11342, Thermo Fisher Scientific) and then incubated at 37 °C for 15 min. SYTOX green is cell impermeant and only stains dead cells. SYTO60 is cell permeant and can diffuse through the cell membrane. After 15 min, the cell suspension was centrifuged at 800 rpm for 5 min, and the supernatant was removed. Finally, the cell pellet was resuspended in 500 µl of 0.85% NaCl solution and transferred to a 5-ml test tube for flow cytometry analysis. The cells were excited at 488 nm for green fluorescence and 561 nm for red fluorescence. The green fluorescence was detected with a 520-nm emission filter; the red fluorescence was detected with a 615-nm emission filter.

2.1.14 Statistical analysis

GraphPad Prism 8.3.0 was used for linear regression analysis, and the slopes of untreated and treated groups were compared with F statistics. Pairwise comparisons were performed using unequal variance t-tests or ANOVA. For statistical significance analysis, the threshold value of P was set as * or # $P < 0.05$, **$P < 0.01$, ***$P < 0.001$, and ****$P < 0.0001$. A minimum of three independent biological replicates (unless otherwise stated) were assessed for all experiments. In all figures, data corresponding to each time point represent the mean value ± standard error.

2.2 Results

2.2.1 Gemcitabine persistence is a slow-growing cell state

Persister cells are defined as a small subpopulation of phenotypic variants that are transiently tolerant to drugs. Once the drug is removed and the persisters are re-cultured in fresh, drug free medium, they form cell populations that exhibit drug sensitivity identical to the original

culture, which distinguishes them from resistant mutants [32]. In this study, persister subpopulations were derived from gemcitabine (GEM)-treated A375 melanoma cell cultures (Figure 2.1a). The A375 cell line has BRAF V600E mutations, leading to excessive cellular proliferation and differentiation and increased cell survival [10]. GEM is a nucleoside that is an analog of deoxycytidine [68] which inhibits DNA replication by incorporating itself at the end of the elongating DNA strand. A375 melanoma cells were treated with GEM (10 x IC_{50}=20 nM, see Supp. Table 2) for 3 days. After the treatment, cells were allowed to recover in fresh, drug-free growth medium and then treated with GEM after recovery to demonstrate the sensitivity of the daughter cells to GEM. Additionally, we treated A375 cells with GEM for 3 days to generate a concentration vs. survival ratio profile (Figure 2.1b); the results showed that the cell survival ratio, that were calculated by normalizing the surviving cell numbers to those in the untreated control groups, did not change significantly at concentrations higher than 10 x IC_{50} (20 nM, see Supp. Table 2) [69,70].

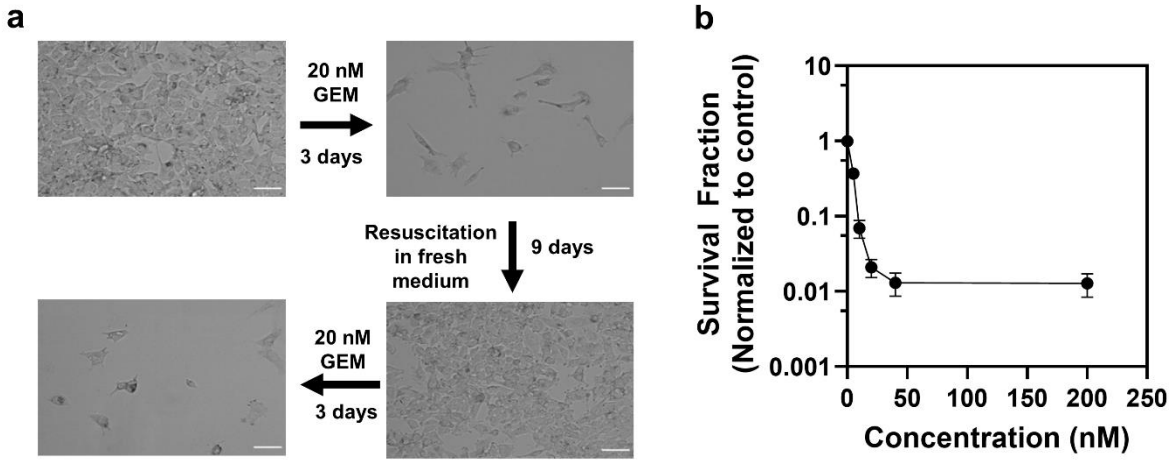

Figure 2.1 Isolating Persister cells. Scale bar: 100 μm. The number of biological replicates (N) =4.

After 3 days of GEM treatment, we gently detached the cells from the flasks, resuspended them in fresh, drug-free growth medium, and incubated them for 24 h to remove dead/late apoptotic cells and collect the persister cells. As shown in the microscope images from the live/dead staining assay (Figure 2.2a), nearly all persister cells were viable. Furthermore, an annexin-V fluorescein

isothiocyanate (FITC)/propidium iodide (PI) assay [63] was performed to detect apoptotic cells. The quadrants of this graph represent (I) live (FITC-/PI-), (II) early apoptotic (FITC+/PI-), (III) late apoptotic (FITC+/PI+) and (IV) dead (FITC-/PI+) cells (Figure 2.2). The data showed that the apoptosis levels in both the parental and surviving persister cell populations were nonsignificant (Figure 2.2b). Unlike drug-resistant mutants, the progenies of persisters are susceptible to cancer drugs; this phenomenon has been demonstrated in many other studies [31,32,57]. Therefore, cells surviving GEM treatment were transferred to fresh medium, regrown, and retreated with GEM to verify the transient state of melanoma persister cells (Figure 2.1a).

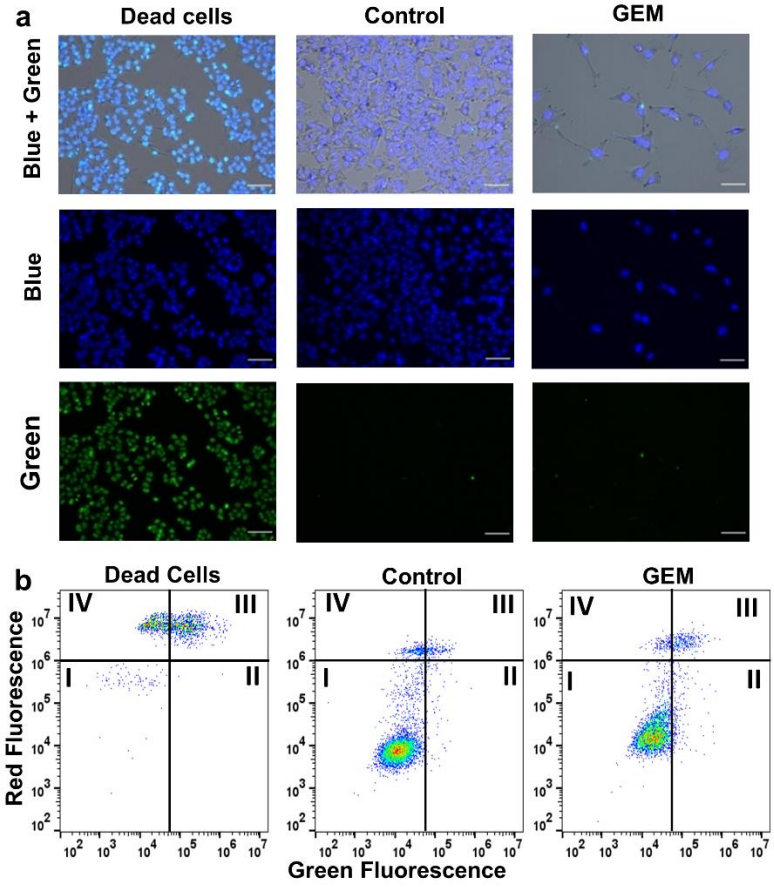

Figure 2.2 Persister cells are live and viable cells.

To measure the growth rate of GEM persister cells, we performed a cell proliferation study using carboxyfluorescein succinimidyl ester (CFSE) dye. For this assay, the cells prestained with

CFSE were treated with GEM or left untreated (control), and the cell proliferation rates of these groups were measured by monitoring the fluorescence dilution rate over time with a flow cytometer. Our results revealed ongoing cell division in the control groups, as evidenced by a reduction in the fluorescent signals, whereas the fluorescent signal was maintained in the treatment groups largely due to a lack of cell proliferation (Figure 2.3b). The mean fluorescence intensity for the first 3 days for each group was integrated into the fluorescence decay equation to calculate the half-life of the fluorescent signal, further showing that cells treated with GEM grew significantly slower than untreated control cells (Figure 2.3a). Our microscope images further showed that the surviving cell populations seemed to be heterogeneous (Figure 2.3a). We noticed that GEM treated cells underwent morphological changes; typically, the cells became elongated or spherical while retaining their fluorescence levels (e.g., cells highlighted with arrows in Figure 2.3c).

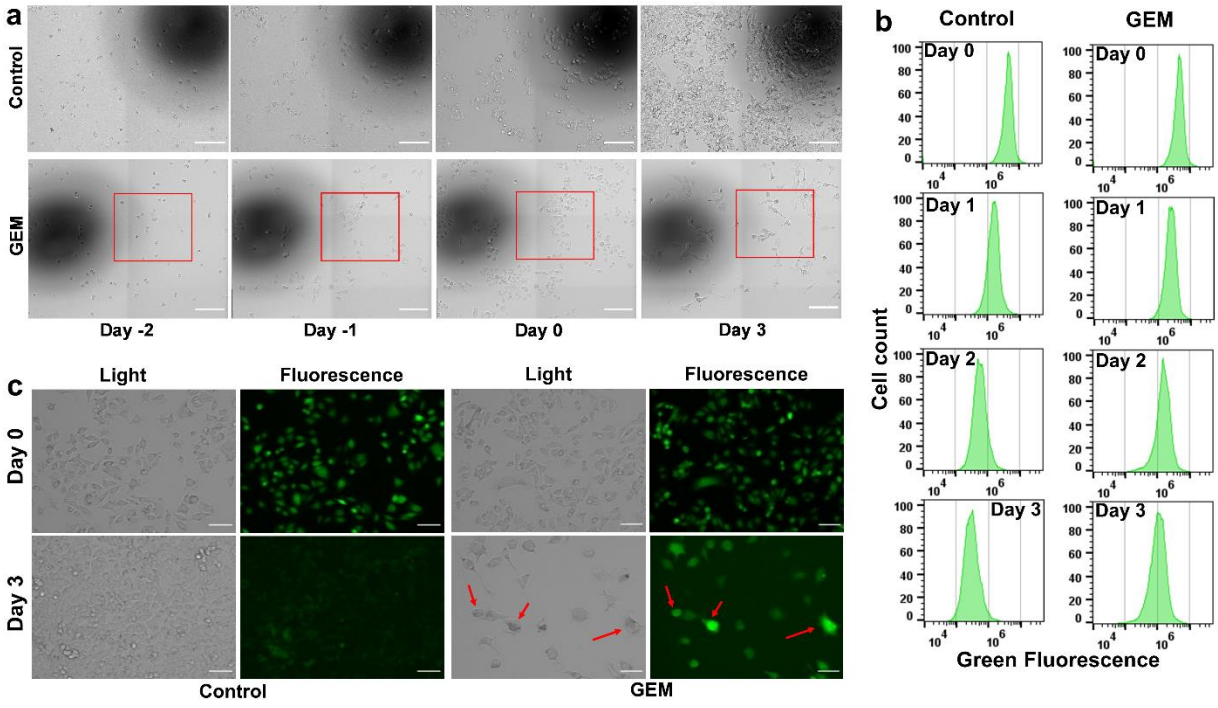

Figure 2.3 Persisters are slow cycling cells. Scale bar: 100 µm

In figure 2.3(a) A375 cells before (days -2 and -1), during (day 0) and after (day 3) GEM (10 x IC_{50}) treatment were monitored with a microscope that is capable of scanning the same area.

The culture vessel was also marked with a black spot to further verify the selected location. Proliferating cells upon GEM treatment either died or entered a cell cycle arrest, leading to morphological changes (highlighted with a box). For figure 2.3(b-c) Melanoma cells prestained with CFSE dye were treated with GEM or left untreated (control), and their fluorescence intensity was monitored at the indicated time points with flow cytometry (b) or florescence microscopy (c).

Melanoma cells can undergo reversible phenotypic transitions in response to drug treatments, which may result in stem cell like characteristics [71,72]. Since high aldehyde dehydrogenase (ALDH) activity and increased expression of stem cell biomarkers, CD271, CD44 and CD34, were shown to be associated with the phenotypic plasticity of melanoma cells [73,74], we performed the ALDEFLUOR assay and flow cytometry analysis to measure these biomarkers in GEM treated cells. Melanoma cells were treated with GEM (10 x IC_{50}) or left untreated for 3 days. Every day, the ALDH activity of the cells was assessed with an ALDEFLUOR assay and a flow cytometer. Cells treated with the ALDH inhibitor 4-(dimethylamino)benzaldehyde (DAEB) served as negative controls (Figure 2.4a). CD271, CD44 and CD34 biomarkers were detected with their respective conjugated antibodies. Cells treated with isotype controls of CD271, CD44 and CD34 were used to determine stem cell biomarker negative (-) and positive (+) cells (Figure 2.4(b-d). Live/dead staining was used to gate the live cells.

Although GEM treatment slightly induced the CD271 expression in the cells, we did not observe a consistent trend in the expression levels of other stem cell biomarkers (CD44 and CD34) and found no significant increase in ALDH activity in GEM persisters compared to untreated control cells (Figure 2.4a-d). Altogether, our data indicate that persister populations studied here are slow-growing cells that are potentially induced by chemotherapeutic treatment. These cells exhibit heterogenous morphology without having a drastic increase in the expression levels of known stem cell biomarkers.

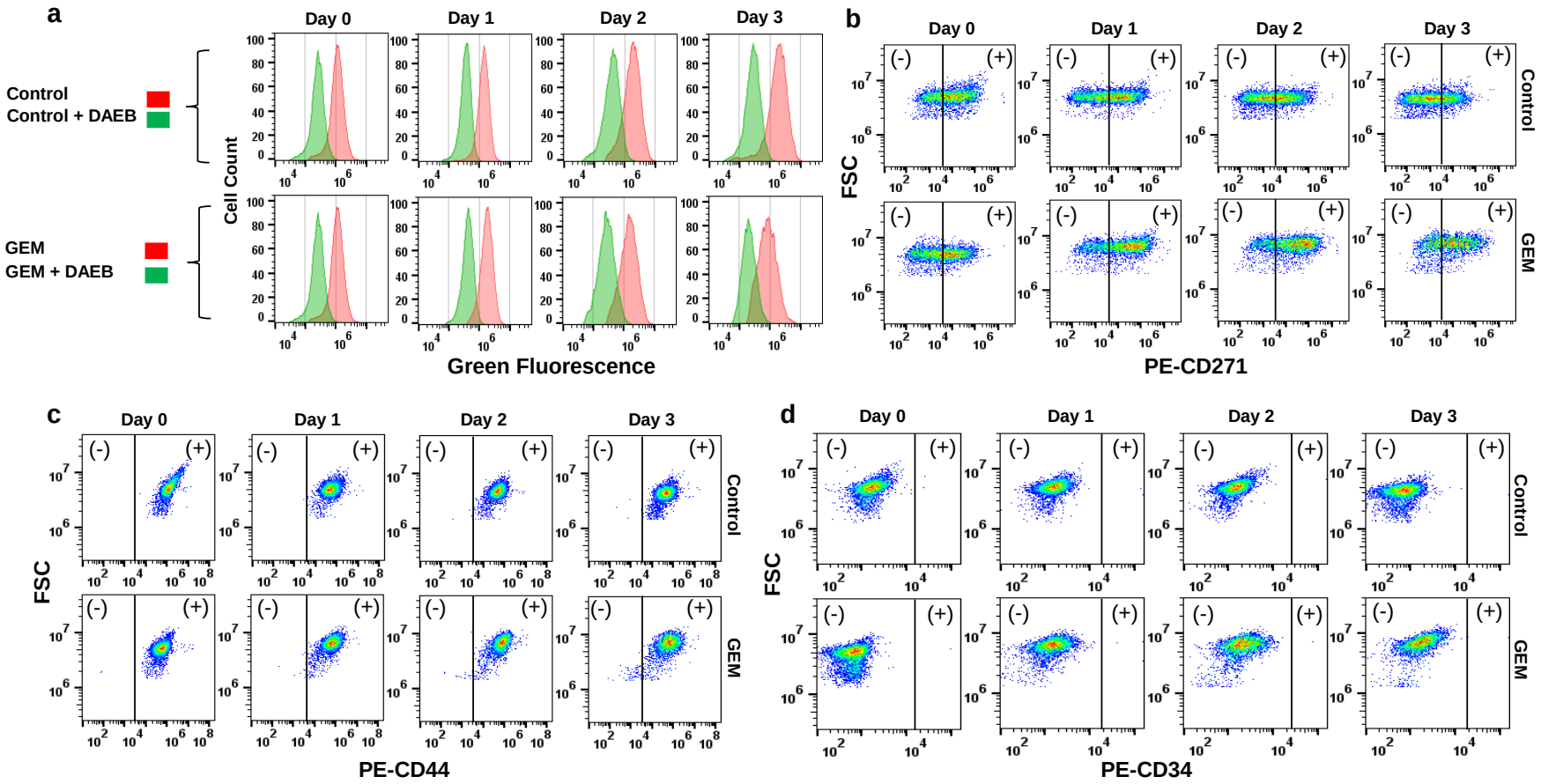

Figure 2.4 Stem cell biomarkers in A375 persister cells.

2.2.2 Persister cells have an altered metabolic state.

Tumor cells undergo metabolic alteration to fulfill the energy requirement, sustain the high rate of cell proliferation, avoid the action of therapeutics and improve the overall survivability of the tumor cells [75]. As persistence is a transient state, we expected that persister cells would undergo metabolic alterations due to their slow or nonproliferating cell state. To identify such metabolic mechanisms, we conducted untargeted metabolomics analysis of GEM-treated cells and untreated control cells. Persisters were generated by treating the cells with 10 x IC_{50} of GEM, and untreated cells were generated by culturing the cells in drug-free growth media. In our study, we measured 689 different metabolites that are part of the superpathways involving the following factors: amino acids, peptides, carbohydrates, energy, lipids, nucleotides, cofactors/vitamin and xenobiotics (Table 2). Unsupervised clustering of the metabolomics data was performed with the Clustergram function in MATLAB. The generated heat maps show metabolite clusters that are upregulated (red) or downregulated (blue) in the treated group compared to the untreated control group. Each column represents a biological replicate; each row represents a metabolite. Pathway enrichment analysis showed that the relative levels of 342 metabolites were significantly altered in the persister subpopulation compared to the control group (Table 2).

Unsupervised hierarchical clustering of the metabolic data of four independent biological replicates of untreated or GEM-treated samples revealed a distinct metabolic alteration taking place in persister cells (Figure 2.5a). While the relative levels of metabolites associated with dipeptides, phospholipids, sphingosines, the urea cycle, gamma-glutamyl amino acid, ceramides, polyamines, tryptophan, sterols, endocannabinoid, phosphatidylcholines (PC), lysophospholipids and sphingomyelins were upregulated, those associated with glycine, serine, threonine, pentose sugars, vitamin B6, glutamate, the Krebs cycle and branched-chain amino acids (BCAAs) were significantly downregulated in persister cells compared to those in control cells (Figure 2.5a-f and Table 2).

Although our metabolomic analysis indicates that the levels of phospholipids (particularly PCs, phosphatidylserine, phosphatidylethanolamine, phosphatidylglycerol, phosphatidylinositol and phosphatidylinositol-phosphates), and sphingolipids with their associated structural elements (ceramide and sphingosine) were considerably upregulated (Figure 2.5f), those involved in one-carbon metabolism (e.g., glycine, serine, and methionine) were distinctively downregulated in GEM-treated cells compared to untreated control cells (Figure 2.5b). Alteration of the lipid metabolism of cancer cells compared to that of nonmalignant cells is a well-studied phenomenon [76]. This metabolic reprogramming has been shown to be highly dependent on the cancer type and stage. Phospholipids are predominant components of the cell membrane that can play an important role in persistence by modulating the expression and activity of multidrug resistance pumps [77]. Sphingolipids are another family of membrane lipids known to play a role in the regulation of cell proliferation, apoptosis, migration and inflammation [78]. One-carbon metabolism, as an indicator of the cell nutrient status, functions in the biosynthesis of nucleotides as well as the maintenance of the redox and methylation states required to support the high rate of proliferation in cancer cells [79].

Cancer cells overexpress amino acid-degrading enzymes to increase their energy production and to provide metabolites for their anabolic processes. BCAAs (such as leucine, isoleucine and valines) are a class of amino acids, and their levels were significantly downregulated in GEM-treated cells (Figure 2.5e). BCAAs are expected to be upregulated in normal cancer cells, as they can be used for various processes such as protein synthesis and energy production [80]. Of the carbohydrate family, the pentose phosphate pathway (PPP) metabolite levels were significantly downregulated in GEM-treated cells (Figure 2.5d). Similar to one-carbon metabolism, the PPP was shown to be important for tumor cells in terms of nicotinamide adenine dinucleotide phosphate (NADPH) production, which is essential for fatty acid synthesis and reactive oxygen species detoxification [81]. The PPP is tightly interconnected with glycolysis and the Krebs cycle, as they share a number of intermediates, including glucose-6-phosphate (G-6-P), pyruvate and acetyl-CoA.

The Krebs cycle is also closely linked to BCAA metabolism, as alpha-ketoglutarate is essential for BCAA metabolism. Our untargeted metabolomics analysis showed that, similar to BCAA and PPP metabolism, the Krebs cycle was significantly altered in GEM-treated cells, as its intermediates (e.g., alpha-ketoglutarate, fumarate, malate, and oxaloacetate) were significantly less abundant in melanoma persisters than in the untreated bulk cell population; however, we did not observe a significant change in glycolysis intermediates, except for pyruvate, in either group (Figure 2.5c). Although our MS analysis shows a metabolic alteration in energy metabolism in persister cells, MS does not directly measure intracellular reaction rates (e.g., mitochondrial activity); such measurements are necessary to link the abundance of these metabolites to their turnover rates.

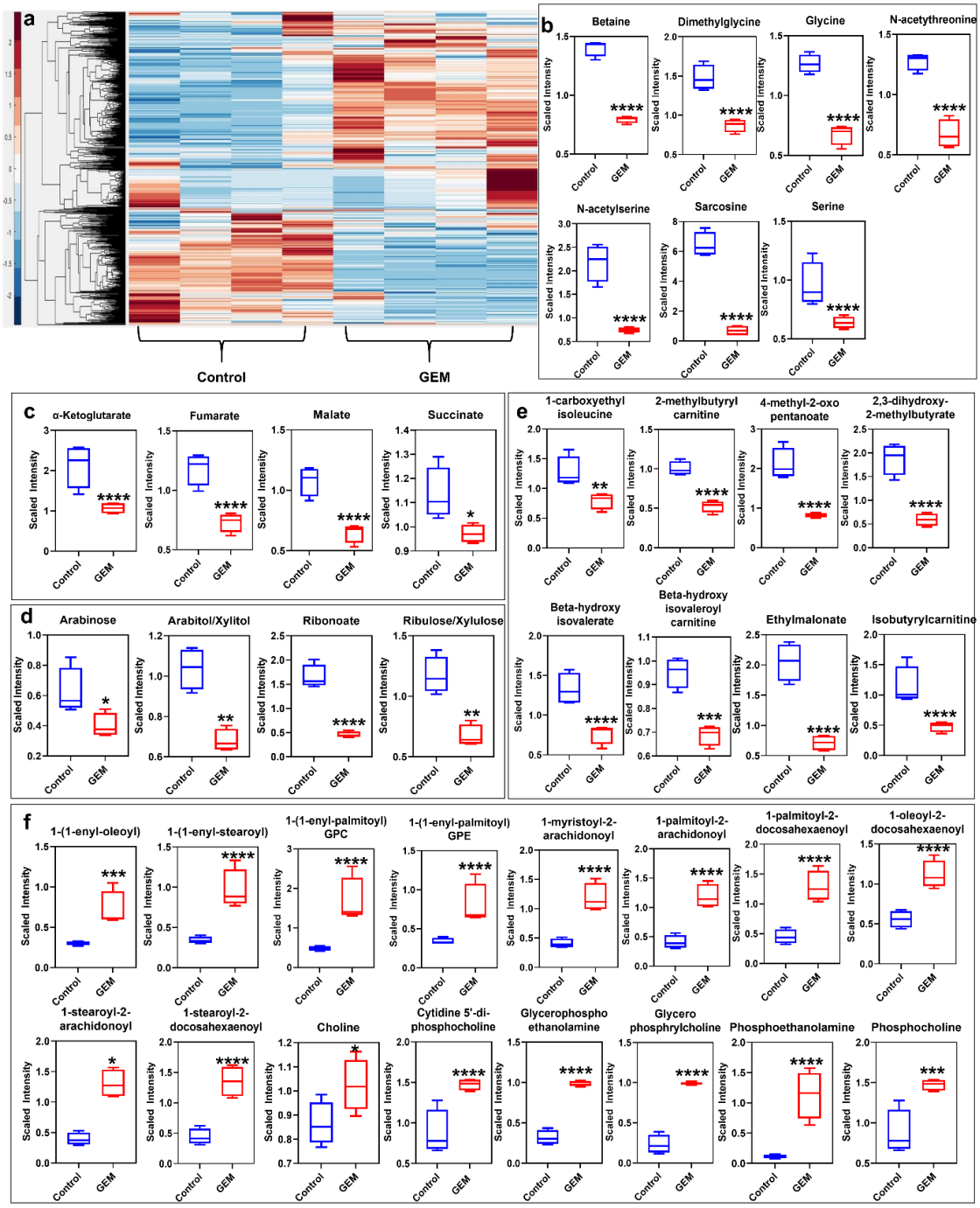

Figure 2.5 Metabolic alterations in GEM persisters. Box plots show the metabolites from the one-carbon metabolism pathway (b), the Krebs cycle (c), the PPP (d), the BCAA metabolism pathways (e), and the lipid metabolism pathway (f). Statistical significance was assessed with ANOVA (* $P < 0.05$, ** $P < 0.01$, *** $P < 0.001$, and **** $P < 0.0001$). N=4

2.2.3 Persister cells have increased mitochondrial activity

Cancer cells are known to use aerobic glycolysis to generate substrates for the anabolic processes needed to support cell proliferation [54,55]. We think that, due to their nonproliferating cell state [31,32], persisters may have increased mitochondrial metabolism. This metabolic alteration may explain the low levels of Krebs cycle intermediates observed in persisters, as the depletion of these substrates is potentially due to faster consumption of these compounds in persisters. To verify this, we measured the mitochondrial activity of the persister cells using MitoPlates (Biolog Inc., Hayward, CA).

For this assay, 30 different substrates associated with glycolysis and the Krebs cycle were screened in a 96-well format. High throughput screening assay was conducted using a modified version of tetrazolium dye. The consumption rates of substrates were monitored by measuring the OD_{590} at the indicated time points (for 100 min total). A kinetic graph was generated to illustrate the consumption of each substrate by measuring the color intensity of a modified tetrazolium dye present in each well. This color change correlates with cellular ETC activities. The obtained data were then clustered (unsupervised) to generate a heat map (Figure 2.6) for all the substrates being studied.

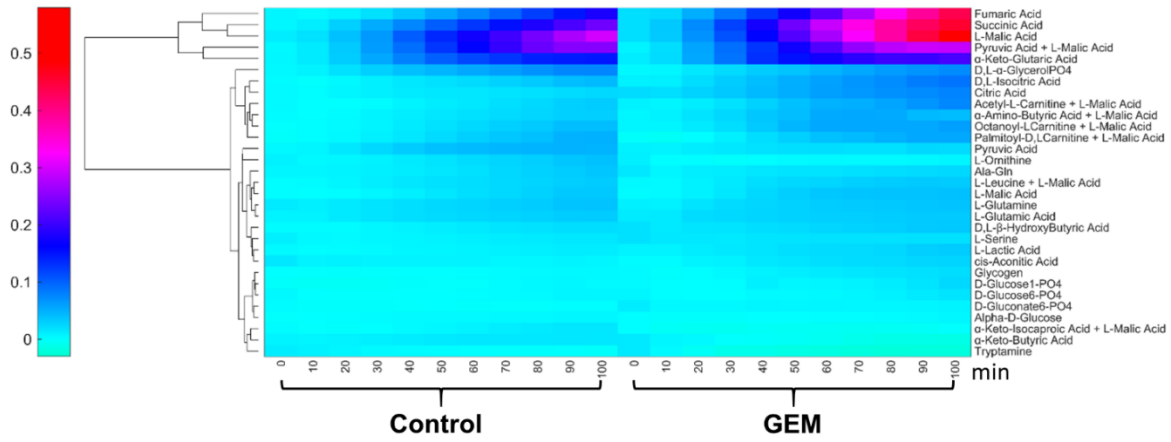

Figure 2.6 Assessing mitochondrial activity of persister cells. N=4.

Of all the substrates that were tested, persister cells had a higher rate of consumption of Krebs cycle metabolites (specifically, the consumption rates of malate, fumarate and succinate) than untreated cells. Mitoplate screening is a high-throughput assay with limited control over the concentrations of substrates in microarrays. As the concentrations of the substrates were not disclosed, to verify the observed results, these assays were repeated in a generic 96-well plate where the metabolites (i.e., malate, fumarate and succinate) were added manually to achieve a final concentration of 4 mM. The data generated from these modified assays were in agreement with our MitoPlate data (Figure 2.7a-c).

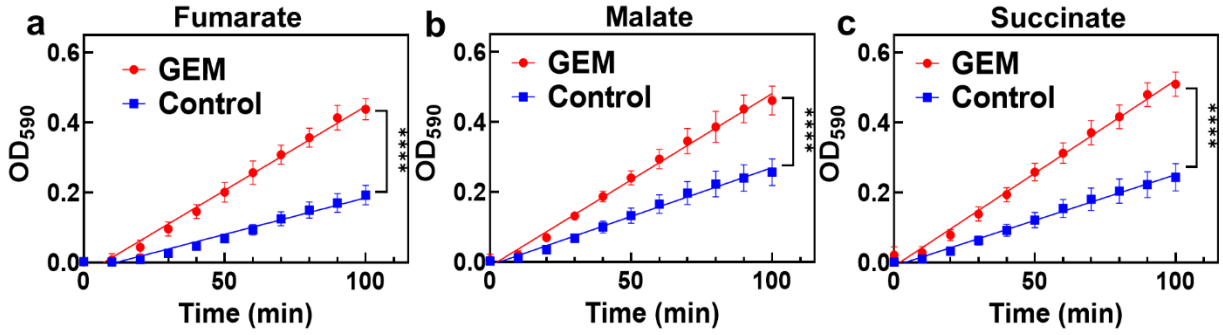

Figure 2.7 Persister cells have higher consumption rate for TCA cycle substrates. Linear regression analysis was performed using F statistics with GraphPad Prism (**** $P<0.0001$). N=4.

To further verify the accuracy of the assays, control experiments, in which ETC complexes were inhibited with rotenone and antimycin A, were conducted. Rotenone is a complex I inhibitor, and antimycin A inhibits complex III of the ETC [82,83]. Therefore, the substrates capable of producing only NADH (i.e., malate and fumarate) and the substrates producing both NADH and FADH2 (i.e., malate, fumarate and succinate) should not give any absorbance reading in the presence of rotenone and antimycin A, respectively, in modified MitoPlate assays.

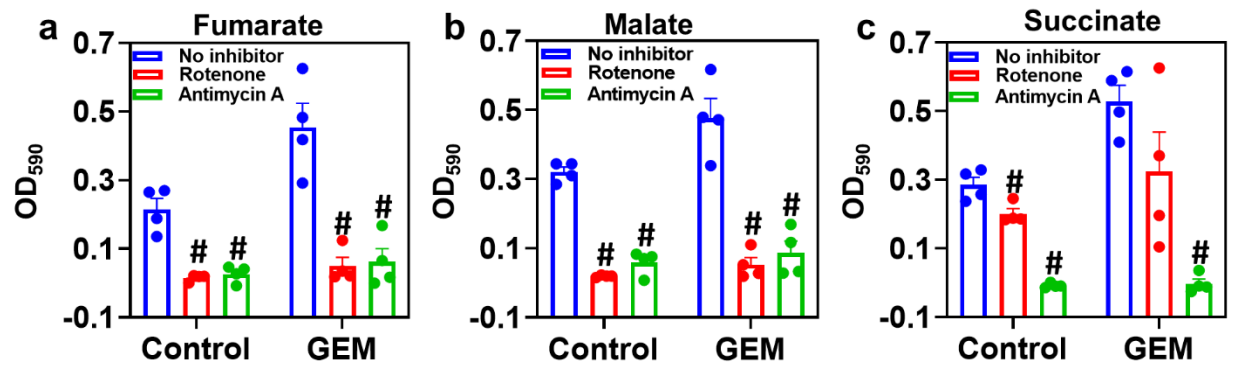

Figure 2.8 Validating efficacy of mitoplate assay. N=4. Statistical significance was assessed by performing pair-wise t-test. # represents a significant difference between the inhibitor (rotenone or antimycin A) and "no inhibitor" groups (P<0.05).

The bar graphs in figure 2.8 represent the OD_{590} data of the modified MitoPlate assays for fumarate (a), malate (b) and succinate (c) and indicate their consumption rates at 100 min in the presence of rotenone (10 µM) or antimycin A (10 µM). The data generated support our argument and validate the efficacy of the assay (Figure 2.8a-c). Of note, MitoPlate data reported here were normalized to "no substrate" controls in which the assays were performed without adding any exogenous Krebs cycle substrates. Therefore, we compared the basal ETC activity of GEM treated with untreated control group by performing regular (Figure 2.9a) or modified MitoPlate (Figure 2.9b) assays without adding any exogenous Krebs cycle substrates. Critically, these "no substrate" data still show that the basal level of persister cell ETC activity is higher than that of the untreated cells (Figure 2.9).

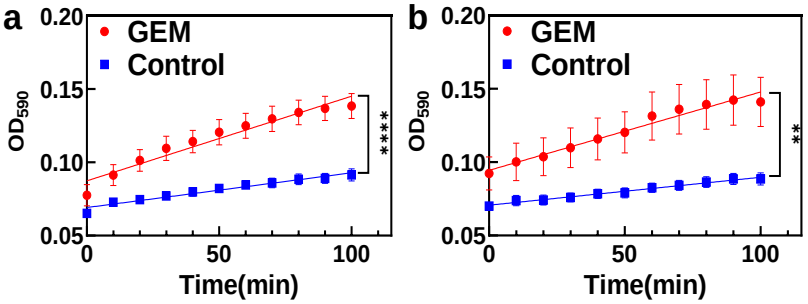

Figure 2.9 The basal ETC activities of GEM persister cells. Linear regression analysis was performed with F statistics using GraphPad Prism (**** P<0.0001, and ** P<0.01). N=4.

Finally, as persistence is a temporary state, the observed metabolic alteration should also be transient. Cells that survived GEM treatment were collected and regrown in fresh growth medium. After 9 days of resuscitation, the cells resumed their growth cycle and started to proliferate (Figure 2.1a). The progenies of the resuscitated cells after the 3rd passage were collected to assess their mitochondrial activity. As expected, the consumption rates of malate, fumarate and succinate in persister progenies were similar to those of untreated control groups (Figure 2.10a-c).

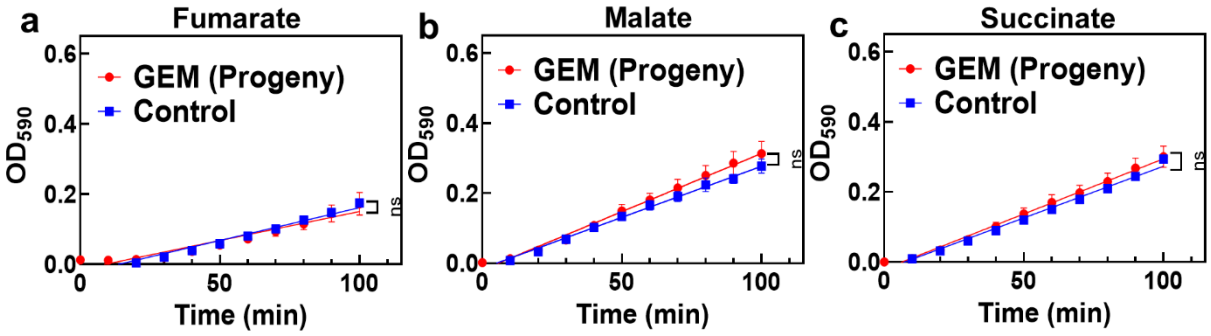

Figure 2.10 Metabolic alteration observed in persister is transient. N=4; ns: the slopes are not significantly different.

2.3 The observed metabolic alteration is independent of GEM concentration and treatment time.

The treatment duration and chemotherapeutic concentration can play a significant role in persister cell metabolism. To assess the effect of the treatment period, A375 cells were treated with GEM (10 x IC_{50}) for 9 days, and the surviving cells were collected for MitoPlate assays, which showed that the consumption rates of Krebs cycle substrates were still higher in GEM-treated cells than in untreated control cells (Figure 2.11a). However, interestingly, the control cells cultured for 9 days had higher consumption rates of Krebs cycle substrates than the control cells cultured for 3 days (control groups in Figure 2.11a-b). This observation might be due to the cell-cycle arrest induced by overpopulation in 9-day cell cultures, which is consistent with our central argument. To assess the effects of drug concentrations on persister metabolism, we isolated persisters by treating

the cells with 100 x IC_{50} GEM for 3 days (Figure 2.11c-d). Similar to the 10 x IC_{50} treatment results, the surviving cells exhibited higher rates of consumption for Krebs cycle substrates than untreated cells (Figure 2.11b and 2.11g-i). Persister cells obtained by 100 x IC_{50} GEM treatment were resuspended for a second round of cell survival and MitoPlate assays, showing that the progenies of persister cells were sensitive to GEM, and the observed metabolic alteration was reversible (Figure 2.11j-l). Persister cells obtained from 100 x IC_{50} GEM treatment were also viable, grew slowly, and exhibited morphological heterogeneity without a consistent trend in the expression of stem cell biomarkers (Figure 2.11c-f), in agreement with the data generated from 10 x IC_{50} treatments. Interestingly, the cells surviving 100 x IC_{50} GEM treatment required ~32 days to resuscitate. This was significantly longer than the resuscitation period of the 10 x IC_{50} treatment group (~9 days), indicating that the resuscitation period is concentration dependent, although increasing the GEM concentration does not affect metabolic alteration.

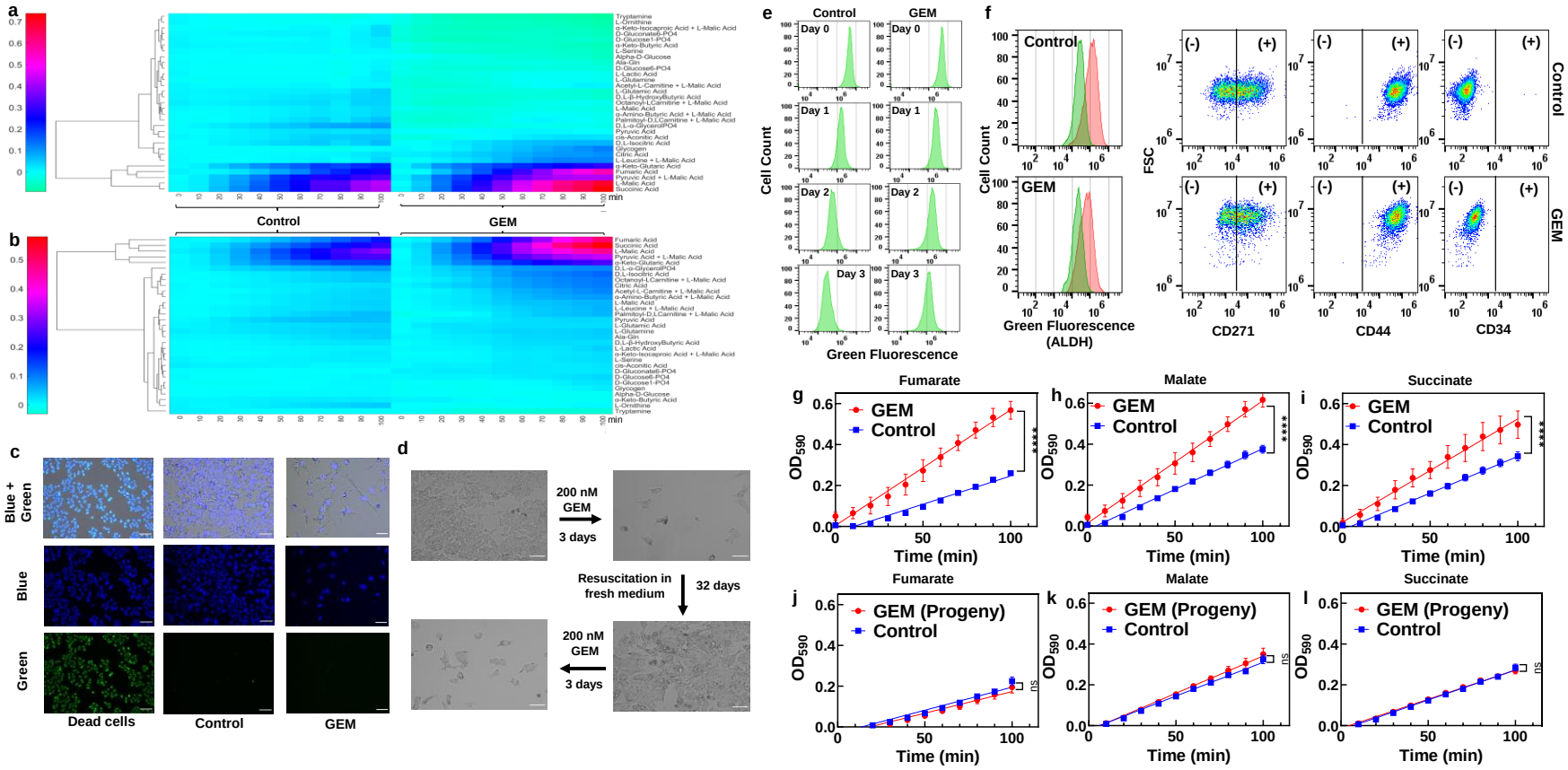

Figure 2.11 Effects of GEM concentration or treatment time on persister metabolism. Linear regression analysis was performed with F statistics using GraphPad Prism (**** P<0.0001). ns: the slopes are not significantly different. N=4.

In figure 2.11, (a-b) A375 cells were treated with GEM (a) at 10 x IC_{50} concentration for 9 days or (b) at 100 x IC_{50} concentration for 3 days, and then, 3 x 10^4 treated cells were transferred to each well of a phenotype microarray that also included a substrate and tetrazolium-based dye. For control, cells were treated with the solvent only. The consumption rates of the substrates were monitored with OD_{590} measurements at the indicated time points (for 100 min total). Unsupervised clustering of absorbance data was performed using MATLAB. N=4. (c) The cells surviving after GEM (100 x IC_{50}=200 nM) treatment were collected and transferred to fresh medium without GEM. The following day, cells were stained with ReadyProbes Cell Viability Imaging dyes to assess live (blue) and dead (green) cells. Dead cells were generated by treating the cells with 70% ethanol for 30 min. "Control" represents the live cells that did not receive GEM treatment. Scale bar: 100 μm. (d) Melanoma cells were treated with GEM (200 nM) for 3 days. After the treatment, cells were allowed to recover in fresh, drug-free growth medium and then treated with GEM (200 nM) again to demonstrate the sensitivity of the daughter cells to GEM. Scale bar: 100 μm. (e) Cells prestained with CFSE dye were treated with GEM (200 nM) or left untreated (control), and their fluorescence intensity was monitored at the indicated time points with flow cytometry. (f) Cells were treated with GEM (200 nM) or left untreated for 3 days. At the end of treatment, the stem cell biomarkers were assessed with an ALDEFLUOR assay and the conjugated antibodies. (g-i) The consumption rates for the selected substrates (4 mM) (fumarate, malate, and succinate) of GEM (200 nM) persisters were measured with the modified MitoPlate assay. (j-l) GEM (200 nM) persister cells were transferred to fresh medium without GEM to stimulate resuscitation. After the third passage, the daughter cells were collected, and their consumption rates for fumarate, malate, and succinate were measured with the modified MitoPlate assay.

2.3.1 Chemotherapeutic-induced metabolic alteration is conserved in melanoma persisters.

Next, we sought to test whether the observed results were also valid for the other chemotherapeutic agents listed in Supp. Table 2.

Table 1: Concentrations of chemotherapeutic agents used for generating persisters.

Chemotherapeutic agents	Classification	IC_{50} (µM)	Working concentration (µM)
Campothecin	Alkaloid	0.01	0.1
Cisplatin	Alkylating agent	13	130
Cytarabine	Antimetabolite	0.5	5
Doxorubicin	Anthracycline antibiotic	0.024	0.24
Etoposide	Alkaloid	6	60
Gemcitabine	Antimetabolite	0.002	0.02
Mitomycin-C	Alkylating agent	0.26	2.6
Paclitaxel	Antimicrotubule agent	0.0147	0.147
Temozolomide	Alkylating agent	272	1360
Vinorelbine	Alkaloid	0.27	2.7

Cytarabine (CYT) is an antimetabolite similar to GEM; camptothecin (CAM), doxorubicin (DOX) and etoposide (ETO) inhibit topoisomerase; cisplatin (CIS) and temozolomide (TEM) are an alkylating agent; vinorelbine (VIN) and paclitaxel (PAC) impair the formation of spindle fibers; and mitomycin-c (MIT) induces cross-linking of DNA [84]. Cells were treated with these therapeutic agents at 10 x IC_{50} doses (Table 1), except TEM, which was applied at 5 x IC_{50}, as the 10 x IC_{50} dose required a high dimethyl sulfoxide (DMSO) solvent content (>1%). A375 cells surviving the chemotherapeutic treatments were collected and transferred to fresh medium without drugs. The following day, cells were stained with ReadyProbes Cell Viability Imaging dyes to assess live (blue) and dead (green) cells. “Control” represents the live cells that did not receive GEM treatment (Figure 2.12). Our data showed that the persister cells retained high cell viability.

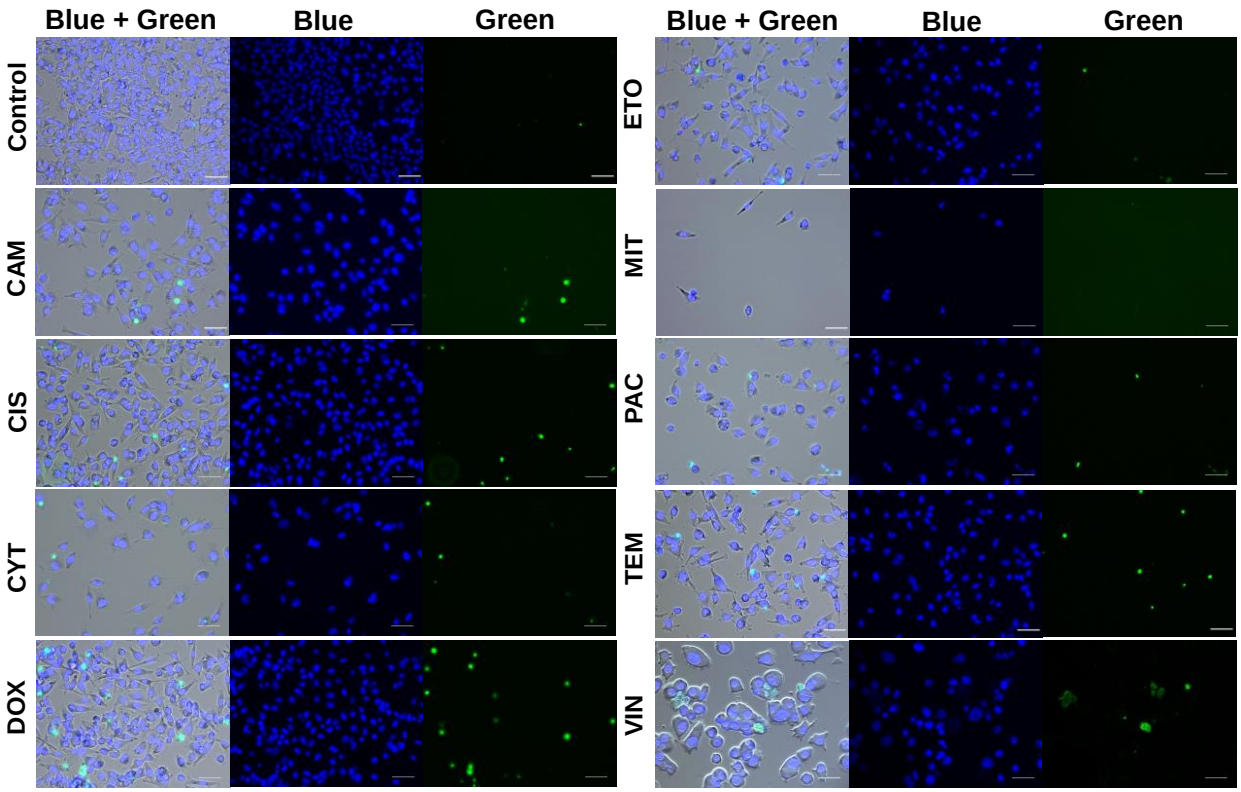

Figure 2.12 Assessing the viability of cells treated with various chemotherapeutic agents. Scale bar: 100 µm**.**

The mitochondrial activity for each treatment was assessed using modified MitoPlate assays. Similar to GEM treatment, cells were treated with the indicated chemotherapeutic agents for 3 days. After treatments, the cells were transferred to a fresh medium and cultured for 24. h. Then, the cells were collected for modified MitoPlate assays to measure the consumption rates of Krebs cycle substrates. Data obtained from mitoplate assay demonstrated that the chemotherapeutic agents generally increased the consumption rates of Krebs cycle substrates in melanoma cells (Figure 2.13).

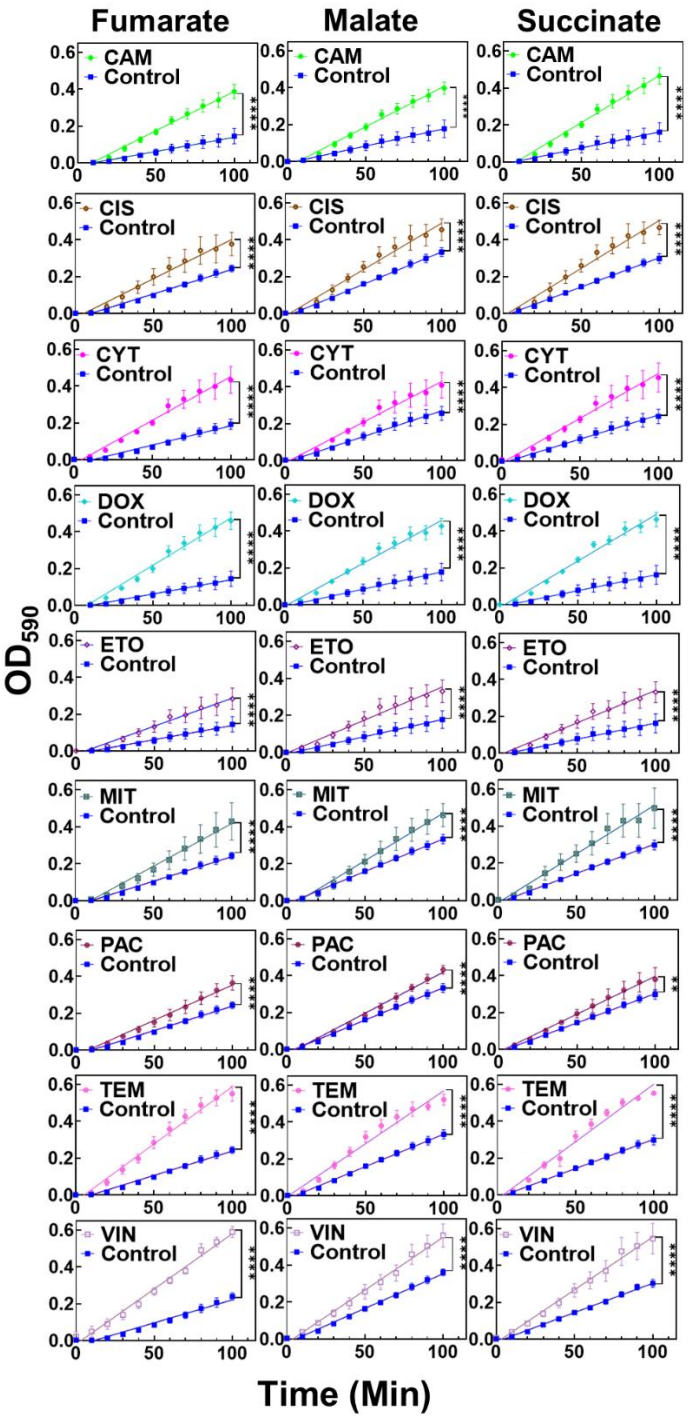

Figure 2.13 Chemotherapeutic treatment enhances krebs cycle activity in melanoma cells. Linear regression analysis was performed using F statistics (**** P<0.0001). N=4**.**

Furthermore, we performed flow cytometer staining assays for stem cell biomarkers for all treatment groups. At the end of treatment, the ALDH activity of the cells was assessed with an

ALDEFLUOR assay and a flow cytometer. Cells treated with the ALDH inhibitor (DAEB) served as negative controls (green). CD271, CD44 and CD34 biomarkers were detected with their respective conjugated antibodies. Cells treated with isotype controls of CD271, CD44 and CD34 were used to determine stem cell biomarker negative (-) and positive (+) cells. Live/dead staining was used to gate the live cells (Figure 2.14). Similar to the results obtained from the GEM treatment, most treatments did not significantly alter cellular stem cell biomarker levels. However, TEM- and MIT-treated cells showed significantly lower ALDH activity than control cells, further supporting that chemotherapeutic persistence may not be directly linked to stem cell phenotypes.

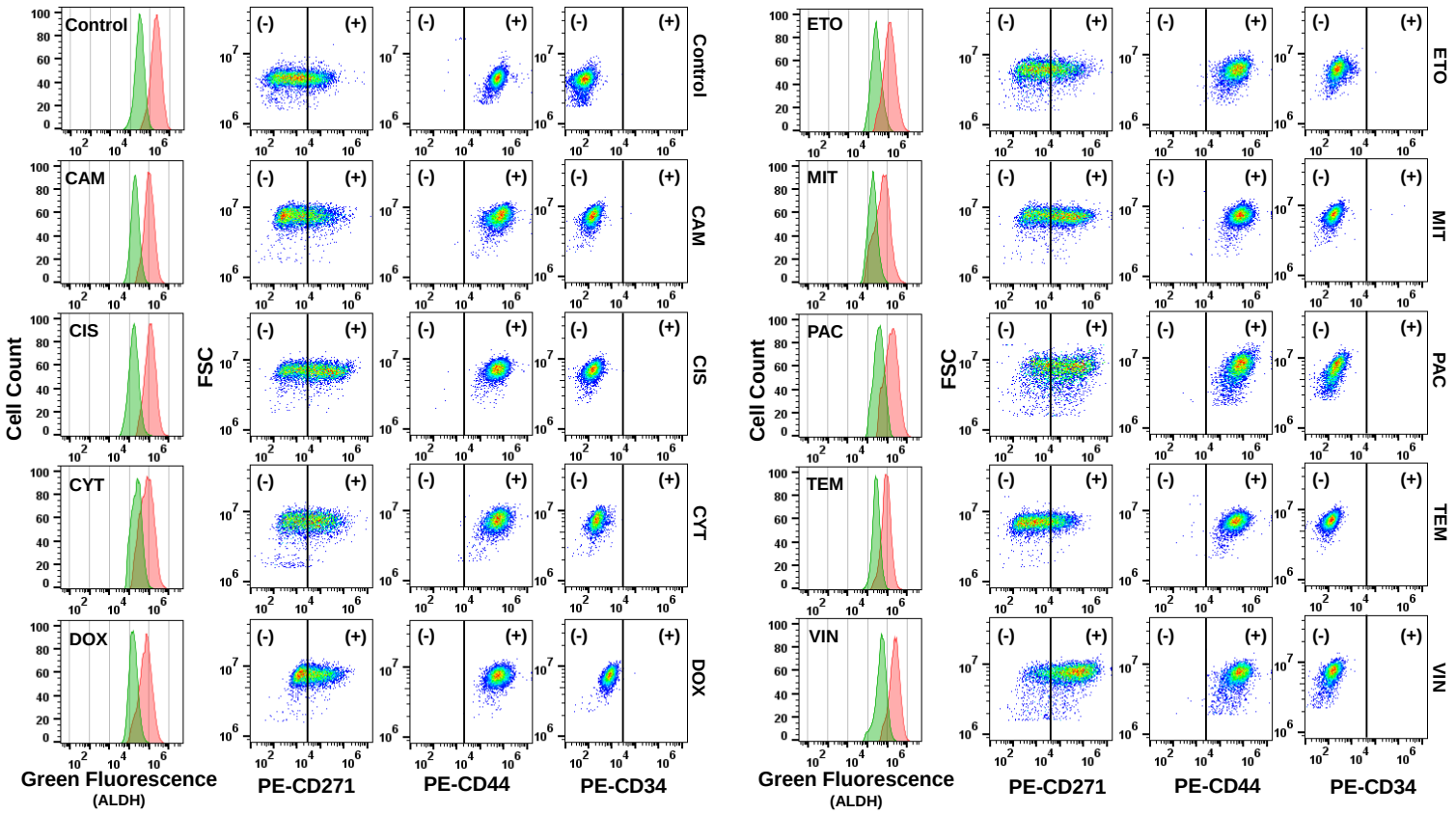

Figure 2.14 Assessing the stem cell biomarkers in A375 persister cells after chemotherapeutic treatments.

Our flow cytometry- and microscopy-based cell proliferation assays with CFSE dye further showed that cells from all treatment groups had undergone a state of negligible growth, indicating that chemotherapeutic-induced growth arrest is conserved in melanoma cells (Figure 2.15 and 2.16).

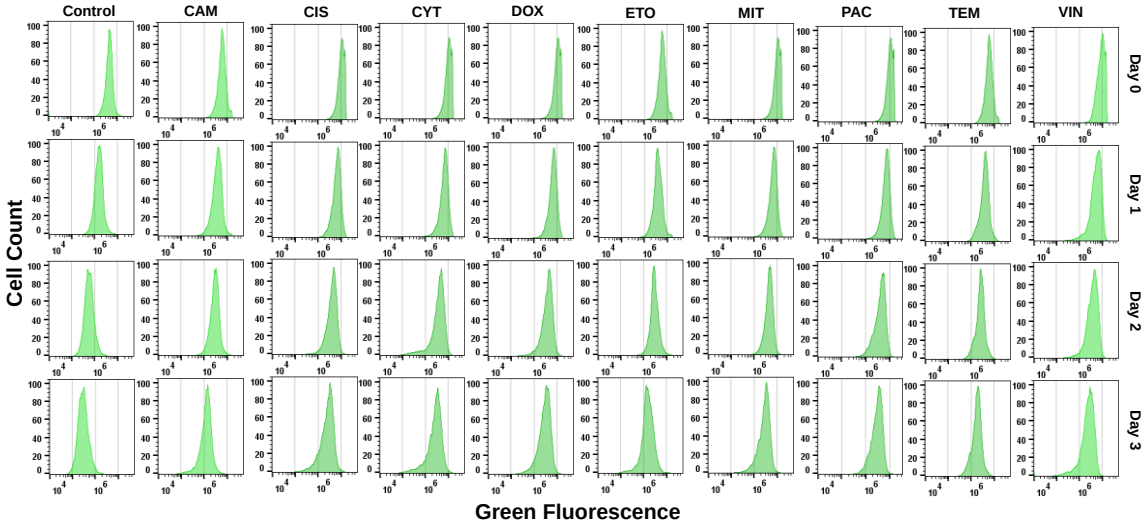

Figure 2.15 Assessing the growth of cells treated with chemotherapeutic agents.

Our microscopy images showed that when compared to the untreated control cells, treated cells had altered morphology with high fluorescence intensity due to the induction of growth arrest (Figure 2.16 vs. control group in Figure 2.3c). Overall, the upregulation of Krebs cycle activity is conserved in melanoma persister populations derived from various chemotherapeutic treatments, despite the diverse morphological changes observed in these persister populations (Figure 2.16 and 2.12).

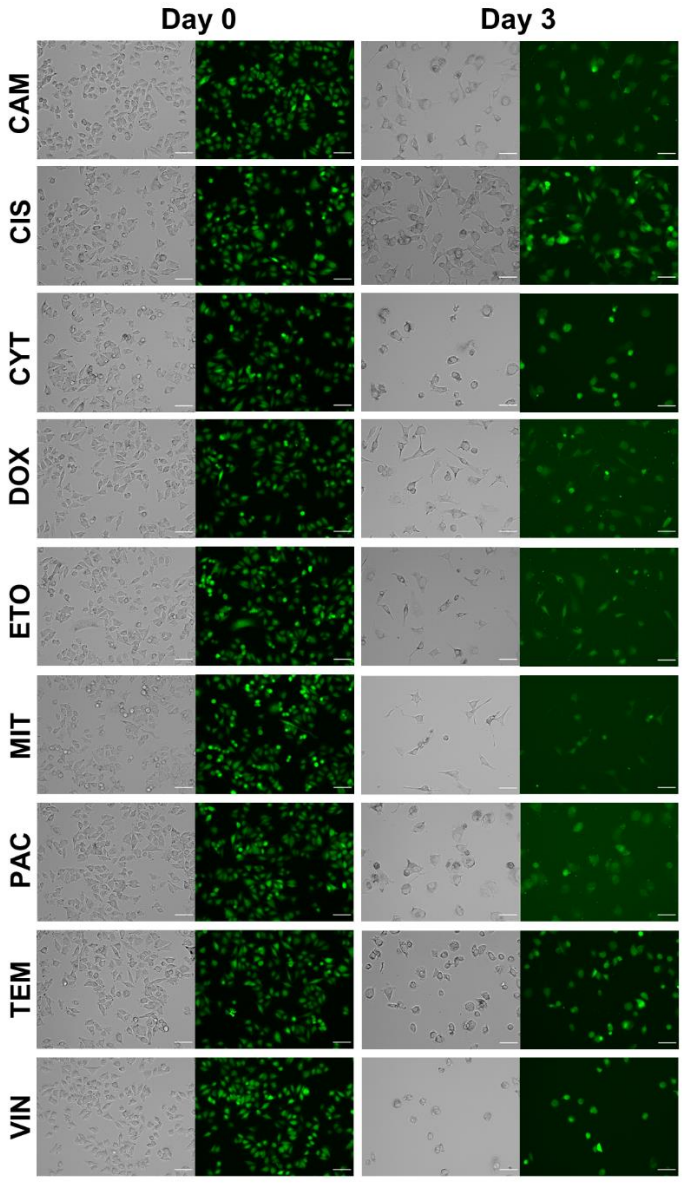

Figure 2.16 Chemotherapeutic drugs morphological changes in persister cells. Scale bar: 100 μm

2.3.2 Phenothiazine drugs can compromise persister survival

We screened a microarray plate (I-1 plates from Biolog, Inc.) with known mitochondrial inhibitors to test the effects of these inhibitors on persister cell viability, as some of these inhibitors, such as gossypol, valinomycin and celastrol, are known to stimulate the production of apoptotic reactive oxygen species [85,86]. The chemical library had four concentrations of each inhibitor, but these concentrations were not disclosed by the company (Biolog, Inc.). As we wanted to identify a

chemical compound that is selectively and effectively lethal to GEM persisters, we focused on the wells with the lowest inhibitor concentrations (Figure 2.17a-b). For this assay, A375 cells incubated in fresh growth medium in a 96-well plate for 24 h were treated with indicated (a) ETC inhibitors (blue) or (b) cotreated with GEM (10x MIC) and ETC inhibitors (red) for 3 days (Figure 2.17). After the treatment, the media in the wells were replaced with fresh, drug-free medium. The cells were incubated in fresh medium for 24 h, and MTT assay was conducted to assess the cell viability.

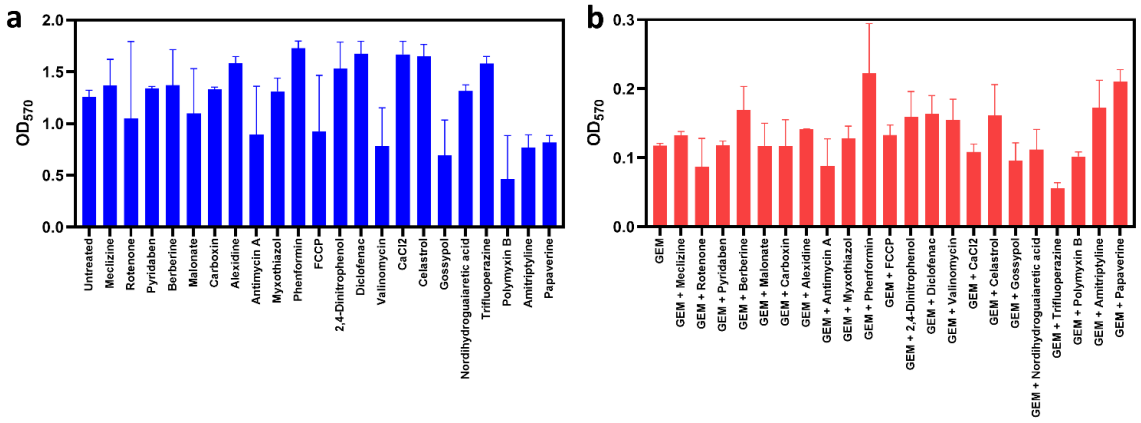

Figure 2.17 High throughput screening of ETC inhibitors. N=2.

Our data revealed that trifluoperazine (TFZ) might be a potential chemotherapeutic adjuvant (Figure 5a-b), although a number of well-known ETC inhibitors, including gossypol, valinomycin, and celastrol, were also found to be effective at higher concentrations (Figure 2.18).

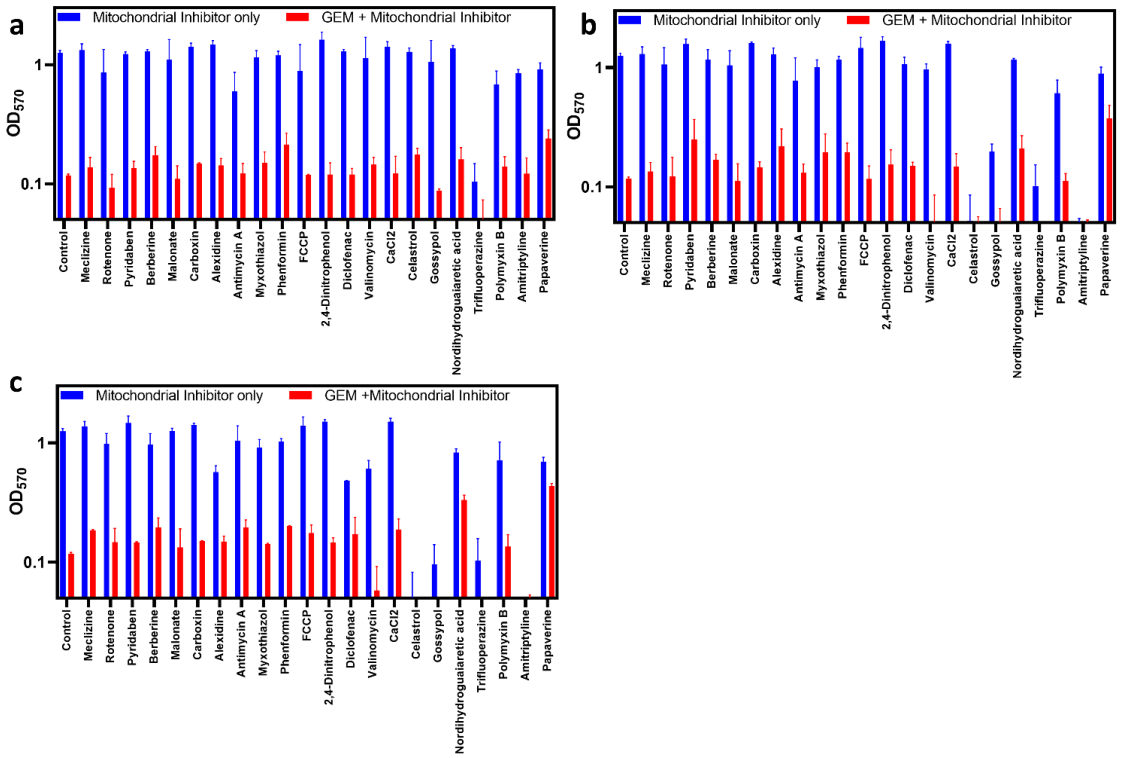

Figure 2.18 Screening for ETC inhibitors that affects persister survival. The graphs represent MTT assay conducted with various concentrations of ETC inhibitors (C): a) C_1, b) C_2 and c) C_3, where $C_1<C_2<C_3$. N=2.

TFZ falls under the class of antipsychotic drugs known as phenothiazines, which have been shown to enhance the cytotoxic effects of chemotherapeutic agents [87]. These drugs have also been shown to inhibit tumor progression by altering the expression levels of proteins related to cell cycle and apoptosis such as CCNE1, CDK4 and BCL-2, and by inhibiting drug efflux pumps [88,89]. To determine whether inhibition of persisters is a more general characteristic of phenothiazines, we tested two additional FDA-approved phenothiazine drugs, thioridazine (TDZ) and fluphenazine (FPZ), which were not in our drug screen. Melanoma cells were treated with phenothiazine drugs (TFZ, TDZ and FPZ) (Figure 2.19a-c) or co-treated with GEM (10xMIC) and phenothiazines (Figure 2.19d-f) at the indicated concentrations for 3 days. After the treatments, the cells were resuspended in fresh drug-free medium and incubated for 24 h. Then, the cell viability was assessed by trypan blue staining using an automated cell counter.

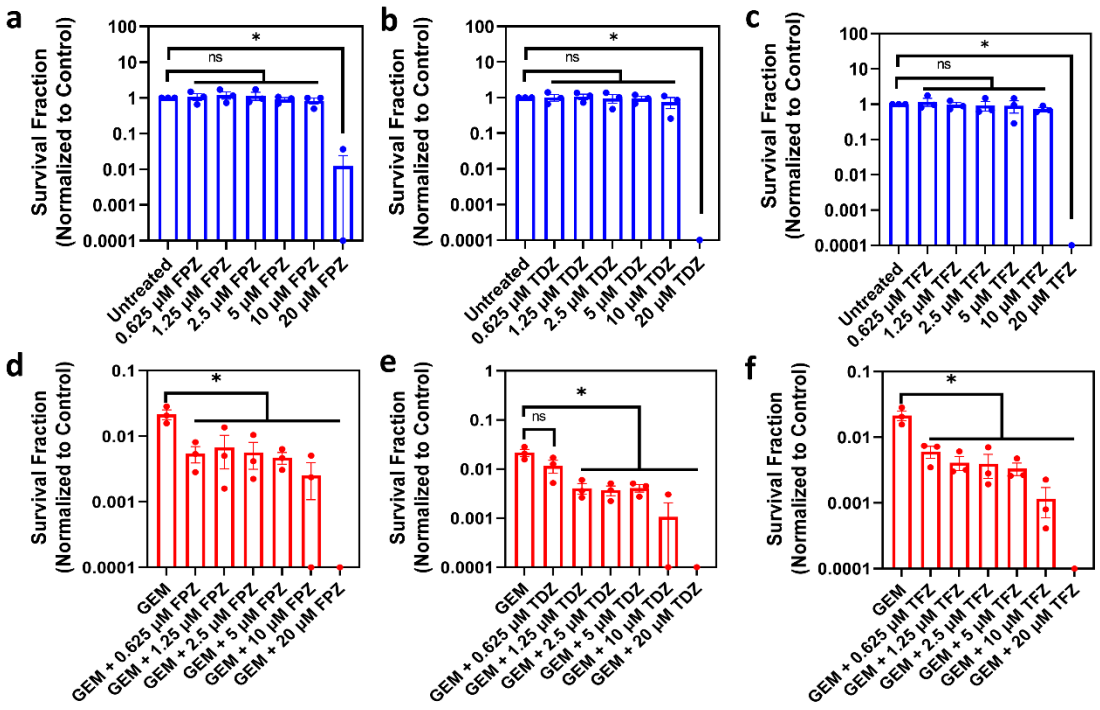

Figure 2.19 Co-treatment with phenothiazines reduces GEM persisters. (a-c) * represents a significant difference between the control and treatment groups (t-test, P<0.05).

Notably, TDZ was recently demonstrated to impair melanoma tumor progression in an animal model [57]. Although all three phenothiazine inhibitors reduced the cell survival fractions across a wide range of concentrations when tested with GEM (Figure 2.19d-f), these inhibitors (at concentrations greater than 10 µM) could also kill the cancer cells in the absence of GEM (Figure 2.19a-c). TFZ was also found to be effective in the presence of most of the chemotherapeutics at the indicated concentrations (Figure 2.20). For this assay, cells were treated with the indicated chemotherapeutic agents and/or TFZ (10 µM) for 3 days. The concentrations of chemotherapeutic agents were 10 x IC_{50}, except TEM, whose concentration was 5 x IC_{50} (see Table 1). After the treatments, the cells were collected and incubated in fresh, drug-free medium for 24 h, and then, the cell viability was assessed with STYO60 (red)/SYTOX (green) dyes using a flow cytometer.

TEM, which is used most often for melanoma patients, has become very effective in the presence of TFZ, as the level of survived cells in cotreatment cultures is around the limit of

detection (Figure 2.20). Although we did not test a wide range of drug concentrations and analyze the synergetic interactions between the drugs in these cotreatments, our results suggest that metabolic inhibitors can potentially boost the effectiveness of the existing chemotherapeutic drugs.

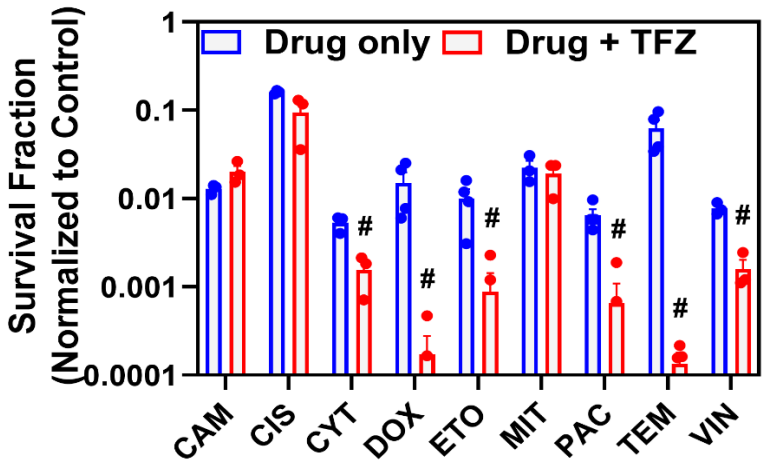

Figure 2.20 Co-treatment with TFZ reduces melanoma persisters. # represents a significant difference between the cotreatment (drug+FPZ) and drug-only groups (t-test, P<0.05).

2.3.3 Chemotherapeutic-induced metabolic alteration is also observed in a metastatic cell line (RPMI-7951)

Finally, we used a metastatic melanoma cell line (RPMI-7951) to assess if the observed metabolic alteration is a global response of melanoma cells to chemotherapeutic treatments. RPMI-7951 cells were treated with GEM (10 x IC_{50}), TEM (5 x IC_{50}) or left untreated for 3 days, and mitoplate assays were performed following the methods described above. Similar to A375 cells, RPMI-7951 cells treated with chemotherapeutics have significantly increased consumption rates of Krebs-cycle substrates (fumarate, malate and succinate) when compared to untreated control groups (Figure 2.21a-f). Furthermore, we co-treated RPMI-7951 cells with TEM and an ETC inhibitor (TFZ) to test the impact of ETC inhibition on RPMI-7951 persistence as described in sections 2.3.2 and 2.1.13. We chose TEM for the co-treatment study as it is one of the preferred chemotherapeutic agents for metastasized melanoma treatments [48]. As expected, our data shows

that co-treated cultures have reduced persister survival compared to the cultures treated with TEM only (Figure 2.21g-h). This observation further shows that targeting the metabolism of drug-tolerant cells can be an effective therapeutic strategy for melanoma cancers.

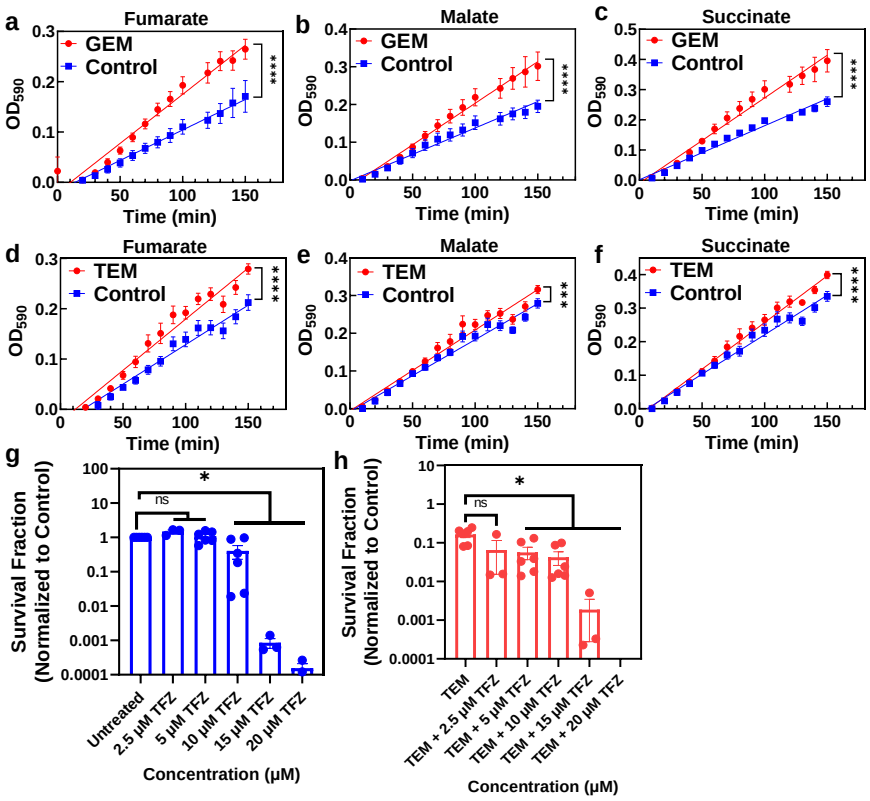

Figure 2.21 Increased consumption of TCA cycle substrates is observed in the RPMI-7951 cell line. Linear regression analysis was performed using F statistics using GraphPad Prism (**** P<0.0001). * represents a significant difference between the control and treatment groups (t-test, P<0.05).

2.4 Discussion

Conventional chemotherapeutic agents target fast-growing cells such as tumor cells. Because of their slow or no-growth state, persister cell tolerance to treatment has been attributed to cell dormancy [32]. Cancer cell dormancy can be induced by various mechanisms, such as the activation of signaling pathways for autophagy, reactive oxygen species production, and DNA damage repair, that are generally triggered by extracellular stress (e.g., nutrient depletion, hypoxia, overpopulation, therapeutics) [90,91]. Cell dormancy is regulated by many external and internal factors via a highly

integrated signaling network and is one of the most common phenotypic states observed in many drug-tolerant cell types. Due to their phenotypic plasticity, melanoma cells may acquire stem cell like characteristics in response to treatments, which may contribute to melanoma cell heterogeneity and drug tolerance. Although persister cells in previous studies were shown to have increased stem cell biomarkers [32,92], we did not observe a drastic change in the expression levels of known stem cell biomarkers in GEM persisters. Our results also indicate that chemotherapeutics may facilitate a transient dormancy, which may lead to the downregulation of anabolic pathways (due to the observed growth arrest), thus diverting glycolytic intermediates to the Krebs cycle, the most efficient energy-producing pathway. This also explains why the abundance of glycolytic metabolites was not altered in persister cells despite the significant alterations in the abundance of Krebs cycle metabolites.

In this study, we first conducted untargeted metabolomics analysis to identify the metabolic pathways that were significantly altered in GEM-treated persister cells compared to control cells. These pathways included the lipid metabolism, BCAA metabolism, one-carbon metabolism, and the Krebs cycle and the PPP. From the lipid superpathways, the levels of phosphatidylcholines, sphingosines, ceramides and lysophospholipids were primarily upregulated in GEM-treated cells. The accumulation of PC due to overexpression of lysophosphatidylcholine acyltransferase 2 (LPCAT2) can induce drug tolerance in cancer cells, as reported by Cotte et al. [93]. The study revealed that LPCAT2 increases the resistance of cancer cells to immunogenic cell death and mediates chemoresistance by promoting the antiapoptotic response to endoplasmic reticulum stressors [93]. Ceramides have been reported to have dual functions in drug resistance. They can induce either chemosensitivity or chemoresistance depending on the structure and length of their fatty acyl chains [94].

BCAA metabolism, which involves essential amino acids, such as valine, leucine and isoleucine, has been studied extensively in cancer cells [95]. It is closely linked to the Krebs cycle, as

alpha-ketoglutarate is needed to initiate the degradation of valine, isoleucine and leucine [95]. Enzymes that catalyze the first step of BCAA degradation, branched-chain aminotransferase 1 (BCAT1) and branched-chain aminotransferase 2 (BCAT2), are commonly upregulated in cancer cells. BCAT1 in particular is associated with cancer cell growth and has been proposed as a prognostic cell marker [95,96]. In addition, many studies have explored BCAT1 as a potential target for cancer therapeutics, as it is also linked to cell proliferation via m-Torc1 activity [97]. BCAA metabolism has been shown to alter gene expression in cancer cells by altering the epigenome. Epigenetic changes can affect several cellular processes that can induce drug tolerance in cancer cells. A recent study by Wang et al. showed that H3K9 demethylation-mediated epigenetic upregulation of BCAT1 can promote tyrosine kinase inhibitor (TKI) tolerance in epidermal growth factor receptor (EGFR)-mutant lung cancer cells [98].

The upstream metabolites of the Krebs cycle are needed for the initiation of PPP metabolism. Along with one-carbon metabolism, the PPP regulates NADPH production in cancer cells [99]. Additionally, it has been hypothesized that slow-growing/drug tolerant cells have an increased rate of PPP metabolism compared to the bulk cancer cell population [100]. Debeb et al. showed that PPP metabolism is upregulated in histone deacetylase inhibitor-induced cancer stem cells and is regulated by an increase in the level of glucose-6-phosphate dehydrogenase (G6PD), a rate-limiting enzyme in PPP metabolism [101].

DNA repair proteins (e.g. DNA double-strand-break repair proteins) have a major role in metabolic reprogramming of persister cells and mediating their responses to chemo- and radiotherapy [102,103]. The study conducted by Cosentino et al., 2011, showed that ATM, a key DNA damage protein, regulates PPP via induction of G6PD to promote NADPH and nucleotide production needed for the DNA damage repair [104]. Phosphorylated ATM also enhances mitochondrial respiration and oxidative phosphorylation by increasing the expression of cytochrome c oxidase 2 and glutaminase

[105–107]. These metabolic alterations, particularly in mitochondria, could enhance the toxicity of chemotherapeutic agents.

Given that MS does not directly measure intracellular reaction rates, subsequent assays are necessary to link the abundance of metabolites to their turnover rates. Our metabolomics data show that the majority of Krebs cycle metabolites were significantly downregulated in GEM-treated cells due to their increased consumption rates, and these findings were verified by MitoPlate assays. It is known that cancer cells prefer aerobic glycolysis; however, as persisters are slow-growing cells, they might not depend on aerobic glycolysis as extensively. The increased mitochondrial metabolism of drug-tolerant cells has been reported across multiple tumor cell lines and in response to a variety of therapeutic challenges [38,57,108], supporting our hypothesis of a conserved, transient metabolic phenomenon mediated by chemotherapeutic treatments. Given that increased mitochondrial metabolism is a potentially conserved characteristic of melanoma persistence, ETC inhibitors can be used as adjuvants for persister therapeutics. Although not all ETC inhibitors can be potent and cytotoxic, our findings show that TFZ was highly effective against TEM-tolerant cells. As TEM is a preferred chemotherapeutic agent for the treatment of metastasized melanoma cancers, a co-treatment regime including TEM and an ETC inhibitor can have a potential clinical application. These findings further highlight the significance of understanding and targeting the key metabolic changes in drug-tolerant persister cells.

It is well established that suppression or lack of apoptosis is one of the major factors that increases chemo-resistance [63,109]. There are several studies claiming that alterations in certain Bcl-2 family members (e.g. Bcl-2 and Bcl-xL expression level) contribute to multidrug resistance [110,111]. Persister cells can escape apoptosis and drug cytotoxicity via transient metabolic alterations. However, how these alterations affect apoptotic pathways and consequently cancer persistence remains to be characterized. Finally, we would like to point out that our study has been conducted in vitro in a controlled environment; therefore, in vivo factors such as cell-cell interactions, micro-

environment in the host, treatment regimens and drug clearance may impact persister cell metabolism. Our future goal is to characterize the metabolic state of persister cells in clinically relevant samples or environments, such as patient-derived tissues and animal models.

In this study, we aimed to evaluate the role of metabolism in melanoma persister cells and the utility of targeting persister cell metabolism as a therapeutic strategy. Melanoma which is the most fatal form of skin cancer is thought to be a chemotherapy-resistant cancer type, and this resistance is potentially facilitated by slow-growing persister cells. Our analysis shows that chemotherapeutic agents can facilitate persister cell formation in melanoma cells and alter cellular metabolism by upregulating the utilization rates of Krebs cycle metabolites. The observed metabolic alteration seems to be independent of drug concentration and treatment time and can be mediated by a wide range of chemotherapeutic agents.

Chapter 3 BRAF-Inhibitor-Induced Metabolic Alterations in A375 Melanoma Cells

Drug tolerance has also been observed as a heterogeneous trait in cancer cells[31]. A sub-population, known as persister cells, have been shown to acquire a transient drug-tolerant state in cancer cell populations [31]. These persisters cells, which are described as slow-cycling cells [33], can act as a reservoir for the emergence of multi-drug resistant mutants and contribute to cancer relapse [112]. Recent evidence shows that persisters have unique metabolic profiles compared to the bulk cancer population.[32,57] In our previous study, we explored the impacts of conventional chemotherapeutics (cytotoxic medications) on persister metabolism and found that chemotherapeutics induce a transient shift from aerobic glycolysis to oxidative phosphorylation [34].

When it comes to targeted therapeutics, melanoma persister cells are generally derived by co-treatment with BRAF/MEK inhibitors [57], making it unclear how persister metabolism is affected by each drug, individually. In this study, with the use of untargeted metabolomics, high-throughput assays (phenotype microarrays), and enzymatic measurements of glucose and lactate levels, we explored BRAF inhibitor-induced persister metabolism. Our integrated approach allowed us to identify energy sources/substrates that are selectively preferred by vemurafenib persisters.

3.1 Materials and Methods:

3.1.1 Cell culture conditions

The melanoma A375 cell line was purchased from American Type Culture Collection (ATCC) (Manassas, VA). If not otherwise specified, all materials were obtained from Fisher Scientific (Waltham, MA). Melanoma cells were cultured in Dulbecco's modified Eagle's medium (DMEM) supplemented with 10% fetal bovine serum (FBS), 100 units penicillin and 100 µg streptomycin/mL. Cells were cultured in a humidified incubator at 37ºC and 5% CO_2. Phenotype microarray plates and assay solutions were purchased from Biolog, Inc. (Hayward, CA). PE-

conjugated antibodies [CD271 (catalog# 557196), CD44 (catalog# 555479), or CD34 (555822)] and their IgG isotype controls were obtained from BD science (San Jose, CA). The ALDEFLUOR assay kit was obtained from STEMCELL Technologies (Cambridge, MA). BRAF inhibitor, vemurafenib (VEM), was dissolved in dimethylsulfoxide (DMSO) to prepare stock solutions.

3.1.2 Generating persister kill curves

To generate biphasic kill curves, 3 x 10^5 cells were seeded in each well of a 6-well plate. The cells were maintained in 3 ml of DMEM for 24 h in a humidified incubator at 37ºC and 5% CO_2. After 24h, the medium was removed and replaced with fresh medium with varying concentrations of VEM. After treating the cells with VEM for 3 days, the surviving cells were washed with 3 ml of Dulbecco's phosphate-buffered saline (DPBS) two times. The cells were detached with 300 µl of trypsin-EDTA (0.25% trypsin and 0.9 mM EDTA), and then collected in 1.5-ml microcentrifuge tubes after adding 1 ml of DMEM which deactivates the trypsin. The cell suspension was centrifuged at 900 revolutions per minute (rpm) for 5 mins and the supernatant was removed. The cell pellet was then re-suspended in fresh DMEM, and live cells were quantified with trypan blue staining [61] using an automated cell counter (catalog# A27977, Thermo Fisher Scientific). The survival ratio was calculated by normalizing the cell count with the total number of cells in the untreated control group. Finally, the survival ratios and drug concentrations were plotted to generate the kill curves.

3.1.3 Isolating persister cells

Approximately 2.5 x 10^6 cells were transferred to 15 ml of DMEM in a T-75 flask. The cells were cultured for 24 h in a humidified incubator maintained at 37°C and 5 % CO_2. After 24 h, the medium was replaced with fresh medium containing 10 µM VEM. After treating the cells with VEM for 3 days, the cells were washed with 10 ml of DPBS two times and detached from the flasks with 2 ml of trypsin-EDTA. Then, 5 ml of DMEM was added to deactivate the trypsin and the cells were centrifuged at 900 rpm for 5 mins. The supernatant was removed, and the cells were

resuspended in fresh DMEM and transferred to a T-75 flask. The cells were further incubated at 37°C in the presence of 5 % CO_2 for 24 h to remove dying/dead cells as they cannot adhere to the flask surface. Following the incubation, the supernatant with dead cells was discarded, and the live cells were detached and collected for the experiments described below. The control group (untreated cells) has undergone the same procedure, receiving the solvent-only (DMSO) treatment.

3.1.4 Assessing the cell viability with microscopy

The viability of cells after VEM treatment was assessed with the ReadyProbes Cell Viability Imaging kit (Blue/Green) (catalog# R37609, Thermo Fisher Scientific) as described by the vendor's protocol as well as in Chapter 2 section 2.1.3.

3.1.5 Apoptosis assay

The annexin-V FITC/PI kit (catalog# P50-929-7; Thermo Fisher Scientific) was used to detect apoptotic cells in VEM treated and untreated cultures, as described in our previous study [34] and in Chapter 2 Section 2.1.4.

3.1.6 Clonogenic survival assay

Cells surviving the VEM treatment were serially diluted by transferring 1 ml of the cell suspension to a 15 ml centrifuge tube containing 9 ml of fresh growth medium (*i.e.*, a 10-fold serial dilution). Then, 3 ml diluted cell suspensions were transferred to the wells of a 6-well plate. The cells were cultured for 12 days for colony formation while replacing the growth medium every 3-4 days. After 12 days, the growth medium was removed, and the cells were washed with 3 ml of DPBS. The cells were then fixed with 1 ml of fixing agent (methanol: acetic acid at 3:1) for 5 mins. After fixing the cells, the cells were stained with crystal violet (0.5%) for 15 mins to visualize and to count the colonies.

3.1.7 Cell count with a flow cytometer

After VEM treatment, the live cells were collected and washed with DPBS twice and resuspended DPBS. Cell viability and enumeration was then performed using SYTOX Green/STYO60 dyes following the method described in Chapter 2 Section 2.1.13. SYTOX green is cell-impermeant and can only diffuse through dead cell membrane while SYTO60 is cell-permeant and can freely diffuse through both live and dead cell membrane. Untreated and ethanol-treated dead cells were used as negative and positive controls.

3.1.8 Cancer stem cell markers

Cells during VEM treatment in flasks were detached and collected at desired time points and centrifuged at 900 rpm for 5 mins. CSCs marker expression was then measured using of PE-conjugated antibodies [CD271 (catalog# 557196), CD44 (catalog# 555479), or CD34 (555822); BD Biosciences, San Jose, CA] following the method described in Chapter 2 section 2.1.11.

3.1.9 ALDEFLUOR assay

At desired time points, cells during VEM treatment were detached, collected, and centrifuged at 900 rpm for 5 mins. The supernatant was removed, and the cell pellet was washed with 5 ml of DPBS. The cells were then resuspended in ALDEFLUOR to perform the ALDEFLUOR assay as described in the Chapter 2 section 2.1.10.

3.1.10 Cell proliferation assay

Cell proliferation assay was conducted with the CellTrace proliferation kit (catalog# C34570, Thermo Fisher Scientific) following the protocol provided by the vendor as well as described in Chapter 2 section 2.1.8.

3.1.11 Metabolomics

Cells were treated with VEM in T-75 flasks for 3 days. After 3 days, the surviving cells were collected, washed with 5 ml of DPBS twice and pooled in a 1.5 ml micro centrifuge tube. The

final cell pellet volume for each group was ~100 µl. The cell pellet was first flash frozen in a dry ice/ethanol bath, and then, stored in -80ºC before shipping the sample to Metabolon, Inc. (Morrisville, NC). Cells treated with solvent (DMSO) only were used as a control group. Metabolomics study including sample extraction, instrumentation and initial data analysis was conducted according to Metabolon's protocols [65]. The MS data were normalized to the protein concentration (assessed by Bradford assay). The normalized data were used for unsupervised hierarchical clustering with the Clustergram function of MATLAB. ANOVA test was used for pairwise comparisons ($P < 0.05$), and a Q-value for each metabolite was assessed to estimate the false discovery rate [65]. Enrichment analysis was performed using overrepresentation analysis (ORA) algorithm of MetaboAnalyst [113]. The metabolites that were significantly different in VEM persisters compared to those in the control group were clustered into two groups: upregulated and downregulated metabolites. The list of compound names (human metabolome database ID) for each group was used as an input for the enrichment analysis, which is based on several libraries containing ~9,000 biologically meaningful metabolite sets. ORA uses hypergeometric test to evaluate if a specific metabolite set or pathway is truly (not by chance) represented within the input list. Finally, the results were provided as dot plots, where the size of the circle represents the Enrichment Ratio (observed hits/predicted) and the color represents the P-value for each metabolite set [114].

3.1.12 Mitoplate assays

After VEM treatment, the cells were collected, resuspended in a fresh drug-free growth medium, and incubated for 24 h. After incubation, the cells were collected, and washed with DPBS twice. The mitochondrial activities of the cells were then assessed following the mitoplate assay as described in Chapter 2 section 2.1.6.

3.1.13 PM-M1 assays

PM-M1 assays were performed using a protocol provided by Biolog, Inc. [115]. After VEM treatment, the cells were collected, resuspended in a fresh drug-free growth medium, and incubated for 24 h. At 24 h, cells were washed with 5 ml of DPBS twice. The cell pellet was resuspended in Biolog IF-M1 medium (catalog# 72301, Biolog, Inc.) supplemented with penicillin/streptomycin, 5% FBS and 0.3 mM glutamine to obtain a cell density of 4 x 10^5 cells per ml. Then, 50 µl of cell suspension was transferred to each well of the PM-M1 plate and incubated at 37 °C for 48 h. At desired time points (t=0, 24h, 48h), 10 µl of tetrazolium-based dye (catalog# 74352, Biolog, Inc.), was added to each well of the PM-M1 plate and incubated for 8 h. The rate of dye reduction was evaluated by measuring absorbance at 590 nm (OD_{590}) every 30 mins. The absorbance readings are subtracted by the baseline (*i.e.*, initial absorbance at t= 0 min) to determine the absolute absorbance change for each substrate. These data are then normalized by subtracting control (glutamine only) measurements.

3.1.14 Glucose and lactate consumption assay

After VEM treatment, cells were collected and resuspended in Biolog IF-M1 medium (catalog# 72301, Biolog, Inc.) supplemented with penicillin/streptomycin, 5% FBS, and 0.3 mM glutamine. When indicated, 4 mM sodium lactate and/or 4 mM glucose were added in the cell suspension. The cell density was adjusted to 4 x 10^5 cells per ml. Then, 500 µl of the cell suspension was transferred to each well of 24-well plate and incubated at 37°C. At desired time points (t= 24 h and 48 h), the cell suspension was removed, centrifuged at 900 rpm for 5 mins, and the supernatant was transferred to 1.5 mL microcentrifuge tube. The glucose and lactate concentrations in samples and standard solutions were measured using glucose colorimetric detection kit (catalog# EIAGLUC, Thermo Fisher Scientific) and lactate assay kit (catalog# MAK064-1KT, Sigma Aldrich) following the vendor's protocol. For the lactate assay, the supernatant was deproteinized with a 10 kDa MWCO spin filter. This additional step was needed as the presence of lactate

dehydrogenase can degrade lactate and interfere with the readings. Standard curves were used to calculate the amount of glucose or lactic acid consumed by the cells daily. The data were then normalized by the number of cells.

3.1.15 Viability assay in minimal medium

After VEM treatment, cells were collected and resuspended in Biolog IF-M1 medium (catalog# 72301) supplemented with penicillin/streptomycin, 5% FBS, and 0.3 mM glutamine. The cell density was adjusted to 4 x 10^5 cells per ml. The cell suspension was further supplemented with 4 mM glucose and/or 4 mM sodium lactate. Then, 500 µL of the cell suspension was transferred to each well of a 24-well plate and incubated at 37°C. At t= 48 h, the cells were collected and resuspended in 500 µL of DPBS. The cells were stained with 0.25 µM SYTOX green and SYTO60 red and incubated for 15 mins at room temperature. Finally, the cells were transferred to a 5 mL test tube and analyzed with a flow cytometer to measure green (excitation: 488 nm/emission: 520 nm) and red (excitation: 561 nm/emission: 586 nm) fluorescence. The live and dead cells were separated based on their fluorescence intensity and the number of live cells were enumerated by the flow cytometer.

3.1.16 Statistical analysis

Unequal variance t-test or ANOVA was used for pairwise comparisons ($P < 0.05$). For PM-M1 assays, substrates whose absorbance was found to be higher than that of no-substrate control were selected for linear regression analysis. The slopes of untreated and treated groups for the selected substrates were compared with F statistics using GraphPad Prism 8.3.0, and the threshold of significance was set to $P < 0.05$. A minimum of three independent biological replicates were performed, and data points in figures denote the mean value ± standard error.

3.2 Results

3.2.1 Vemurafenib persister cells are slow-cycling cells that are reversibly drug-tolerant.

Drug-tolerant persister cells were generated by treating A375 cells with vemurafenib (VEM) (Figure 3.1). VEM, which is commonly used as a targeted therapy for melanoma with the BRAF V600E positive mutation, is a competitive inhibitor of the mutated BRAF protein [116]. To generate a kill curve (survival ratio vs. VEM concentration) (Figure 3.1), we treated A375 cells with VEM at indicated concentrations for 3 days. After treatment, surviving cells were collected for assessing their viability with trypan blue staining. The survival fraction was calculated by normalizing the number of live cells in the treatment culture with the total number of cells in the untreated control group.

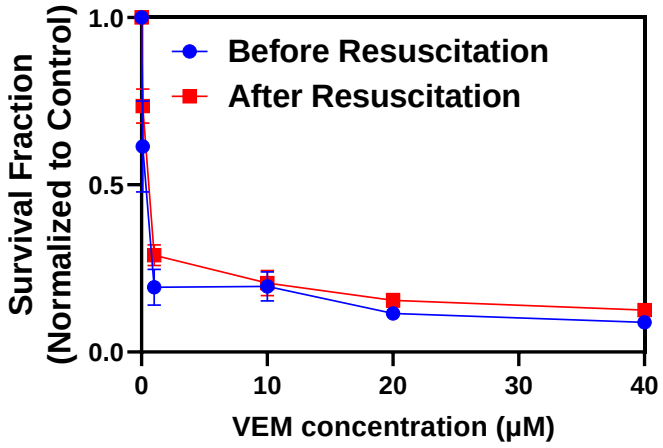

Figure 3.1 Biphasic kill curves shows that a small fraction of cancer cells can survive drug treatment. Number of biological replicates (N) = 4.

The data shows that the half maximal inhibitory concentration (IC_{50}) of VEM for A375 cells was ~100 nM, and the treatment concentration higher than 10 x IC_{50} did not significantly affect the persister ratio (*i.e.*, cell survival ratio) [34]. As persisters survive high concentrations of drugs, persister cells were isolated by treating A375 cells with VEM at 100 x IC_{50} concentration for 3 days, consistent with previous studies [34,60,98]. After treatment, the cells were cultured in fresh, drug-free growth medium for 24 h to remove dead/apoptotic cells. The cell viability imaging assay

and fluorescence microscopy were used to validate that the isolated persisters were viable cells (Figure 3.2a). Furthermore, the annexin-V apoptosis assay was used to quantify the apoptotic cells in our samples [63].

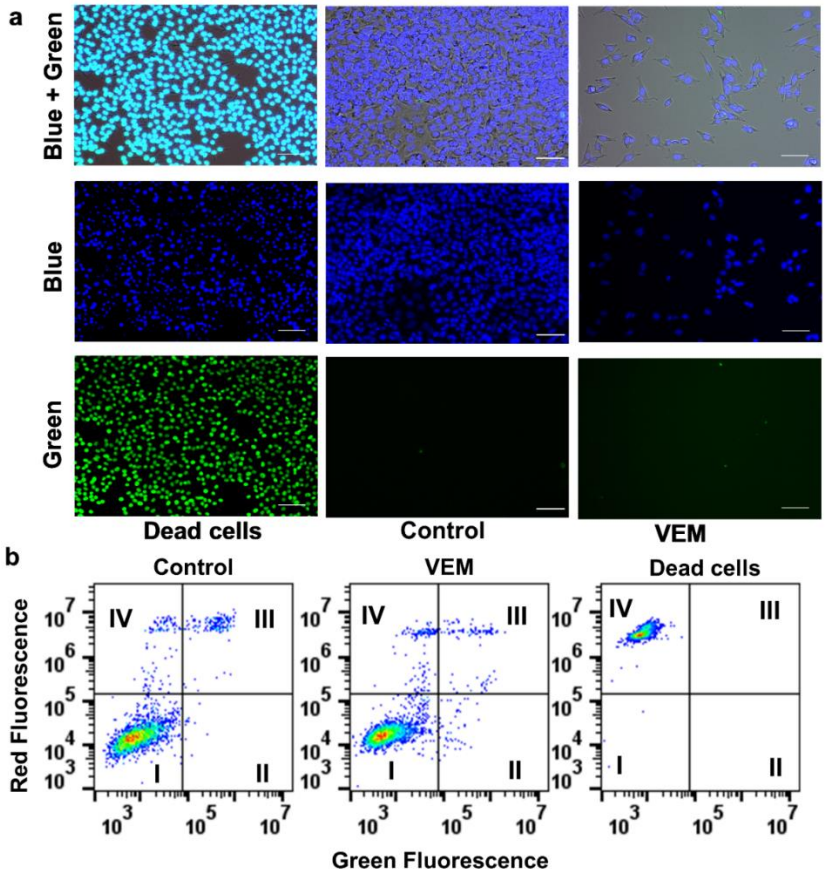

Figure 3.2 Persisters are live and viable cells. Dead cells were generated by treating the cells with 70% ethanol for 30 min. "Control" represents the live cells that did not receive VEM treatment.

For the apoptosis assay, A375 cells after VEM treatment were collected and cultured in a fresh, drug-free growth medium for 24 h. Then, cells were stained with annexin-V/ Fluorescein Isothiocyanate (FITC) conjugate and Propidium Iodide (PI). Of note, PI is a membrane impermeant dye that can only penetrate the damaged, permeable membranes of dead cells. During the early stages of apoptosis, phosphatidylserine (PS) is exposed towards the outer leaflets of the cell membrane, which has high specificity towards annexin-V in the presence of calcium [62]. The cell populations were gated to represent (I) live (FITC-/PI-), (II) early apoptotic (FITC+/PI-), (III) late

apoptotic (FITC+/PI+) and (IV) dead (FITC-/PI+) cells. Our analysis showed that the isolated persister cells are not apoptotic (Figure 3.2b).

Since persister cells are reversibly tolerant to treatments, we re-cultured these cells in a fresh medium and treated the daughter cells (*i.e*., progenies) with VEM (Figure 3.1). As expected, the progenies of the persister cells were sensitive to VEM treatment. Cell viability assay was performed STYO60/SYTOX green staining as described in section 2.1.13. We also conducted clonogenic survival assays (CSAs) to assess the persister cells' colonization capability (section 3.1.6) and used live/dead cell fluorescent probes and flow cytometry to quantify persister cells after removal of drug. The data show that persister and colony counts were not significantly different (Figure 3.3), verifying that persister cells largely colonized upon removal of VEM.

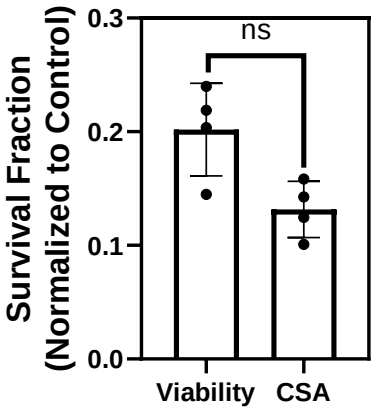

Figure 3.3 Persister cells are capable of resuscitating in drug free environment. ns: not significant (t-test, $P<0.05$). N= 4.

As persister cells are described as slow-cycling cells, we performed cell proliferation analysis with carboxyfluorescein succinimidyl ester (CFSE), a fluorescent dye which can readily diffuse through cell membranes and produce a stable fluorescent signal [117]. The cells were stained with the dye and cultured for 3 days either in the presence or absence of VEM. The cell proliferation was assessed for treated and untreated groups by monitoring the dilution of the fluorescent signal with flow cytometry. As expected, our flow cytometry analysis shows that the VEM-treated

cultures retained a higher signal of fluorescence compared to the untreated control group (Figure 3.4a). Furthermore, we imaged CFSE loaded cells before and after treatment with fluorescence microscopy (Figure 3.4b), demonstrating that the VEM-treated cells underwent morphological changes, and retained higher green fluorescence compared to the untreated control.

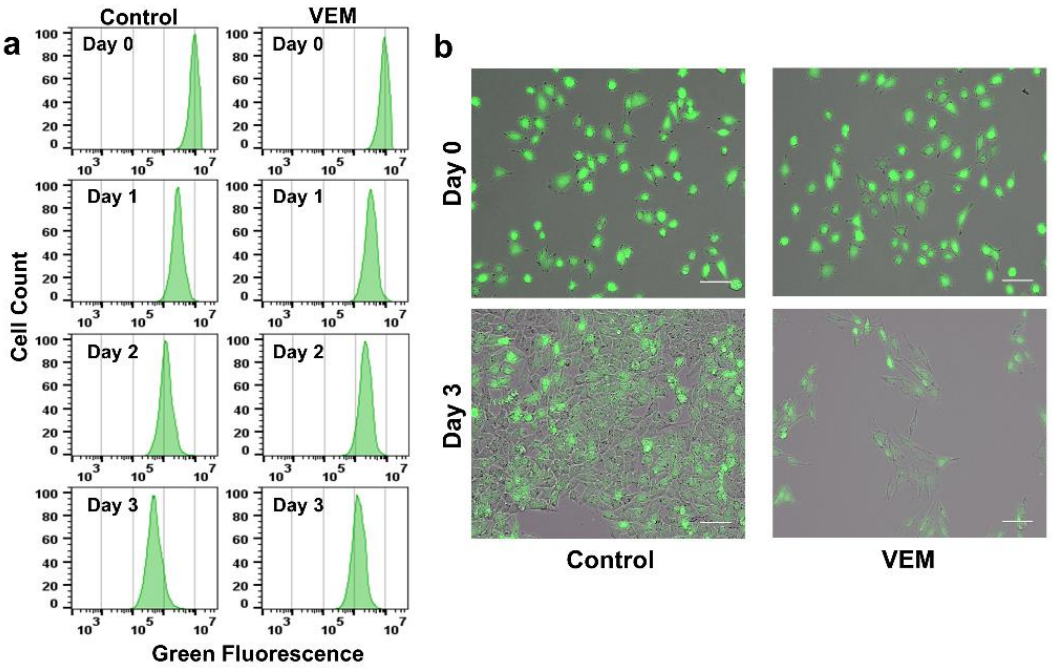

Figure 3.4 Persisters are slow growing cells. N = 4.

This observation further supports the notion that persister cells are slow-proliferating cells, potentially induced by VEM treatment. Finally, to assess the impact of the treatment period, cells were treated with VEM (100 x IC_{50}) for 9 days, and the surviving cells were assessed using the aforementioned assays. As represented in figure 3.5, Cells surviving 9-day VEM treatment were stained with ReadyProbesCell Viability Imaging dyes to assess live (blue) and dead (green) cells (Figure 3.5a). For apoptosis assay, Cells surviving 9-day VEM treatment were stained with annexin-V/FITC and PI to detect apoptotic cells (figure 3.5b). And finally for cell proliferation assay, cells pre-stained with CFSE dye were treated with VEM or left untreated (control), and their fluorescence intensity was monitored at the indicated time points with florescence microscopy

(Figure 3.5c). Our observations showed that the effects of 9-day treatment on cell viability, morphology, and growth were very similar to those obtained from 3-day treatment (Figure 3.5).

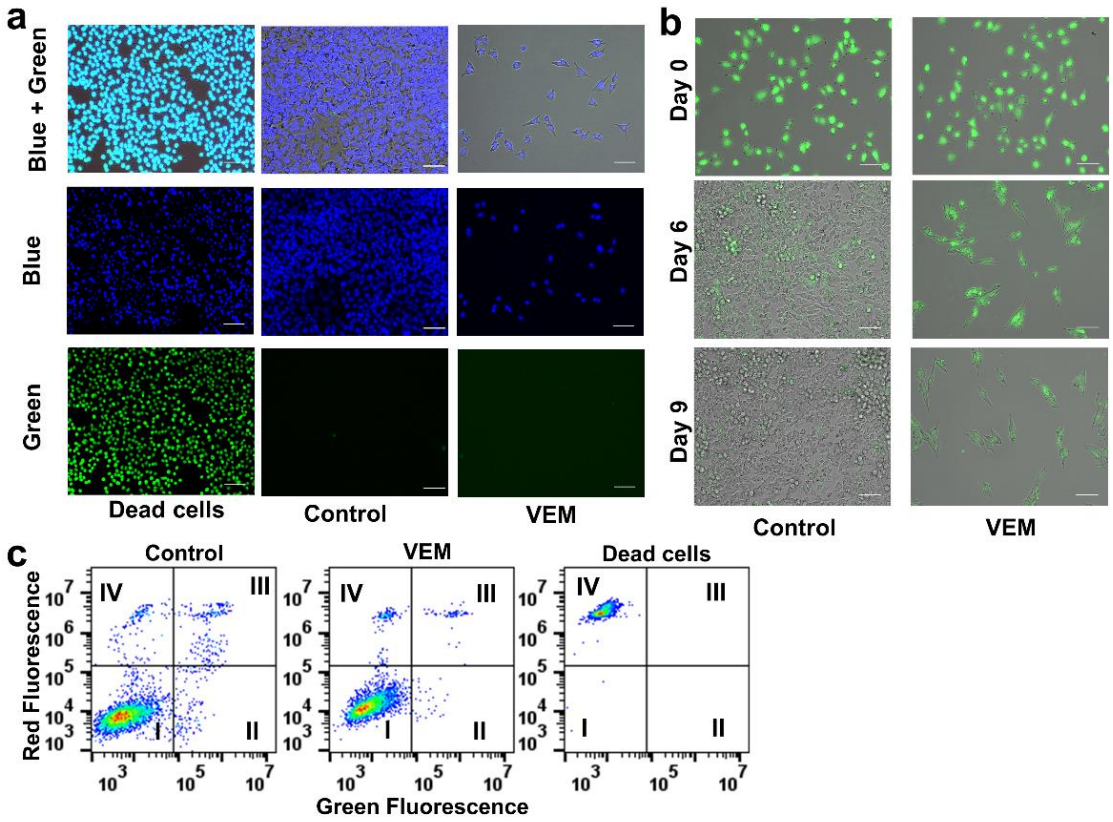

Figure 3.5 Effects of prolonged VEM treatment on cell viability, proliferation, and morphology. Scale bar: 100 μm.

3.2.2 VEM treatment affects the expression levels of cancer stem cell biomarkers.

As cancer stem cells (CSCs) are often associated with dormancy, slow growth, and drug tolerance, we measured the common melanoma CSCs biomarkers (CD271, CD44, CD34, and aldehyde dehydrogenase activity) (Figure 3.6) to determine if the isolated persisters are CSCs [118]. At indicated time points, the ALDH activity of cells (red) was assessed with the ALDEFLOUR assay. Cells treated with ALDH inhibitor 4-(dimethylamino) benzaldehyde, DAEB, (blue) were used as a negative control. Expressions of CSC biomarkers (CD271, CD44 and CD34) were measured with their respective Phycoerythrin (PE)-conjugated antibodies. Cells treated with their

isotype controls were used to determine CSC negative (-) and positive (+) cells. There was no significant difference in CD34 and CD44 expression between persister and untreated control cells (Figure 3.6c-d). However, the expression level of CD271 was gradually increased in VEM-treated cells when compared to untreated cells (Figure 3.6b). This observation has previously been reported by Rambow *et al.*, where they showed that, upon BRAF inhibition, melanoma cells demonstrated a high expression of nerve growth factor receptor (NGFR or CD271) [119].

Additionally, it has been shown that a transient overexpression of CD271 can result in a phenotypic switch to a low proliferative and highly invasive state in cells while increasing the tolerance of cells to BRAF inhibitors [120]. With the ALDEFLUOR assay, we measured the activity of aldehyde dehydrogenase (ALDH) – a functional biomarker of melanoma stem cells – in both persisters and untreated control groups. On the contrary to our expectation, VEM treated cells showed lower ALDH activity compared to untreated control cells (Figure 3.6a). As CSCs have higher levels of stem cell markers than the bulk population, our observations indicate that VEM persisters are not necessarily preexisting cancer stem cells, and drug treatment can up- or down-regulate the expression levels of CSC biomarkers in the cells.

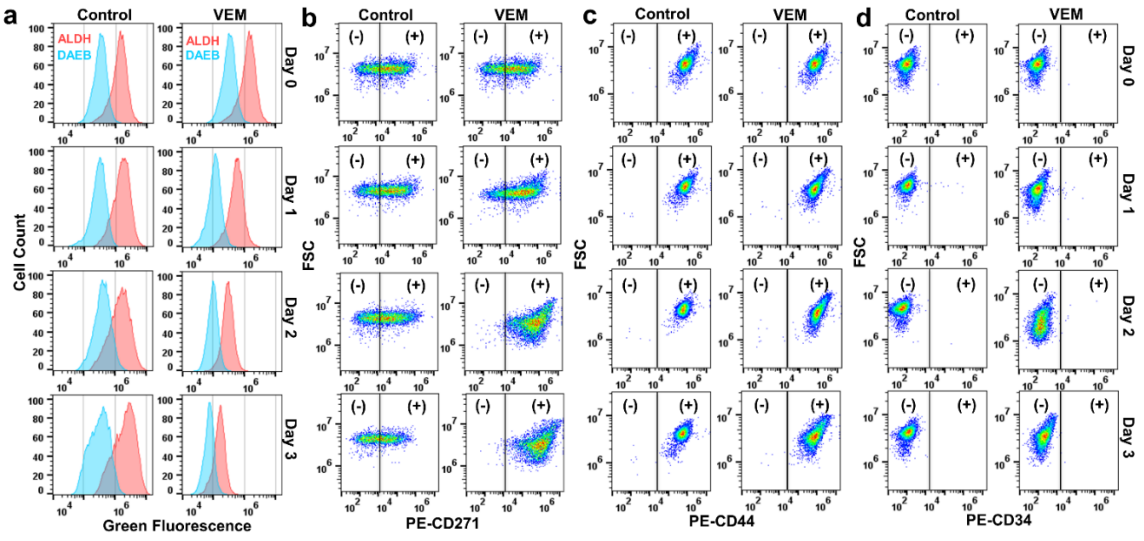

Figure 3.6 Expression of CSC markers in VEM persister cells.

3.2.3 VEM-induced persister cells exhibit an altered metabolic profile.

Metabolic rewiring is a common hallmark of cancer persister cells. Persisters undergo such alterations to meet their energy requirements and enable their survival in the presence of therapeutics. These metabolic alterations can be unique or conserved in various persister phenotypes [31,32,57]. After confirming that VEM persisters are live, reversibly drug-tolerant cells that are different from CSCs, we conducted untargeted metabolomics to study and identify persister-specific metabolic alterations. For the metabolomics study, persister cells were generated by treating the cells with VEM (100 x IC_{50}) for 3 days. The metabolomics library consisted of 689 metabolites from the following super pathways: amino acids, peptides, carbohydrates, energy, lipids, nucleotides, cofactors/vitamin and xenobiotics. The metabolomics data were normalized based on the total protein concentration, and the statistical analysis was conducted with ANOVA test ($P<0.05$) (Figure 3.7). The data generated with metabolomics were clustered (unsupervised) using the Clustergram function in MATLAB.

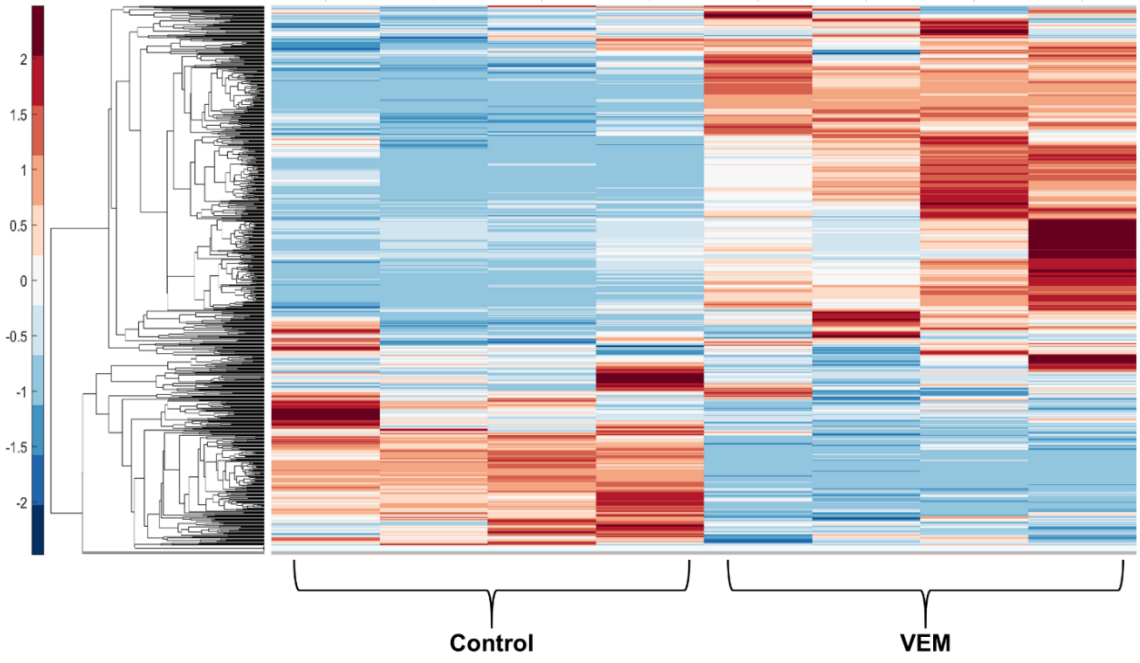

Figure 3.7 Clustergram of metabolomics dataset for VEM persisters. Each column represents a biological replicate; each row represents a metabolite. N=4.

We also performed pathway enrichment analysis with Metaboanalyst for subsets of metabolites that were either upregulated or downregulated in persister cells (Figure 3.8-3.10) [113]. Our data show that the concentrations of 469 metabolites were significantly altered in persister cells when compared to the untreated control group (Figure 3.7-3.10 and Tables 3). Figure 3.8 represents a simplified metabolic network of persister cells where, Red and blue represent upregulated and downregulated metabolites in persisters when compared to the control group, respectively. Our data showed that ~67.6 % (317) of the identified metabolites were significantly upregulated while ~32.4 % (152) were downregulated in persister cells compared to the untreated control (Table 3).

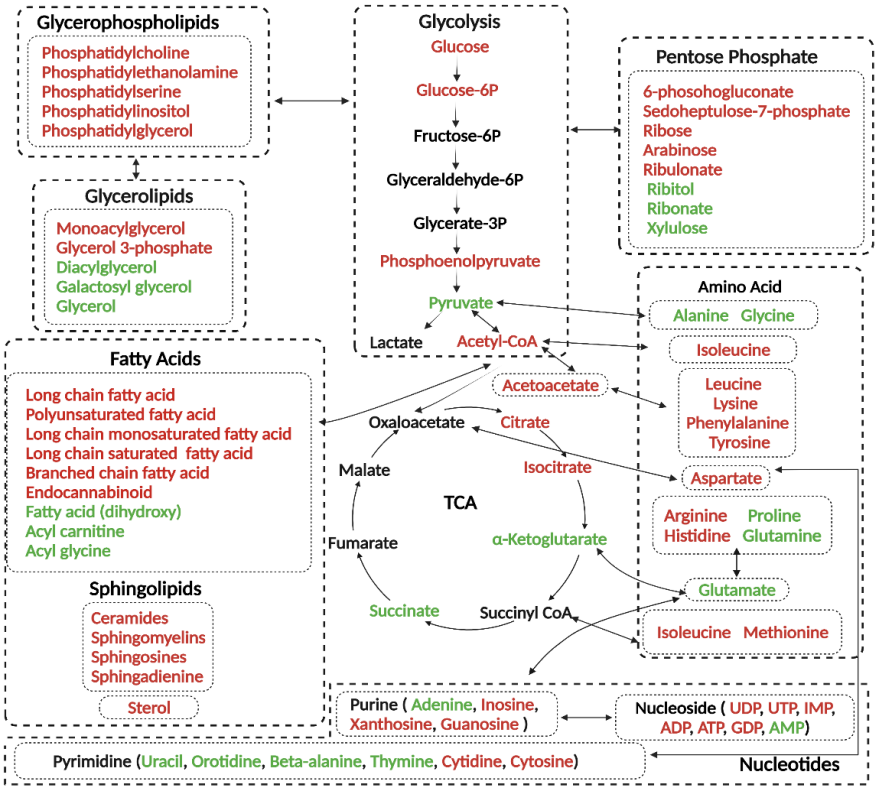

Figure 3.8 Metabolic prolife of VEM persister cells. (Created with Biorender)

Of the 317 upregulated metabolites, 161 were involved in the lipid super pathway. The enrichment analysis further validated that a majority of the metabolites that were upregulated in persister cells were involved in lipid biosynthesis (Figure 3.8 and 3.9). Phosphatidylcholine (PC), phosphatidylethanolamide (PE), monoacylglycerol, lysophospholipid, and sphingomyelins were

primarily upregulated while metabolites involved in fatty acid metabolism were downregulated in persister cells (Figure 3.10 and Table 3).

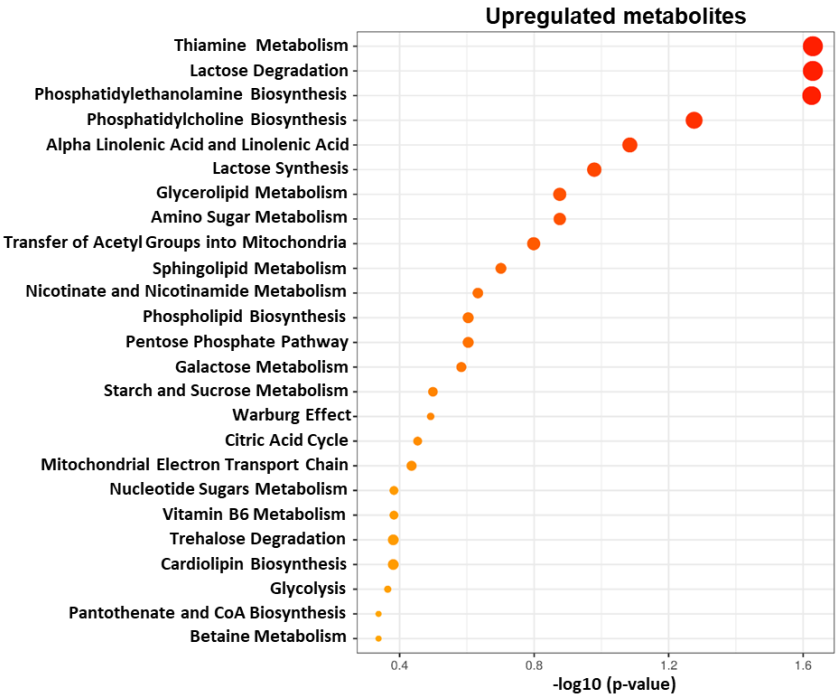

Figure 3.9 Pathway enrichment analysis for upregulated metabolites in VEM persisters. Enrichment analysis was performed using overrepresentation analysis (ORA) algorithm of MetaboAnalyst.

In addition to lipids, metabolites associated with lysine, purine/pyrimidine, thiamine, and lactose metabolism were upregulated while one-carbon (betaine, glycine and serine), branched-chain amino acid (BCAA), and glutamate metabolism were downregulated in persisters compared to control cells (Figure 3.10 and Table 3).

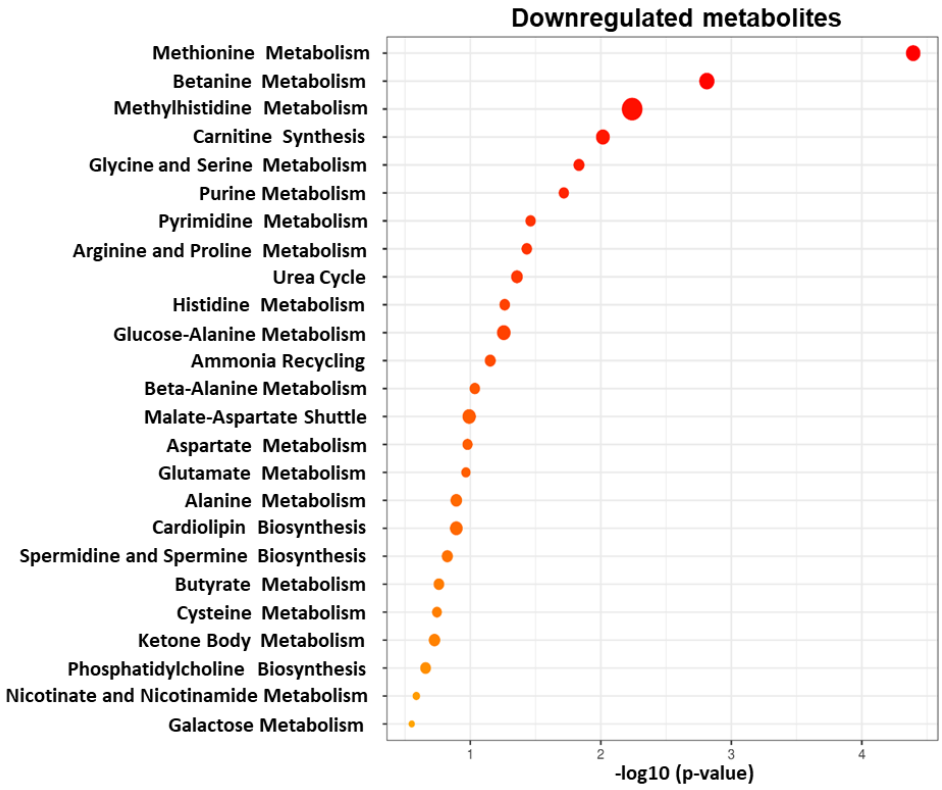

Figure 3.10 Pathway enrichment analysis for downregulated metabolites in VEM persisters. Enrichment analysis was performed using overrepresentation analysis (ORA) algorithm of MetaboAnalyst.

Our data also show an alteration of carbohydrate metabolism; particularly, glucose and glucose 6-phosphate were significantly upregulated in persister cells. Interestingly, although we did not observe significant alterations in metabolic intermediates of glycolysis and tricarboxylic acid (TCA) cycle, two TCA cycle substrates, alpha-ketoglutarate and succinate, were downregulated in persister cells (Figure 3.8). The observed effect could be attributed to the overall alteration of amino acid metabolism as alpha-ketoglutarate and succinate are involved in various pathways including BCAA, Gamma-aminobutyric acid (GABA) shunt, and glutamate metabolism (Figure 3.8). Overall, while our metabolomics data identified specific metabolites that are significantly altered in persisters, it is not clear which substrates/carbon sources persister cells efficiently use to maintain the biosynthesis of these detected molecules. Therefore, additional experiments (see below) are needed to further characterize persister cell metabolism.

3.2.4 TCA cycle activity of persister cells is not significantly different from that of control cells.

We have used phenotype microarrays (Biolog Inc., Hayward, CA) to determine the metabolites that are efficiently utilized by persister cells. Mitoplate arrays, which mainly include TCA cycle substrates, were used to assess the rate of oxidative phosphorylation of VEM-treated and untreated control cells. This assay employs a tetrazolium dye which produces water-soluble formazan crystals when reduced by mitochondrial reductases. The rate of metabolism of specific metabolites is measured by monitoring the color change associated with formazan production (optical density at 590 nm, OD_{590}) with a plate reader. Also, the cells are permeabilized with saponin so that the tetrazolium dye can be intracellularly reduced by mitochondria.

In our previous study, we showed that the levels of TCA metabolites were down-regulated in drug-tolerant cells (obtained from chemotherapeutic treatments) because of the increased consumption rates of these intermediates by the cells [34]. From the mitoplate assays, we observed a slight increase in the consumption of succinate in VEM persister cells (Figure 5.1). This observation corroborates our metabolomics data, which showed an overall downregulation of succinate molecules in VEM persisters compared to the untreated control. However, no significant difference was observed in the consumption rates of other TCA cycle metabolites (Figure 5.1). Although drug-tolerant cells are generally shown to be less dependent on aerobic glycolysis (the Warburg effect) and more reliant on oxidative phosphorylation [41,57,58], our metabolomics and mitoplate data do not show this trend in VEM persisters.

3.2.5 Lactic acid consumption is significantly up-regulated in VEM persister cells.

A phenotype microarray (PM-M1) (Biolog Inc.) containing 91 carbon and nitrogen substrates was used to identify metabolites that are efficiently catabolized by persisters. Similar to the mitoplate assay, cellular metabolic activities are measured by a tetrazolium dye in the PM-M1 assay. However, unlike the mitoplate assay, cells are not permeabilized in the PM-M1 assay, in which the cells are cultured for 2 days in a minimal medium supplemented with FBS, glutamine,

and the substrate of interest (see chapter 3 section 3.1.13). Phenotype microarrays (PM-M1 array) were used to measure the consumption rates of various substrates in VEM persister and control groups at (a) 0 h, (b) 24 h, and (c) 48 h respectively in Figure 3.11. Consumption rates were measured with a tetrazolium-based dye at 590 nm (OD_{590}). The absorbance was normalized by using t = 0 h and glutamine control data. The data points and error bars represent the mean and the standard error.

We consistently observed that carbon sources such as D-turanose, D-mannose, glycogen, and D-maltose were consumed less by persisters when compared to control cells (Figure 5.2-4.4). We also observed significant differences in glucose, lactic acid, inosine, and adenosine metabolism between persisters and untreated cells (Figure 3.11 and Figures 5.2-5.4).

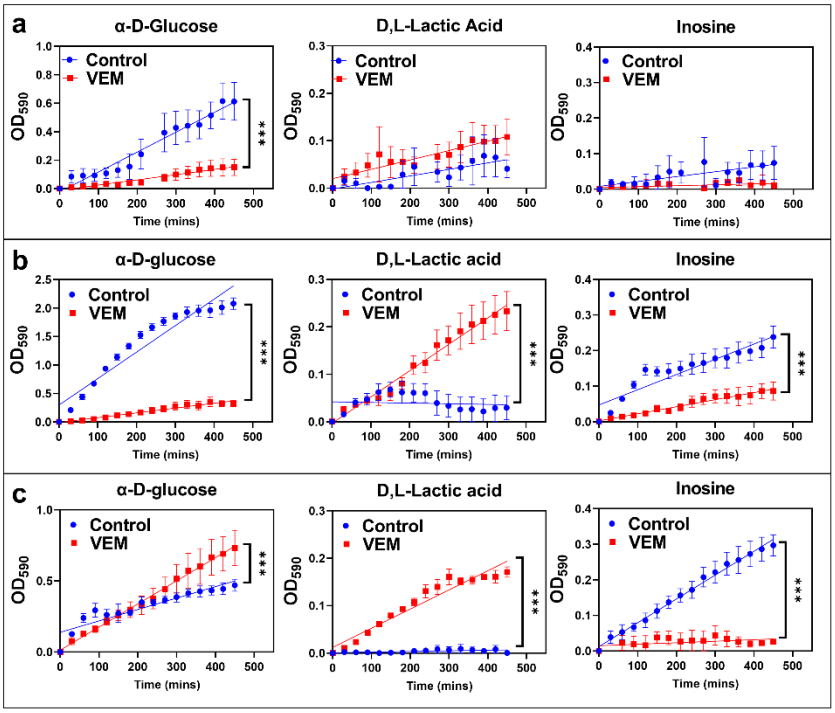

Figure 3.11 Assessing the consumption rates of various substrate in VEM persister cells. Statistical analysis was performed using a linear regression analysis (F-Statistics, ***p< 0.001). N= 4.

Interestingly, although untreated cells seemed to have higher consumption rates of glucose at t = 0 h and 24 h, the glucose consumption rates were found to be low in persister cells at initial time points (Figure 3.11). Increased intracellular concentrations of glucose and glucose 6-phosphate in persister cells determined by metabolomics analysis (Figure 3.8) may be due to the decreased consumption rates of these metabolites by the persister cells (Figure 3.11). On the other hand, lactate metabolism is significantly upregulated in persister cells (Figure 3.11), while the metabolism of inosine and adenosine are more active in control cells (Figure 3.11 and Figures 5.2-5.4). Lactic acid is a byproduct of glycolysis and glutaminolysis, and increased levels of lactate production in cancer cells have been extensively studied and linked with increased aerobic glycolysis. However, the observed difference in lactic acid utilization (Figure 3.11) may be due to conversion of lactic acid to pyruvate and acetyl-coA which serve as metabolic intermediates for lipid and amino acid metabolism in persister cells (Figure 3.8). Lastly, both adenosine and inosine are nucleosides that have been linked to cell proliferation and cell death in cancer cells [121], and both metabolites are preferred by untreated control cells (Figure 3.11). This observation is in alignment with our metabolomics data as we see an accumulation in the inosine and adenosine-containing metabolites in persister cells potentially due to their reduced consumption rates in the cells.

3.2.6 Persister cells have increased viability in minimal medium.

To further validate the phenotype microarray data, we measured glucose and lactic acid concentrations in the cultures in which VEM-treated and untreated control cells were cultured in the presence of glucose or lactic acid under PM-M1 assay conditions. Therefore, after treatment with VEM, cells were cultured in a minimal medium consisting of either glucose or lactic acid. Then, we measured the glucose/lactate consumption rate using enzymatic kits (described in section 3.1.14) and the viability of the cells (see section 3.1.15) for 48 h (Figure 3.12). Our results show that while glucose consumption at t = 24 h was significantly higher in untreated control cells compared to VEM persisters, the glucose consumption of persister cells increased to a level similar

to the untreated control by 48 h (Figure 3.12a), consistent with our PM-M1 results (Figure 3.11). Both glucose consumption and phenotype microarray data verify the existence of a longer lag phase in persister cells. We also measured the number of viable cells (although confluent cell cultures were used for PM-M1 assays as described in Materials and Methods) and showed that the number of cells was slightly higher in the control group in the presence of glucose; however, the difference between persister and control groups was not statistically significant (Figure 3.12b). Our measurement of lactic acid in untreated control samples showed minimal or no changes in lactic acid concentration; therefore, we were not able to calculate the lactic acid consumption by control cells. However, VEM persister cells were able to consume lactic acid (Figure 3.12c), as predicted by PM-M1 data (Figure 3.11). Interestingly, cell count data showed that, by 48 h, the survival ratio of untreated control cells was significantly lower compared to VEM persister cells in a minimal medium containing lactic acid (Figure 3.12d).

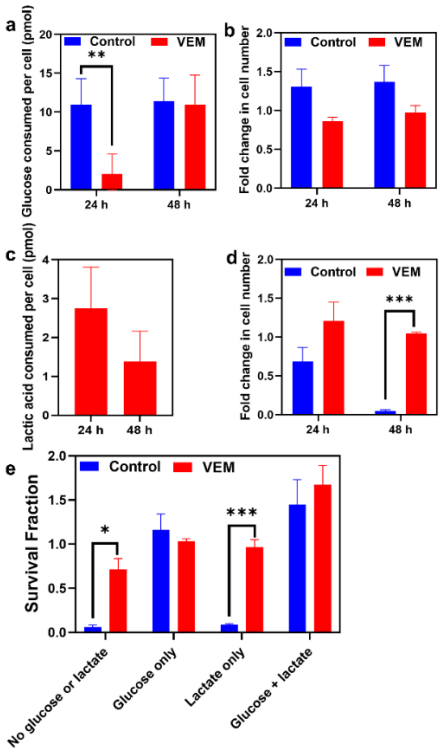

Figure 3.12 Measurement of glucose and lactic acid consumption. Statistical comparison was conducted with a pairwise t-test (*p< 0.5, **p< 0.01, and ***p< 0.001).

3.3 Discussion

The emergence of drug-tolerant persister cells has become one of the major challenges in cancer treatment. The ability of persister cells to avoid conventional therapeutics can lead to a high relapse rate and poses a significant challenge in the complete eradication of tumor cells. With this study, we aimed to characterize the metabolic profiles of persisters that are tolerant to vemurafenib, a BRAF inhibitor. Identifying metabolic pathways of tolerant cells can offer potential therapeutic targets, which has been an overarching goal of many recent studies. Methods employing various transcriptomics techniques (RNA-seq, single-cell RNA-seq, DNA microarrays) have been utilized to explore the metabolic alterations in persister cells [31,32,57]. Our study employs untargeted metabolomics which can provide a global/comprehensive analysis of the persister metabolome. Although recent studies have explored the advantages of metabolic flux analysis with isotope-labeled metabolites, this does not provide a broad overview of the persister metabolome.

Although untargeted metabolomics is a powerful tool [122], discerning whether the identified metabolites are consumed by the cells or are the products of certain pathways is quite challenging. To address this issue, we employed phenotype microarray assays that measure the utilization rates of various substrates via a tetrazolium dye. The key underlying mechanism of this assay is that the utilization rate of a substrate correlates with the rate of dye reduction; thus, these assays in combination with metabolomics can allow us to infer if a given biochemical source is being catabolized. In addition, we employed a modified version of the microarray assay, namely the mitoplate assay, which measures the consumption rates of substrates associated with the TCA cycle. The modified version of the tetrazolium dye is expected to be reduced by electrons primarily released from cytochromes. This technique can indeed be used to infer the rate of oxidative phosphorylation in the sample being tested. The most popular method for assessing oxidative phosphorylation is the seahorse assay, which measures the oxygen consumption rate (OCR) as well

as the glycolytic flux [123]. However, the seahorse assay does not provide insights on the utilization rates of substrates contributing to the increased OCR.

Our metabolic analysis showed that almost half of the upregulated metabolites in persister cells are associated with lipid metabolism. Our subsequent assays indicate that carbon sources, such as lactate, are potentially diverted to anabolic pathways associated with lipid and amino acid metabolism in persisters. Lactate is utilized for many cellular processes involved in metastasis, angiogenesis and more importantly, immunosuppression of cancer [124]. Furthermore, lactic acid can be reversibly converted to pyruvate and acetyl-coA which may act as an energy source for fatty acid oxidation [125] or serve as metabolic intermediates for certain amino acid and lipid metabolism (Figure 3.8).

The alteration of lipid metabolism in drug-tolerant cells has been shown by prior studies [126]. PC, PE, lysophospholipid, and sphingomyelins are major components of cell membranes and play significant roles in cell proliferation, apoptosis, and cell migration [77]. Phospholipids and sphingolipids are also closely associated with drug resistance and tumor progression in multiple cancers including melanoma [127]. Delgado-Goni *et al*. demonstrated that limiting the exogenous lipid content resulted in an overall increase in VEM sensitivity for resistant BRAF-mutated melanoma cells [128]. *De novo* fatty acids are continually used by cancer cells to synthesize lipids required for membrane production and to provide energy through β-oxidation [129].

Nucleotide metabolism (pyrimidine and purine) represents another class of metabolites that was altered in persister cells. With microarray experiments, we observed that persister cells had lower consumption rates for adenosine and inosine compared to untreated cells. This difference was noticeably greater in the inosine consumption rate. Inosine can be produced by the catabolism of adenosine. Soares *et al*. have shown that adenosine causes cell proliferation by activating the adenosine receptor, AR, while inosine enhances proliferation by activating the receptor A_3AR [130]. One carbon metabolism, which was shown to be down-regulated in persister cells, can be used for

biosynthesis of nucleotides [131]. Along with pentose phosphate pathway (PPP), one carbon metabolism is involved in NADPH production, and the maintenance of redox and methylation states are required for cell proliferation [79]. Lastly, in the amino acid metabolism, metabolites involved in BCAA were significantly altered in persister cells. BCAA metabolism in cancer has been extensively studied as it is required for many cellular processes including protein synthesis and energy production [95,132]. Branched chain aminotransferase 1/2 (BCAT1/ BCAT1) enzymes, which are involved in BCAA degradation, are proposed to be a prognostic marker for cancer [133]. Study by Wang *et al*. also demonstrated that epigenetic upregulation of BCAT1 can promote tolerance to tyrosine kinase inhibitor in lung cancer cells [98].

Along with lipid metabolism, we expected that persister cells would have a significant difference in energy metabolism, primarily in the TCA cycle and oxidative phosphorylation. Studies have shown persister cells generally exhibit an increased rate of oxidative phosphorylation compared to bulk tumor populations [41,57]. However, in this study, we did not see a significant difference in the consumption rates of TCA substrates except for succinate. This can be a result of differences in experimental details between studies. For instance, we generated persister cells with a single drug treatment while the majority of the studies have used combinations of BRAF/MEK inhibitors and/or chemotherapeutics. A study conducted by Parmenter *et al*. showed similar outcomes where single treatment with BRAF inhibitor resulted in a decrease in OCR of melanoma cells [134] although they speculated that long-term treatments may eventually shift persister metabolism towards oxidative phosphorylation.

In this study, we showed that VEM persisters can utilize lactate more efficiently than untreated control cells. Although investigating the molecular mechanism underlying this observed phenomenon is beyond the scope of this study, we hypothesize that targeted therapeutics (*e.g.*, the BRAF inhibitor, VEM) potentially induce cell dormancy by directly inhibiting cell-proliferation signaling pathways. Oncogenic mutations in RAS genes (KRAS, NRAS, and HRAS) or RAF genes

(RAF-1, BRAF, and A-RAF) occur in many cancer types, including the melanoma cells [135]. BRAF is a serine/threonine-protein kinase and acts upstream in several signaling pathways (*e.g.*, MEK/ERK, PI3K/AKT) that promote aerobic glycolysis and enhance the expression of enzymes involved in anabolic pathways (*e.g.*, protein and lipid synthesis) by activating various transcription factors, such as HIF1/2, MYC, FoxO and STAT3 [135,136]. These transcription factors are known to induce glucose transporters and glycolytic and anabolic enzymes [137–141]. Studies show that metabolism of drug-tolerant melanoma cells may be associated with increased mitochondrial oxidative phosphorylation and decreased glycolysis and lactate synthesis [142–145], which may indeed increase lactate consumption in the cells. Lactate consumption can interrupt cellular energy homeostasis by deactivating AMP-activated protein kinase (AMPK) resulting in overexpression of regulatory element-binding protein 1 (SREBP1), Stearoyl-CoA, and desaturase-1 [146]. Upregulation of these enzymes protects cells against ferroptosis by increasing the production of exogenous monounsaturated fatty acids [146].

The existence of persisters is a major obstacle in cancer therapy. Eradication of these drug-tolerant cells is a monumental challenge because the mechanisms underlying their formation and survival are highly complex and diverse. The therapeutic promise of targeting a metabolic mechanism in persister cells garners noteworthy attention in the field, as metabolism represents a rich source of targets for anti-persister strategies [32,57]. Although we focused on melanoma cells, the suggested methodologies integrating untargeted metabolomics and phenotype microarrays can be readily extrapolated to other cell lines, enabling assessment of the physiological capabilities of a wide variety of persisters.

Chapter 4 Summary and Future Directions

4.1 Summary

With the use of metabolomics, high-throughput screening of microarrays, and in-vitro bioassays, we studied the metabolic alterations induced by chemo or targeted therapeutics in melanoma persister cells. We conducted viability, apoptosis, cell proliferation, and biomarker assays to show that persisters are slow cycling viable cells. The metabolic datasets generated in these studies present potential therapeutic targets for developing anti-persister therapies.

With our first study, we demonstrated that conventional chemotherapeutic agents induce a transient metabolic alteration which led to downregulation of Krebs cycle substrates in persister cells. Furthermore, with the use of microarrays that consisted of various mitochondrial substrates and a tetrazolium dye-based bioenergetics assay, we demonstrated that persister cells consumed succinate, malate, and fumarate at a higher rate compared to untreated bulk cancer population. Finally, with microarrays consisting of various mitochondrial inhibitors, we screened for potential metabolic inhibitors that can lead to an overall reduction in persister levels in melanoma cells. We showed that upon co-treatment with trifluoperazine, an electron transport inhibitor, persister levels were significantly reduced in melanoma cell lines.

In the second study, we characterized the metabolic alterations in melanoma persisters induced by vemurafenib, a BRAF inhibitor, treatment. Our results showed that vemurafenib persisters exhibited a transient metabolic alteration primarily in amino acid and lipid metabolism without a significant alteration in the TCA cycle when compared to untreated control cells. When we conducted a tetrazolium-based bioenergetics assay with microarrays consisting of various carbon sources, we found that the consumption of glucose, adenosine, inosine, and lactic acid was significantly different in persisters compared to control cell. Interestingly, persister cells utilize lactate more efficiently than untreated melanoma cells and survive in a minimal medium that

includes lactate as a sole carbon source while the untreated cells could not survive in this minimal medium. Additional studies are needed to characterize the underlying mechanism behind this phenomenon.

4.2 Cell signaling analysis and in-vivo studies

Genetic alteration in different cell signaling pathways that controls various cellular functions, cell-cycle progression, differentiation, and apoptosis is a hallmark of cancer cells. Mutation of proto-oncogenes to oncogenes results in hyperactivation of these pathways while mutations in tumor suppressors genes can affect the regulatory mechanism of cell signaling pathways. Alterations in many signaling pathways including, PI3K-Akt, Ras-ERK, Wnt signaling, RAS/MAP kinase, and more have been associated with tumor cells.[147–149] These mutations have been exploited as and proven to be potential targets for cancer therapy.[150–154] However, as with conventional chemotherapy, acquired resistance has become a key challenge in achieving complete treatment. One of the ways cells overcome such therapeutic approaches is through alteration of transcriptional regulators.[39] Therefore, to understand the underlying mechanism of drug tolerance, understating the key transcriptional changes and active signaling pathways in persister cells is necessary.

Since metabolism is closely linked with cell signaling and transcription, we conducted a high-throughput screening using a commercially available antibody array. For this assay, A375 cells were treated with GEM (orange) or left untreated (blue) either for (a) 1 day or (b) 3 days. The surviving cells were collected, and their total protein was extracted for western blotting with the antibody array (Figure 4.1). We screened for potential targets in NF-κβ, TGF-β, MAPK, AKT, and JAK/STAT pathways using a chemiluminescence detection method. Our results showed that during treatment with GEM, cells showed a significant upregulation in phosphorylation of cJUN protein. This difference was transient as prolonged exposure to GEM led to no significant difference in cJUN activity compared to untreated cells (Figure 4.1).

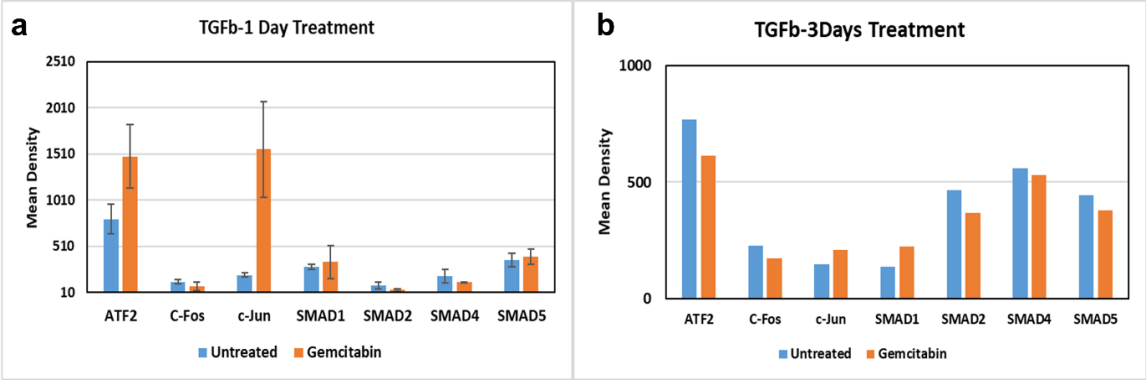

Figure 4.1 High throughput screening of signaling proteins in GEM persisters.

We further verified this observation with western blotting and as expected cells after the therapeutic pressure expressed higher level of phospho-cJUN than untreated bulk cancer cells. Finally, we co-treated the cells with the cJun inhibitor, JNK-IN-8. JNK-IN-8 is a very selective, potent, and irreversible inhibitor for phosphorylation of cJUN.[155] Upon treatment with GEM in presence of JNK-IN-8, we observed that the cells were capable of surviving the therapeutic pressure. We further performed co-treatment with JNK and various other cancer drugs including camptohecin (CAM), cytarabine (CYT), azacitidine (AZA), methotrexate (MET), and capecitabine (CAP). We observed that the viability was increased only for AZA, CYT, and GEM. All these three drugs fall under the category of antimetabolite and are analogs of cytidine. This led us to believe that cJUN phosphorylation is involved in the maintenance of the persister state. However, additional experiments are needed to understand the mechanism and roles of cJUN phosphorylation in the persister cells.

cJUN is a part of the activator protein-1 (AP-1) complex and is associated with various cellular activities such as proliferation, apoptosis, survival, differentiation, migration, tumorigenesis, and more.[156–160] The AP-1 family is a collective term for dimers formed by proteins of JUN, FOS, activating transcription factor (ATF), and musculoaponeurotic fibrosarcoma (MAF).[160,161] cJun is one of the most extensively studied proteins from the AP-1 family and has been associated with cancer cell signaling. Growth factors external stimuli have shown to

significantly affect the transcriptional and DNA binding activity of cJun.[162–165] The initial step results in phosphorylation of cJun in response to the stimulus.[166,167] Phosphorylation of cJun can initiate AP-1 activation however, phospho-cJun are unstable and exist transiently.[168,169] cJun has been shown to affect cell growth and regulate apoptosis in multiple ways.[170–173] In cancer cells, cJun has shown to be overexpressed in various tissue types including lung[174], breast,[175] and colon cancer[176]. Such high levels of cJun were associated with proliferation, angiogenesis as well as invasiveness of the tumor cells. Although cJun is generally linked with oncogenic effects as it is shown to regulate genes involved in tumor development such as cyclin D1 (simulates proliferation), Fas (inhibition of apoptosis), CD 44 (simulates invasiveness), and proliferin (simulates angiogenesis),[177–181] mechanism of cJun interactions is complex and can vary depending on how cJun undergoes dimerization. Although cJun homodimer generally has oncogenic activity, cJun-JunB heterodimer tends to repress such functions.[182] In melanoma cells, Ramsdale *et al.* have shown that the abundance of cJun maintained inherent and adaptive resistance to BRAF inhibitors.[183] These factors highlight the significance of cell signaling and cJun in cancer cells.

Transcriptional regulators have been a significant factor in persister phenotype. Taniguchi *et al.* demonstrated that Osimertinib treated lung cancer cells entered a slow-growing persister state via upregulation of kinase receptor, AXL.[184] This activation of AXL induces epithelial-mesenchymal transition (EMT) which leads to acquired resistance to various therapeutic agents.[185] Wnt/β-catenin pathway, which is significant for stem cell phenotype, was shown to be activated during EGFR inhibition via Notch3-dependent pathway which resulted in the survival of persister cells.[186,187] This transient shift in the cell signaling pathway can be attributed to the metabolic remodeling we observed in persister cells. Therefore, to understand the underlying mechanism of transcriptional regulation of cJun, we need to perform in-depth transcriptional analysis in persister cells. We are also generating stable A375 cells that will be transfected with cJun reporter plasmid to monitor the overall cJun activity pre-, during, and post-treatment with cancer drugs. We will also

be conducting the co-treatment assay with mitochondrial or cJun inhibitors with chemotherapeutic agents *in-vivo*. With the data generated with transcriptomics and *in-vivo* studies, we can have a deeper insight into the persister phenotype, which enables us to develop effective anti-persister therapies to bolster cancer treatment.

Supplementary Data

Table 2 Metabolomics dataset for GEM treated A375 cells.

Super Pathway	Sub Pathway	Biochemical Name	Fold Change	p-value	q-value
Amino Acid	Glycine, Serine and Threonine Metabolism	glycine	0.53	1.720E-06	0.000
		sarcosine	0.11	1.129E-06	0.000
		dimethylglycine	0.59	1.000E-04	0.000
		betaine	0.57	1.157E-05	0.000
		serine	0.67	6.000E-04	0.001
		N-acetylserine	0.34	2.320E-08	0.000
		threonine	1.58	4.000E-04	0.001
		N-acetylthreonine	0.53	3.000E-04	0.001
	Alanine and Aspartate Metabolism	alanine	1.11	1.953E-01	0.136
		N-acetylalanine	0.65	6.000E-04	0.001
		aspartate	1.06	5.664E-01	0.309
		N-acetylaspartate (NAA)	0.80	7.800E-03	0.010
		asparagine	1.19	5.440E-02	0.048
		N-acetylasparagine	0.79	8.640E-02	0.070
		hydroxyasparagine**	0.47	2.400E-03	0.004
	Glutamate Metabolism	glutamate	0.94	4.031E-01	0.241
		glutamine	0.99	9.233E-01	0.433
		alpha-ketoglutaramate*	0.63	7.370E-02	0.062
		N-acetylglutamate	0.48	2.420E-07	0.000
		N-acetylglutamine	0.75	6.000E-03	0.008
		4-hydroxyglutamate	0.30	1.118E-10	0.000
		glutamate, gamma-methyl ester	0.91	7.535E-01	0.381
		pyroglutamine*	0.34	6.481E-08	0.000
		N-acetyl-aspartyl-glutamate (NAAG)	0.52	2.344E-05	0.000
		beta-citrylglutamate	0.64	4.207E-05	0.000
		carboxyethyl-GABA	6.24	1.588E-10	0.000
		S-1-pyrroline-5-carboxylate	0.77	5.481E-01	0.302
	Histidine Metabolism	histidine	2.04	6.383E-06	0.000
		1-methylhistidine	2.46	1.000E-04	0.000
		3-methylhistidine	2.08	9.000E-04	0.002
		N-acetylhistidine	2.06	2.359E-06	0.000
		N-acetyl-3-methylhistidine*	1.86	1.000E-04	0.000
		N-acetyl-1-methylhistidine*	1.96	3.200E-03	0.005
		trans-urocanate	0.88	4.313E-01	0.253
		imidazole propionate	0.18	9.405E-11	0.000

Table 2 Continued

		formiminoglutamate	0.83	2.202E-01	0.150
		imidazole lactate	**0.14**	4.368E-11	0.000
		carnosine	**1.90**	1.186E-05	0.000
		1-methyl-4-imidazoleacetate	**0.51**	2.191E-05	0.000
		1-methyl-5-imidazoleacetate	**0.15**	8.930E-11	0.000
		1-ribosyl-imidazoleacetate*	**0.27**	2.649E-06	0.000
		4-imidazoleacetate	1.02	7.578E-01	0.381
		histidine methyl ester	1.11	2.492E-01	0.166
	Lysine Metabolism	lysine	0.98	8.579E-01	0.417
		N2-acetyllysine	**3.99**	1.291E-05	0.000
		N6-acetyllysine	**0.66**	5.000E-04	0.001
		N6-methyllysine	**1.26**	3.070E-02	0.031
		N6,N6-dimethyllysine	**0.72**	5.340E-02	0.047
		N6,N6,N6-trimethyllysine	**1.63**	3.749E-05	0.000
		hydroxy-N6,N6,N6-trimethyllysine*	**1.45**	4.500E-03	0.006
		5-hydroxylysine	**1.59**	1.550E-02	0.017
		5-(galactosylhydroxy)-L-lysine	**2.16**	1.082E-05	0.000
		fructosyllysine	1.17	3.992E-01	0.239
		saccharopine	**3.57**	5.785E-05	0.000
		2-aminoadipate	**1.90**	7.300E-03	0.009
		glutarylcarnitine (C5-DC)	**1.80**	5.120E-02	0.046
		pipecolate	0.93	5.261E-01	0.295
		6-oxopiperidine-2-carboxylate	**0.82**	6.230E-02	0.054
		cadaverine	**0.87**	6.200E-03	0.008
		N-acetyl-cadaverine	0.44	1.661E-01	0.119
		5-aminovalerate	**0.69**	1.000E-03	0.002
		N,N,N-trimethyl-5-aminovalerate	**0.44**	1.223E-06	0.000
	Phenylalanine Metabolism	phenylalanine	1.09	2.020E-01	0.139
		N-acetylphenylalanine	**1.24**	7.020E-02	0.059
		1-carboxyethylphenylalanine	**0.77**	5.130E-02	0.046
		phenylpyruvate	1.35	3.038E-01	0.194
		phenyllactate (PLA)	**0.74**	8.940E-02	0.072
		phenethylamine	1.60	1.651E-01	0.119
	Tyrosine Metabolism	tyrosine	1.18	1.045E-01	0.082
		N-acetyltyrosine	**1.65**	3.150E-05	0.000
		1-carboxyethyltyrosine	**0.41**	4.248E-06	0.000
		4-hydroxyphenylpyruvate	**1.28**	4.290E-02	0.040
		3-(4-hydroxyphenyl)lactate	**0.62**	2.818E-05	0.000
		phenol sulfate	**1.45**	4.350E-02	0.041
		3-methoxytyrosine	**2.35**	1.000E-04	0.000
		o-Tyrosine	**6.27**	6.572E-05	0.000

Table 2 Continued

		O-methyltyrosine	0.55	9.599E-06	0.000
	Tryptophan Metabolism	tryptophan	1.31	6.800E-03	0.009
		N-acetyltryptophan	1.20	1.551E-01	0.114
		C-glycosyltryptophan	0.71	1.180E-02	0.014
		tryptophan betaine	0.39	1.818E-05	0.000
		kynurenine	2.02	5.896E-06	0.000
		kynurenate	1.96	6.500E-03	0.008
		serotonin	2.65	5.000E-04	0.001
		tryptamine	1.21	4.761E-01	0.274
		indolelactate	1.51	7.460E-02	0.062
		indoleacetate	1.27	2.042E-01	0.140
	Leucine, Isoleucine and Valine Metabolism	leucine	1.13	8.110E-02	0.066
		N-acetylleucine	1.29	9.660E-02	0.076
		1-carboxyethylleucine	1.16	1.995E-01	0.138
		4-methyl-2-oxopentanoate	0.39	3.735E-05	0.000
		alpha-hydroxyisocaproate	0.85	2.544E-01	0.168
		isovalerylglycine	0.76	3.955E-01	0.238
		isovalerylcarnitine (C5)	0.62	2.510E-02	0.026
		beta-hydroxyisovalerate	0.58	4.000E-04	0.001
		beta-hydroxyisovaleroylcarnitine	0.72	2.700E-03	0.004
		3-methylglutaconate	0.78	1.180E-02	0.014
		isoleucine	1.08	2.493E-01	0.166
		N-acetylisoleucine	0.89	8.353E-01	0.409
		1-carboxyethylisoleucine	0.63	1.500E-03	0.003
		3-methyl-2-oxovalerate	0.41	6.100E-03	0.008
		2-hydroxy-3-methylvalerate	0.89	4.476E-01	0.260
		2-methylbutyrylcarnitine (C5)	0.52	3.000E-04	0.001
		2-methylbutyrylglycine	0.68	8.120E-02	0.066
		tiglylcarnitine (C5:1-DC)	0.68	3.200E-03	0.005
		3-hydroxy-2-ethylpropionate	0.91	8.408E-01	0.411
		ethylmalonate	0.35	2.953E-07	0.000
		methylsuccinate	0.63	3.400E-03	0.005
		valine	1.11	1.276E-01	0.097
		N-acetylvaline	1.08	4.188E-01	0.247
		1-carboxyethylvaline	0.55	1.600E-03	0.003
		3-methyl-2-oxobutyrate	0.39	1.900E-03	0.003
		alpha-hydroxyisovalerate	0.96	6.967E-01	0.356
		isobutyrylcarnitine (C4)	0.42	1.640E-05	0.000
		3-hydroxyisobutyrate	1.08	6.664E-01	0.348
		2,3-dihydroxy-2-methylbutyrate	0.32	6.113E-07	0.000
	Methionine, Cysteine, SAM and Taurine Metabolism	methionine	1.15	6.960E-02	0.059

Table 2 Continued

		N-acetylmethionine	1.71	7.000E-04	0.001
		N-formylmethionine	0.93	4.241E-01	0.249
		S-methylmethionine	1.44	2.529E-01	0.168
		methionine sulfone	1.46	1.450E-02	0.016
		methionine sulfoxide	3.87	3.464E-07	0.000
		N-acetylmethionine sulfoxide	3.21	7.478E-05	0.000
		S-adenosylmethionine (SAM)	1.18	6.120E-02	0.053
		S-adenosylhomocysteine (SAH)	0.68	7.261E-05	0.000
		2,3-dihydroxy-5-methylthio-4-pentenoate (DMTPA)*	0.77	2.030E-02	0.021
		homocysteine	0.65	4.530E-02	0.042
		cystathionine	0.19	4.333E-11	0.000
		cysteine	1.38	3.720E-02	0.036
		N-acetylcysteine	0.87	4.612E-01	0.267
		S-methylcysteine sulfoxide	1.23	3.129E-01	0.198
		S-carboxyethylcysteine	3.79	3.215E-08	0.000
		hypotaurine	0.58	2.000E-03	0.003
		taurine	0.52	1.400E-03	0.002
		N-acetyltaurine	0.37	7.960E-07	0.000
	Urea cycle; Arginine and Proline Metabolism	arginine	1.55	9.000E-04	0.002
		argininosuccinate	0.77	2.096E-01	0.144
		ornithine	4.81	1.035E-05	0.000
		3-amino-2-piperidone	6.24	6.616E-05	0.000
		2-oxoarginine*	1.20	2.017E-01	0.139
		citrulline	1.15	9.590E-02	0.076
		proline	0.52	2.000E-04	0.000
		dimethylarginine (SDMA + ADMA)	1.49	6.300E-03	0.008
		N-acetylarginine	1.17	3.570E-02	0.035
		N-delta-acetylornithine	1.54	1.300E-03	0.002
		trans-4-hydroxyproline	1.80	1.945E-05	0.000
		pro-hydroxy-pro	0.56	1.760E-02	0.019
		N-methylproline	0.53	1.100E-03	0.002
		N,N,N-trimethyl-alanylproline betaine (TMAP)	1.44	5.700E-03	0.008
		N-monomethylarginine	1.45	4.080E-02	0.039
	Creatine Metabolism	creatine	0.72	2.000E-04	0.001
		creatinine	0.75	6.000E-03	0.008
		creatine phosphate	0.61	7.000E-04	0.001
	Polyamine Metabolism	putrescine	0.28	5.825E-07	0.000
		N-acetylputrescine	0.65	3.683E-01	0.224
		N-acetyl-isoputreanine	2.34	6.216E-07	0.000
		spermidine	1.84	7.499E-05	0.000
		N('1)-acetylspermidine	6.76	4.302E-08	0.000

Table 2 Continued

		diacetylspermidine*	1.69	6.000E-04	0.001
		spermine	0.53	5.020E-02	0.046
		N(1)-acetylspermine	3.04	1.081E-06	0.000
		N1,N12-diacetylspermine	3.34	9.971E-06	0.000
		5-methylthioadenosine (MTA)	1.06	3.538E-01	0.217
		4-acetamidobutanoate	0.79	8.060E-02	0.066
	Guanidino and Acetamido Metabolism	1-methylguanidine	1.46	7.520E-02	0.063
		4-guanidinobutanoate	0.37	1.990E-10	0.000
	Glutathione Metabolism	glutathione, reduced (GSH)	1.22	5.110E-02	0.046
		glutathione, oxidized (GSSG)	1.04	6.088E-01	0.326
		cyclic dGSH	1.10	2.839E-01	0.184
		cysteine-glutathione disulfide	1.28	2.298E-01	0.155
		S-methylglutathione	1.33	3.700E-02	0.036
		cysteinylglycine	1.36	1.400E-03	0.002
		5-oxoproline	1.16	5.890E-02	0.052
		2-hydroxybutyrate/2-hydroxyisobutyrate	0.92	2.288E-01	0.155
		ophthalmate	9.26	1.349E-07	0.000
		S-(1,2-dicarboxyethyl)glutathione	0.75	1.810E-02	0.019
		4-hydroxy-nonenal-glutathione	0.85	3.196E-01	0.202
		CoA-glutathione*	1.07	5.684E-01	0.309
Peptide	Gamma-glutamyl Amino Acid	gamma-glutamylcysteine	1.13	3.075E-01	0.196
		gamma-glutamylglutamate	0.85	1.564E-01	0.114
		gamma-glutamylglutamine	2.84	2.232E-06	0.000
		gamma-glutamylhistidine	3.63	1.000E-04	0.000
		gamma-glutamylisoleucine*	2.45	1.343E-07	0.000
		gamma-glutamylleucine	3.71	2.141E-07	0.000
		gamma-glutamylmethionine	1.57	1.250E-02	0.014
		gamma-glutamylphenylalanine	1.76	2.000E-04	0.000
		gamma-glutamylthreonine	8.52	1.104E-08	0.000
		gamma-glutamyltryptophan	1.19	6.540E-02	0.056
		gamma-glutamyltyrosine	1.64	8.500E-03	0.010
		gamma-glutamylvaline	3.32	5.218E-08	0.000
	Dipeptide	alanylleucine	2.16	1.000E-03	0.002
		glycylisoleucine	3.83	4.799E-05	0.000
		glycylleucine	2.37	1.100E-03	0.002
		glycylvaline	2.03	4.700E-03	0.006
		isoleucylglycine	4.22	4.277E-05	0.000
		leucylglycine	3.53	4.000E-04	0.001
		phenylalanylalanine	3.11	4.000E-04	0.001
		phenylalanylglycine	2.81	2.000E-04	0.000
		prolylglycine	1.30	3.440E-02	0.034

Table 2 Continued

		threonylphenylalanine	1.66	1.840E-02	0.020
		tryptophylglycine	3.28	8.662E-05	0.000
		tyrosylglycine	3.14	4.000E-04	0.001
		valylglutamine	1.77	2.800E-03	0.004
		valylglycine	4.24	2.000E-04	0.000
		valylleucine	4.40	1.000E-04	0.000
		leucylglutamine*	3.66	3.415E-05	0.000
	Acetylated Peptides	phenylacetylglycine	0.61	1.830E-02	0.020
Carbohydrate	Glycolysis, Gluconeogenesis, and Pyruvate Metabolism	glucose	1.42	6.397E-01	0.339
		glucose 6-phosphate	1.61	1.063E-01	0.082
		fructose 1,6-diphosphate/glucose 1,6-diphosphate/myo-inositol diphosphates	1.41	3.129E-01	0.198
		dihydroxyacetone phosphate (DHAP)	0.66	5.011E-01	0.285
		3-phosphoglycerate	0.64	1.312E-01	0.099
		phosphoenolpyruvate (PEP)	1.94	6.100E-02	0.053
		pyruvate	0.49	8.908E-06	0.000
		lactate	0.93	4.810E-01	0.276
		glycerate	1.66	2.590E-02	0.026
	Pentose Phosphate Pathway	6-phosphogluconate	1.12	6.351E-01	0.337
		sedoheptulose-7-phosphate	2.11	8.100E-03	0.010
	Pentose Metabolism	ribose	1.63	2.290E-02	0.024
		ribitol	0.44	2.058E-06	0.000
		ribonate	0.28	2.668E-08	0.000
		ribulose/xylulose	0.57	1.900E-03	0.003
		arabinose	0.64	1.690E-02	0.018
		arabitol/xylitol	0.66	3.000E-03	0.004
		arabonate/xylonate	0.67	4.830E-02	0.044
		ribulonate/xylulonate/lyxonate*	0.91	5.735E-01	0.311
	Disaccharides and Oligosaccharides	lactose	2.36	4.300E-03	0.006
	Fructose, Mannose and Galactose Metabolism	fructose	1.62	1.577E-01	0.115
		mannitol/sorbitol	1.17	2.878E-01	0.186
		mannose	0.91	9.128E-01	0.433
		galactitol (dulcitol)	1.10	3.856E-01	0.233
		galactonate	0.37	6.797E-06	0.000
	Nucleotide Sugar	adenosine-5'-diphosphoglucose	1.00	1.000E+00	0.453
		UDP-glucose	0.71	1.540E-02	0.017
		UDP-galactose	0.87	2.402E-01	0.161
		UDP-glucuronate	1.74	4.782E-06	0.000
		guanosine 5'-diphospho-fucose	1.19	7.410E-02	0.062
		UDP-N-acetylglucosamine/galactosamine	1.62	3.800E-03	0.005
		cytidine 5'-monophospho-N-acetylneuraminic acid	1.19	9.160E-02	0.073

Table 2 Continued

	Aminosugar Metabolism	glucosamine-6-phosphate	1.39	3.470E-01	0.214
		glucuronate	1.06	5.874E-01	0.316
		N-acetylglucosamine 6-phosphate	3.88	9.388E-07	0.000
		N-acetyl-glucosamine 1-phosphate	0.42	1.560E-05	0.000
		N-acetylneuraminate	0.20	1.663E-10	0.000
		N-acetylglucosaminylasparagine	1.10	1.633E-01	0.118
		erythronate*	0.61	2.000E-04	0.000
		N-acetylglucosamine/N-acetylgalactosamine	1.38	4.220E-02	0.040
		N-glycolylneuraminate	0.29	2.271E-07	0.000
	Advanced Glycation End-product	N6-carboxymethyllysine	1.25	3.388E-01	0.210
Energy	TCA Cycle	citrate	0.97	8.156E-01	0.401
		aconitate [cis or trans]	0.97	8.607E-01	0.417
		isocitrate	0.78	5.115E-01	0.288
		alpha-ketoglutarate	0.50	6.391E-05	0.000
		succinylcarnitine (C4-DC)	0.94	5.808E-01	0.314
		succinate	0.86	6.740E-02	0.057
		fumarate	0.62	8.000E-04	0.001
		malate	0.60	4.892E-05	0.000
		oxaloacetate	0.54	8.800E-03	0.010
		2-methylcitrate/homocitrate	1.14	3.210E-01	0.202
	Oxidative Phosphorylation	acetylphosphate	0.37	4.748E-01	0.274
		phosphate	0.94	4.168E-01	0.246
Lipid	Fatty Acid Synthesis	malonylcarnitine	1.07	5.732E-01	0.311
	Fatty Acid Metabolism	acetyl CoA	1.39	1.431E-01	0.107
		oleoyl CoA	0.83	5.022E-01	0.285
		arachidonoyl CoA	1.20	4.096E-01	0.244
	Short Chain Fatty Acid	butyrate/isobutyrate (4:0)	1.15	8.506E-01	0.415
	Medium Chain Fatty Acid	heptanoate (7:0)	0.95	6.118E-01	0.327
		(2 or 3)-decenoate (10:1n7 or n8)	0.73	2.534E-01	0.168
		5-dodecenoate (12:1n7)	0.81	4.886E-01	0.279
	Long Chain Saturated Fatty Acid	myristate (14:0)	0.88	6.567E-01	0.345
		pentadecanoate (15:0)	1.09	9.300E-01	0.436
		palmitate (16:0)	1.04	9.014E-01	0.428
		margarate (17:0)	1.74	6.412E-01	0.339
		stearate (18:0)	1.19	8.837E-01	0.425
		nonadecanoate (19:0)	1.67	6.630E-01	0.347
		arachidate (20:0)	1.40	8.705E-01	0.420
	Long Chain Monounsaturated Fatty Acid	myristoleate (14:1n5)	0.80	6.143E-01	0.327
		palmitoleate (16:1n7)	1.01	7.971E-01	0.394
		10-heptadecenoate (17:1n7)	2.29	5.463E-01	0.302
		oleate/vaccenate (18:1)	1.50	7.546E-01	0.381

Table 2 Continued

		10-nonadecenoate (19:1n9)	2.08	5.591E-01	0.306
		eicosenoate (20:1)	1.24	9.468E-01	0.440
		erucate (22:1n9)	1.24	9.700E-01	0.445
	Long Chain Polyunsaturated Fatty Acid (n3 and n6)	eicosapentaenoate (EPA; 20:5n3)	7.71	1.698E-01	0.121
		heneicosapentaenoate (21:5n3)	**6.00**	8.550E-02	0.069
		docosapentaenoate (n3 DPA; 22:5n3)	6.82	1.369E-01	0.103
		docosahexaenoate (DHA; 22:6n3)	3.49	3.250E-01	0.204
		docosatrienoate (22:3n3)	2.37	6.166E-01	0.328
		nisinate (24:6n3)	2.25	5.518E-01	0.303
		hexadecadienoate (16:2n6)	1.61	5.112E-01	0.288
		linoleate (18:2n6)	2.46	4.573E-01	0.265
		linolenate [alpha or gamma; (18:3n3 or 6)]	1.41	6.969E-01	0.356
		dihomo-linoleate (20:2n6)	4.51	1.962E-01	0.136
		dihomo-linolenate (20:3n3 or n6)	3.18	2.404E-01	0.161
		arachidonate (20:4n6)	**8.11**	9.690E-02	0.076
		docosatrienoate (22:3n6)*	3.63	2.027E-01	0.139
		docosapentaenoate (n6 DPA; 22:5n6)	3.30	2.339E-01	0.157
		docosadienoate (22:2n6)	1.26	9.160E-01	0.433
		mead acid (20:3n9)	5.21	1.290E-01	0.098
	Fatty Acid, Branched	(12 or 13)-methylmyristate (a15:0 or i15:0)	1.07	9.402E-01	0.439
		(14 or 15)-methylpalmitate (a17:0 or i17:0)	1.26	9.816E-01	0.448
		(16 or 17)-methylstearate (a19:0 or i19:0)	1.21	9.358E-01	0.438
	Fatty Acid, Dicarboxylate	dimethylmalonic acid	1.54	1.644E-01	0.119
		glutarate (C5-DC)	1.09	6.824E-01	0.354
		2-hydroxyglutarate	**0.51**	5.000E-04	0.001
		2-hydroxyadipate	**1.67**	3.660E-02	0.036
		3-hydroxyadipate*	**1.42**	6.180E-02	0.053
		maleate	**0.72**	2.220E-02	0.023
		dodecadienoate (12:2)*	1.30	4.552E-01	0.264
	Fatty Acid Metabolism (also BCAA Metabolism)	butyrylcarnitine (C4)	**0.51**	1.000E-04	0.000
		propionylcarnitine (C3)	**0.57**	5.110E-05	0.000
		methylmalonate (MMA)	**1.87**	4.900E-03	0.007
	Fatty Acid Metabolism (Acyl Glycine)	N-palmitoylglycine	**0.28**	8.620E-02	0.070
	Fatty Acid Metabolism (Acyl Carnitine, Short Chain)	acetylcarnitine (C2)	**0.53**	3.000E-04	0.001
	Fatty Acid Metabolism (Acyl Carnitine, Medium Chain)	hexanoylcarnitine (C6)	**0.55**	1.600E-03	0.003
		octanoylcarnitine (C8)	**0.59**	2.550E-02	0.026
		decanoylcarnitine (C10)	0.74	3.327E-01	0.207
		laurylcarnitine (C12)	**0.46**	4.100E-03	0.006
	Fatty Acid Metabolism (Acyl Carnitine, Long Chain Saturated)	myristoylcarnitine (C14)	**0.26**	8.516E-06	0.000
		pentadecanoylcarnitine (C15)*	**0.56**	3.300E-02	0.032

Table 2 Continued

		palmitoylcarnitine (C16)	0.42	1.300E-03	0.002
		margaroylcarnitine (C17)*	0.92	7.562E-01	0.381
		stearoylcarnitine (C18)	0.83	5.493E-01	0.302
		arachidoylcarnitine (C20)*	0.65	1.435E-01	0.107
	Fatty Acid Metabolism (Acyl Carnitine, Monounsaturated)	cis-4-decenoylcarnitine (C10:1)	0.77	2.603E-01	0.172
		5-dodecenoylcarnitine (C12:1)	0.40	2.000E-03	0.003
		myristoleoylcarnitine (C14:1)*	0.52	3.180E-02	0.032
		palmitoleoylcarnitine (C16:1)*	0.30	8.000E-04	0.002
		oleoylcarnitine (C18:1)	0.44	1.470E-02	0.016
		eicosenoylcarnitine (C20:1)*	0.52	3.180E-02	0.032
		erucoylcarnitine (C22:1)*	0.70	1.259E-01	0.096
	Fatty Acid Metabolism (Acyl Carnitine, Polyunsaturated)	linoleoylcarnitine (C18:2)*	0.59	6.280E-02	0.054
		linolenoylcarnitine (C18:3)*	0.43	4.900E-03	0.007
		dihomo-linoleoylcarnitine (C20:2)*	0.70	2.750E-01	0.180
		arachidonoylcarnitine (C20:4)	0.58	9.280E-02	0.074
		dihomo-linolenoylcarnitine (C20:3n3 or 6)*	0.56	7.710E-02	0.064
		adrenoylcarnitine (C22:4)*	0.72	3.670E-01	0.223
		docosapentaenoylcarnitine (C22:5n3)*	0.65	4.109E-01	0.244
		docosahexaenoylcarnitine (C22:6)*	0.28	2.250E-02	0.024
	Fatty Acid Metabolism (Acyl Carnitine, Hydroxy)	(R)-3-hydroxybutyrylcarnitine	0.53	4.188E-05	0.000
		(S)-3-hydroxybutyrylcarnitine	0.36	2.340E-06	0.000
		3-hydroxyhexanoylcarnitine (1)	1.33	1.428E-01	0.107
		3-hydroxydecanoylcarnitine	1.05	6.544E-01	0.345
		3-hydroxypalmitoylcarnitine	0.71	1.553E-01	0.114
		3-hydroxyoleoylcarnitine	0.87	4.331E-01	0.253
	Carnitine Metabolism	deoxycarnitine	0.69	5.200E-03	0.007
		carnitine	0.47	1.000E-04	0.000
	Ketone Bodies	3-hydroxybutyrate (BHBA)	0.77	5.240E-02	0.047
	Fatty Acid Metabolism (Acyl Choline)	palmitoylcholine	5.15	5.000E-04	0.001
		oleoylcholine	3.86	6.000E-04	0.001
		palmitoloelycholine	2.66	8.400E-03	0.010
		linoleoylcholine*	1.90	5.120E-02	0.046
		docosahexaenoylcholine	6.46	6.452E-07	0.000
		arachidonoylcholine	1.52	3.270E-02	0.032
	Fatty Acid, Monohydroxy	4-hydroxybutyrate (GHB)	1.74	1.400E-03	0.002
		2-hydroxypalmitate	1.34	9.702E-01	0.445
		2-hydroxystearate	1.38	9.634E-01	0.444
		3-hydroxyhexanoate	1.31	4.003E-01	0.239
		3-hydroxyoctanoate	0.95	9.141E-01	0.433
		3-hydroxydecanoate	1.05	6.838E-01	0.354
		3-hydroxytridecanoate	1.07	9.162E-01	0.433

Table 2 Continued

		3-hydroxylaurate	1.04	7.625E-01	0.382
		3-hydroxymyristate	0.90	7.395E-01	0.375
		3-hydroxypalmitate	0.98	7.395E-01	0.375
		3-hydroxystearate	1.08	8.621E-01	0.417
		3-hydroxyoleate*	1.16	8.267E-01	0.405
		9-hydroxystearate	**0.24**	5.220E-02	0.047
	Fatty Acid, Dihydroxy	2S,3R-dihydroxybutyrate	0.96	8.701E-01	0.420
		2R,3R-dihydroxybutyrate	**0.58**	7.800E-03	0.010
		2,4-dihydroxybutyrate	0.98	9.765E-01	0.446
	Endocannabinoid	oleoyl ethanolamide	**2.15**	5.000E-04	0.001
		palmitoyl ethanolamide	**1.37**	6.740E-02	0.057
		stearoyl ethanolamide	**2.15**	6.000E-04	0.001
		arachidonoyl ethanolamide	**2.95**	2.970E-02	0.030
		N-myristoyltaurine*	**4.27**	1.840E-02	0.020
		N-arachidonoyltaurine	**10.42**	4.520E-02	0.042
		N-oleoyltaurine	**7.72**	5.150E-02	0.046
		N-stearoyltaurine	5.27	1.054E-01	0.082
		N-palmitoyltaurine	**6.33**	9.480E-02	0.075
		N-linoleoyltaurine*	**10.28**	3.960E-02	0.038
		linoleoyl ethanolamide	1.62	8.903E-01	0.427
		palmitoleoyl ethanolamide*	0.87	6.583E-01	0.345
		N-oleoylserine	1.64	5.583E-01	0.306
	Inositol Metabolism	myo-inositol	**0.48**	8.017E-07	0.000
		inositol 1-phosphate (I1P)	**2.32**	3.000E-04	0.001
	Phospholipid Metabolism	choline	**1.19**	2.740E-02	0.028
		choline phosphate	**1.69**	1.000E-03	0.002
		cytidine 5'-diphosphocholine	**1.56**	1.000E-04	0.000
		glycerophosphorylcholine (GPC)	**4.29**	4.159E-06	0.000
		phosphoethanolamine	**10.38**	5.707E-08	0.000
		cytidine-5'-diphosphoethanolamine	**2.02**	2.050E-06	0.000
		glycerophosphoethanolamine	**3.13**	6.434E-07	0.000
		glycerophosphoserine*	**0.81**	1.180E-02	0.014
		glycerophosphoinositol*	**0.82**	4.760E-02	0.044
		trimethylamine N-oxide	**0.54**	1.390E-06	0.000
	Phosphatidylcholine (PC)	1-myristoyl-2-palmitoyl-GPC (14:0/16:0)	0.87	2.250E-01	0.153
		1-myristoyl-2-arachidonoyl-GPC (14:0/20:4)*	**2.89**	5.208E-05	0.000
		1,2-dipalmitoyl-GPC (16:0/16:0)	0.85	2.309E-01	0.155
		1-palmitoyl-2-palmitoleoyl-GPC (16:0/16:1)*	**0.79**	6.420E-02	0.055
		1-palmitoyl-2-stearoyl-GPC (16:0/18:0)	1.07	6.751E-01	0.351
		1-palmitoyl-2-oleoyl-GPC (16:0/18:1)	1.03	7.647E-01	0.383

Table 2 Continued

		1-palmitoyl-2-arachidonoyl-GPC (16:0/20:4n6)	2.90	5.381E-05	0.000
		1-palmitoyl-2-docosahexaenoyl-GPC (16:0/22:6)	2.86	2.000E-04	0.000
		1-palmitoleoyl-2-linolenoyl-GPC (16:1/18:3)*	0.66	3.800E-03	0.005
		1-stearoyl-2-oleoyl-GPC (18:0/18:1)	1.20	1.796E-01	0.127
		1-stearoyl-2-linoleoyl-GPC (18:0/18:2)*	1.00	9.715E-01	0.445
		1-stearoyl-2-arachidonoyl-GPC (18:0/20:4)	3.32	1.431E-05	0.000
		1-stearoyl-2-docosahexaenoyl-GPC (18:0/22:6)	3.07	3.005E-05	0.000
		1,2-dioleoyl-GPC (18:1/18:1)	0.81	1.467E-01	0.109
		1-oleoyl-2-docosahexaenoyl-GPC (18:1/22:6)*	1.99	1.600E-03	0.003
		1,2-dilinoleoyl-GPC (18:2/18:2)	1.30	1.749E-01	0.125
	Phosphatidylethanolamine (PE)	1,2-dipalmitoyl-GPE (16:0/16:0)*	0.74	5.130E-02	0.046
		1-palmitoyl-2-oleoyl-GPE (16:0/18:1)	0.76	4.910E-02	0.045
		1-palmitoyl-2-arachidonoyl-GPE (16:0/20:4)*	1.23	1.660E-01	0.119
		1-palmitoyl-2-docosahexaenoyl-GPE (16:0/22:6)*	2.08	4.000E-04	0.001
		1-stearoyl-2-oleoyl-GPE (18:0/18:1)	1.02	9.223E-01	0.433
		1-stearoyl-2-arachidonoyl-GPE (18:0/20:4)	1.27	7.780E-02	0.064
		1-oleoyl-2-linoleoyl-GPE (18:1/18:2)*	1.08	5.434E-01	0.302
		1-oleoyl-2-arachidonoyl-GPE (18:1/20:4)*	1.63	6.600E-03	0.008
		1-oleoyl-2-docosahexaenoyl-GPE (18:1/22:6)*	1.83	7.000E-04	0.001
	Phosphatidylserine (PS)	1-palmitoyl-2-oleoyl-GPS (16:0/18:1)	0.63	9.900E-03	0.012
		1-stearoyl-2-oleoyl-GPS (18:0/18:1)	0.83	2.274E-01	0.154
		1-stearoyl-2-arachidonoyl-GPS (18:0/20:4)	1.60	2.560E-02	0.026
	Phosphatidylglycerol (PG)	1-palmitoyl-2-oleoyl-GPG (16:0/18:1)	1.16	5.663E-01	0.309
	Phosphatidylinositol (PI)	1-palmitoyl-2-oleoyl-GPI (16:0/18:1)*	0.98	9.375E-01	0.438
		1-palmitoyl-2-arachidonoyl-GPI (16:0/20:4)*	1.66	4.640E-02	0.043
		1-stearoyl-2-oleoyl-GPI (18:0/18:1)*	0.91	7.823E-01	0.389
		1-stearoyl-2-arachidonoyl-GPI (18:0/20:4)	1.24	6.699E-01	0.349
		1-oleoyl-2-arachidonoyl-GPI (18:1/20:4)*	1.46	9.110E-02	0.073
	Lysophospholipid	1-palmitoyl-GPC (16:0)	1.23	2.739E-01	0.179
		2-palmitoyl-GPC (16:0)*	1.16	9.415E-01	0.439
		1-palmitoleoyl-GPC (16:1)*	0.91	4.396E-01	0.257
		2-palmitoleoyl-GPC (16:1)*	0.78	5.300E-02	0.047
		1-stearoyl-GPC (18:0)	1.95	1.900E-03	0.003
		1-oleoyl-GPC (18:1)	1.07	7.994E-01	0.395
		1-lignoceroyl-GPC (24:0)	1.08	6.935E-01	0.356
		1-palmitoyl-GPE (16:0)	1.47	1.090E-01	0.084
		1-stearoyl-GPE (18:0)	1.95	2.200E-03	0.003
		2-stearoyl-GPE (18:0)*	0.97	9.602E-01	0.443

Table 2 Continued

		1-oleoyl-GPE (18:1)	**1.50**	1.300E-03	0.002
		1-linoleoyl-GPE (18:2)*	**1.37**	9.500E-03	0.011
		1-arachidonoyl-GPE (20:4n6)*	**1.42**	1.200E-03	0.002
		1-palmitoyl-GPS (16:0)*	1.86	5.476E-01	0.302
		1-stearoyl-GPS (18:0)*	**2.58**	1.300E-03	0.002
		1-oleoyl-GPS (18:1)	1.63	5.646E-01	0.309
		1-palmitoyl-GPG (16:0)*	0.78	5.480E-01	0.302
		1-stearoyl-GPG (18:0)	1.04	8.952E-01	0.428
		1-oleoyl-GPG (18:1)*	1.03	7.724E-01	0.385
		1-palmitoyl-GPI (16:0)	2.24	4.138E-01	0.245
		1-stearoyl-GPI (18:0)	1.63	6.295E-01	0.334
		1-oleoyl-GPI (18:1)	**1.98**	4.830E-02	0.044
		1-arachidonoyl-GPI (20:4)*	2.20	3.467E-01	0.214
	Plasmalogen	1-(1-enyl-palmitoyl)-2-oleoyl-GPE (P-16:0/18:1)*	0.88	3.003E-01	0.193
		1-(1-enyl-palmitoyl)-2-linoleoyl-GPE (P-16:0/18:2)*	0.93	5.335E-01	0.299
		1-(1-enyl-palmitoyl)-2-palmitoyl-GPC (P-16:0/16:0)*	**1.34**	7.580E-02	0.063
		1-(1-enyl-palmitoyl)-2-palmitoleoyl-GPC (P-16:0/16:1)*	1.06	6.958E-01	0.356
		1-(1-enyl-palmitoyl)-2-arachidonoyl-GPE (P-16:0/20:4)*	**1.35**	1.900E-02	0.020
		1-(1-enyl-palmitoyl)-2-oleoyl-GPC (P-16:0/18:1)*	**1.29**	9.970E-02	0.078
		1-(1-enyl-stearoyl)-2-oleoyl-GPE (P-18:0/18:1)	0.88	4.872E-01	0.279
		1-(1-enyl-palmitoyl)-2-arachidonoyl-GPC (P-16:0/20:4)*	**5.25**	6.756E-07	0.000
		1-(1-enyl-palmitoyl)-2-linoleoyl-GPC (P-16:0/18:2)*	**1.79**	6.600E-03	0.008
		1-(1-enyl-stearoyl)-2-arachidonoyl-GPE (P-18:0/20:4)*	**1.59**	3.100E-03	0.005
	Lysoplasmalogen	1-(1-enyl-palmitoyl)-GPC (P-16:0)*	**3.43**	1.440E-05	0.000
		1-(1-enyl-palmitoyl)-GPE (P-16:0)*	**2.35**	9.000E-04	0.002
		1-(1-enyl-oleoyl)-GPE (P-18:1)*	**2.36**	1.000E-03	0.002
		1-(1-enyl-stearoyl)-GPE (P-18:0)*	**2.83**	6.281E-05	0.000
	Glycerolipid Metabolism	glycerol	0.90	2.895E-01	0.187
		glycerol 3-phosphate	**1.86**	2.590E-02	0.026
		glycerophosphoglycerol	0.89	2.651E-01	0.174
	Monoacylglycerol	1-myristoylglycerol (14:0)	0.69	4.992E-01	0.284
		1-pentadecanoylglycerol (15:0)	1.13	9.427E-01	0.439
		1-palmitoylglycerol (16:0)	0.83	5.305E-01	0.297
		1-palmitoleoylglycerol (16:1)*	0.57	3.258E-01	0.204
		1-margaroylglycerol (17:0)	1.22	8.985E-01	0.428
		1-oleoylglycerol (18:1)	0.95	6.941E-01	0.356
		1-linoleoylglycerol (18:2)	1.31	9.677E-01	0.445
		1-dihomo-linolenylglycerol (20:3)	1.57	9.893E-01	0.451

Table 2 Continued

		1-arachidonylglycerol (20:4)	2.17	4.427E-01	0.258
		1-docosahexaenoylglycerol (22:6)	1.45	9.923E-01	0.452
		2-myristoylglycerol (14:0)	0.72	5.479E-01	0.302
		2-palmitoylglycerol (16:0)	0.95	7.658E-01	0.383
		2-palmitoleoylglycerol (16:1)*	0.65	5.071E-01	0.287
		2-oleoylglycerol (18:1)	1.07	8.570E-01	0.417
		2-linoleoylglycerol (18:2)	1.80	7.405E-01	0.375
		2-arachidonoylglycerol (20:4)	2.43	5.460E-01	0.302
		2-docosahexaenoylglycerol (22:6)*	1.75	7.586E-01	0.381
		1-heptadecenoylglycerol (17:1)*	0.97	7.726E-01	0.385
		2-heptadecenoylglycerol (17:1)*	1.42	8.861E-01	0.426
	Diacylglycerol	palmitoyl-oleoyl-glycerol (16:0/18:1) [2]*	**0.38**	4.000E-04	0.001
		oleoyl-arachidonoyl-glycerol (18:1/20:4) [2]*	1.33	6.146E-01	0.327
	Galactosyl Glycerolipids	galactosylglycerol	**0.65**	1.200E-03	0.002
	Sphingolipid Synthesis	3-ketosphinganine	**5.91**	2.306E-10	0.000
		sphinganine	**2.35**	5.000E-04	0.001
		sphingadienine	**3.00**	3.400E-03	0.005
		phytosphingosine	1.17	2.284E-01	0.155
	Dihydroceramides	N-palmitoyl-sphinganine (d18:0/16:0)	**3.08**	1.170E-02	0.014
		N-stearoyl-sphinganine (d18:0/18:0)*	**3.64**	1.420E-02	0.016
	Ceramides	N-palmitoyl-sphingosine (d18:1/16:0)	**2.33**	4.800E-03	0.007
		N-stearoyl-sphingosine (d18:1/18:0)*	**2.04**	8.600E-03	0.010
		N-palmitoyl-sphingadienine (d18:2/16:0)*	**1.87**	6.600E-03	0.008
		ceramide (d18:1/14:0, d16:1/16:0)*	**1.79**	1.420E-02	0.016
		ceramide (d18:1/17:0, d17:1/18:0)*	**3.31**	2.400E-03	0.004
		ceramide (d16:1/24:1, d18:1/22:1)*	1.88	5.181E-01	0.291
		ceramide (d18:2/24:1, d18:1/24:2)*	1.34	2.250E-01	0.153
	Hexosylceramides (HCER)	glycosyl-N-stearoyl-sphinganine (d18:0/18:0)*	**5.23**	2.300E-03	0.003
		glycosyl-N-palmitoyl-sphingosine (d18:1/16:0)	1.32	1.955E-01	0.136
		glycosyl-N-stearoyl-sphingosine (d18:1/18:0)	1.51	1.098E-01	0.084
		glycosyl-N-behenoyl-sphingadienine (d18:2/22:0)*	1.36	2.785E-01	0.182
		glycosyl ceramide (d18:1/20:0, d16:1/22:0)*	**2.13**	7.000E-03	0.009
		glycosyl ceramide (d16:1/24:1, d18:1/22:1)*	**2.52**	8.600E-03	0.010
		glycosyl ceramide (d18:1/23:1, d17:1/24:1)*	**1.67**	7.280E-02	0.061
		glycosyl ceramide (d18:2/24:1, d18:1/24:2)*	1.08	8.017E-01	0.395
	Lactosylceramides (LCER)	lactosyl-N-palmitoyl-sphingosine (d18:1/16:0)	**1.92**	2.000E-04	0.001
		lactosyl-N-stearoyl-sphingosine (d18:1/18:0)*	**2.07**	8.000E-04	0.002
		lactosyl-N-behenoyl-sphingosine (d18:1/22:0)*	**1.79**	1.590E-02	0.017
		lactosyl-N-nervonoyl-sphingosine (d18:1/24:1)*	**1.79**	2.500E-03	0.004

Table 2 Continued

	Dihydrosphingomyelins	myristoyl dihydrosphingomyelin (d18:0/14:0)*	1.59	3.720E-02	0.036
		palmitoyl dihydrosphingomyelin (d18:0/16:0)*	1.81	1.470E-02	0.016
		behenoyl dihydrosphingomyelin (d18:0/22:0)*	2.16	3.950E-02	0.038
		sphingomyelin (d18:0/18:0, d19:0/17:0)*	2.90	1.800E-03	0.003
		sphingomyelin (d18:0/20:0, d16:0/22:0)*	2.67	1.900E-03	0.003
	Sphingomyelins	palmitoyl sphingomyelin (d18:1/16:0)	1.37	2.330E-02	0.024
		stearoyl sphingomyelin (d18:1/18:0)	1.42	6.300E-03	0.008
		behenoyl sphingomyelin (d18:1/22:0)*	1.90	2.610E-02	0.026
		tricosanoyl sphingomyelin (d18:1/23:0)*	1.31	2.634E-01	0.173
		lignoceroyl sphingomyelin (d18:1/24:0)	1.42	1.973E-01	0.137
		sphingomyelin (d18:2/23:1)*	1.26	2.817E-01	0.183
		sphingomyelin (d18:2/24:2)*	0.91	6.481E-01	0.342
		sphingomyelin (d17:1/14:0, d16:1/15:0)*	1.10	6.643E-01	0.347
		sphingomyelin (d18:1/14:0, d16:1/16:0)*	1.28	1.349E-01	0.102
		sphingomyelin (d18:2/14:0, d18:1/14:1)*	0.81	1.899E-01	0.134
		sphingomyelin (d17:1/16:0, d18:1/15:0, d16:1/17:0)*	1.29	1.647E-01	0.119
		sphingomyelin (d17:2/16:0, d18:2/15:0)*	1.24	3.289E-01	0.205
		sphingomyelin (d18:2/16:0, d18:1/16:1)*	1.17	3.269E-01	0.205
		sphingomyelin (d18:1/17:0, d17:1/18:0, d19:1/16:0)	1.92	2.200E-03	0.003
		sphingomyelin (d18:1/18:1, d18:2/18:0)	1.10	4.098E-01	0.244
		sphingomyelin (d18:1/20:0, d16:1/22:0)*	1.76	3.900E-03	0.005
		sphingomyelin (d18:1/21:0, d17:1/22:0, d16:1/23:0)*	2.03	1.290E-02	0.015
		sphingomyelin (d18:1/22:1, d18:2/22:0, d16:1/24:1)*	1.37	9.860E-02	0.077
		sphingomyelin (d18:1/22:2, d18:2/22:1, d16:1/24:2)*	1.50	4.958E-01	0.283
		sphingomyelin (d18:2/23:0, d18:1/23:1, d17:1/24:1)*	1.38	1.925E-01	0.135
		sphingomyelin (d18:1/24:1, d18:2/24:0)*	1.23	3.718E-01	0.225
		sphingomyelin (d18:2/24:1, d18:1/24:2)*	0.98	8.964E-01	0.428
	Sphingosines	sphingosine	1.97	1.200E-02	0.014
		sphingosine 1-phosphate	1.58	4.440E-02	0.042
		hexadecasphingosine (d16:1)*	3.35	1.200E-03	0.002
		heptadecasphingosine (d17:1)	2.11	1.660E-02	0.018
		eicosanoylsphingosine (d20:1)*	4.11	2.000E-04	0.001
	Mevalonate Metabolism	3-hydroxy-3-methylglutarate	0.34	2.425E-09	0.000
	Sterol	cholesterol	0.95	5.815E-01	0.314
		7-dehydrocholesterol	3.44	7.249E-07	0.000
		4-cholesten-3-one	1.27	4.720E-01	0.272
		beta-sitosterol	1.70	1.500E-02	0.017
		campesterol	1.59	1.948E-01	0.136

Table 2 Continued

		7-hydroxycholesterol (alpha or beta)	1.61	1.840E-02	0.020
	Primary Bile Acid Metabolism	glycochenodeoxycholate	1.62	1.879E-01	0.133
		taurochenodeoxycholate	1.64	1.439E-01	0.107
	Secondary Bile Acid Metabolism	glycodeoxycholate	1.30	6.860E-01	0.354
Nucleotide	Purine Metabolism, (Hypo)Xanthine/Inosine containing)	AICA ribonucleotide	0.17	4.685E-05	0.000
		inosine 5'-monophosphate (IMP)	0.44	9.070E-02	0.073
		inosine	0.85	5.107E-01	0.288
		hypoxanthine	0.82	3.632E-01	0.221
		xanthine	1.02	7.842E-01	0.389
		xanthosine	1.56	6.010E-02	0.052
		N1-methylinosine	2.81	6.000E-04	0.001
		2'-deoxyinosine	0.12	3.792E-06	0.000
		urate	0.48	1.100E-03	0.002
		allantoin	0.80	1.130E-02	0.013
	Purine Metabolism, Adenine containing	adenosine 5'-triphosphate (ATP)	0.95	9.180E-01	0.433
		adenosine 5'-diphosphate (ADP)	1.00	8.198E-01	0.402
		adenosine 5'-monophosphate (AMP)	0.96	8.753E-01	0.422
		adenosine 3',5'-cyclic monophosphate (cAMP)	0.72	2.200E-03	0.003
		adenylosuccinate	0.51	5.200E-03	0.007
		adenosine	1.04	5.939E-01	0.319
		adenine	0.71	3.070E-02	0.031
		N1-methyladenosine	1.86	1.224E-05	0.000
		N6-methyladenosine	0.86	6.713E-01	0.349
		N6-carbamoylthreonyladenosine	1.15	8.380E-02	0.068
		2'-deoxyadenosine 5'-diphosphate	0.58	7.700E-03	0.010
		2'-deoxyadenosine 5'-monophosphate	0.04	6.235E-12	0.000
		2'-deoxyadenosine	0.24	2.000E-04	0.000
		diadenosine triphosphate	0.93	5.821E-01	0.314
		N6-succinyladenosine	1.16	3.533E-01	0.217
	Purine Metabolism, Guanine containing	guanosine 5'- diphosphate (GDP)	0.94	8.059E-01	0.397
		guanosine 5'- monophosphate (5'-GMP)	0.78	5.680E-02	0.050
		guanosine	0.76	1.927E-01	0.135
		guanine	1.39	1.185E-01	0.091
		7-methylguanine	0.60	6.049E-05	0.000
		N2-methylguanosine	1.21	1.059E-01	0.082
		N2,N2-dimethylguanosine	0.83	8.090E-02	0.066
		2'-deoxyguanosine	0.25	2.427E-05	0.000
	Pyrimidine Metabolism, Orotate containing	dihydroorotate	0.21	9.000E-03	0.011
		orotate	0.14	3.000E-04	0.001
		orotidine	0.02	4.900E-14	0.000

Table 2 Continued

	Pyrimidine Metabolism, Uracil containing	uridine 5'-triphosphate (UTP)	1.09	6.865E-01	0.354
		uridine 5'-diphosphate (UDP)	0.79	3.963E-01	0.238
		uridine 5'-monophosphate (UMP)	0.84	3.901E-01	0.235
		uridine 3'-monophosphate (3'-UMP)	**2.99**	6.800E-03	0.009
		uridine	**0.71**	1.540E-02	0.017
		uracil	0.67	1.892E-01	0.134
		pseudouridine	1.08	3.396E-01	0.210
		5,6-dihydrouridine	**1.36**	8.000E-04	0.001
		2'-O-methyluridine	1.11	3.174E-01	0.201
		5-methyluridine (ribothymidine)	**0.22**	1.196E-05	0.000
		2'-deoxyuridine	0.63	1.521E-01	0.112
		3-ureidopropionate	**0.22**	1.211E-09	0.000
		beta-alanine	**0.35**	1.419E-06	0.000
		3-(3-amino-3-carboxypropyl)uridine*	**0.59**	1.066E-05	0.000
	Pyrimidine Metabolism, Cytidine containing	cytidine triphosphate	1.69	2.915E-01	0.188
		cytidine diphosphate	**1.47**	7.830E-02	0.064
		cytidine 5'-monophosphate (5'-CMP)	**1.19**	6.650E-02	0.057
		cytidine	**1.30**	7.000E-02	0.059
		cytosine	**1.54**	2.770E-02	0.028
		3-methylcytidine	**1.86**	2.751E-05	0.000
		5-methylcytidine	**0.50**	9.964E-07	0.000
		2'-deoxycytidine 5'-monophosphate	**0.73**	4.660E-02	0.043
		2'-deoxycytidine	0.80	7.086E-01	0.362
		2'-O-methylcytidine	**1.94**	9.866E-06	0.000
	Pyrimidine Metabolism, Thymine containing	thymidine 5'-monophosphate	0.99	9.003E-01	0.428
		thymidine	1.31	1.510E-01	0.112
		thymine	**0.59**	1.450E-02	0.016
		5,6-dihydrothymine	**0.91**	6.200E-03	0.008
		3-aminoisobutyrate	0.74	1.125E-01	0.086
	Purine and Pyrimidine Metabolism	methylphosphate	**1.51**	3.270E-02	0.032
Cofactors and Vitamins	Nicotinate and Nicotinamide Metabolism	quinolinate	1.13	7.972E-01	0.394
		nicotinamide	0.96	9.494E-01	0.440
		nicotinamide ribonucleotide (NMN)	**0.64**	4.970E-02	0.045
		nicotinamide riboside	1.17	1.525E-01	0.112
		nicotinamide adenine dinucleotide (NAD+)	**0.77**	4.400E-03	0.006
		nicotinamide adenine dinucleotide reduced (NADH)	**0.57**	1.650E-02	0.018
		nicotinamide adenine dinucleotide phosphate reduced (NADPH)	0.66	3.726E-01	0.225
		1-methylnicotinamide	**1.33**	2.030E-02	0.021
		trigonelline (N'-methylnicotinate)	**0.73**	5.680E-02	0.050

Table 2 Continued

		adenosine 5'-diphosphoribose (ADP-ribose)	0.95	8.581E-01	0.417
	Riboflavin Metabolism	riboflavin (Vitamin B2)	**1.42**	2.000E-04	0.000
		flavin adenine dinucleotide (FAD)	1.02	6.927E-01	0.356
		flavin mononucleotide (FMN)	0.92	4.302E-01	0.252
	Pantothenate and CoA Metabolism	pantoate	**0.45**	3.477E-05	0.000
		pantothenate	0.92	3.631E-01	0.221
		pantetheine	**1.59**	2.900E-03	0.004
		phosphopantetheine	**1.76**	1.420E-02	0.016
		3'-dephosphocoenzyme A	**2.31**	3.900E-03	0.005
		coenzyme A	1.15	2.997E-01	0.193
	Ascorbate and Aldarate Metabolism	2-O-methylascorbic acid	1.00	9.660E-01	0.445
		threonate	1.00	1.000E+00	0.453
		gulonate*	**0.54**	4.711E-05	0.000
	Tocopherol Metabolism	alpha-tocopherol	1.04	7.237E-01	0.369
	Biotin Metabolism	biotin	0.84	5.854E-01	0.315
	Folate Metabolism	folate	1.00	1.000E+00	0.453
		5-methyltetrahydrofolate (5MeTHF)	**0.49**	1.000E-04	0.000
	Pterin Metabolism	pterin	0.73	3.395E-01	0.210
	Hemoglobin and Porphyrin Metabolism	bilirubin (Z,Z)	0.75	1.338E-01	0.101
	Thiamine Metabolism	thiamin (Vitamin B1)	**2.83**	1.975E-06	0.000
		thiamin monophosphate	1.50	1.782E-01	0.127
		thiamin diphosphate	1.50	1.073E-01	0.083
		5-(2-Hydroxyethyl)-4-methylthiazole	**2.57**	2.201E-05	0.000
	Vitamin A Metabolism	retinol (Vitamin A)	**1.73**	7.000E-04	0.001
	Vitamin B6 Metabolism	pyridoxine (Vitamin B6)	**0.04**	8.950E-13	0.000
		pyridoxamine	**0.66**	8.100E-03	0.010
		pyridoxamine phosphate	0.89	3.036E-01	0.194
		pyridoxal phosphate	**0.68**	2.000E-04	0.001
		pyridoxal	**0.56**	4.753E-05	0.000
		pyridoxate	**4.53**	5.221E-08	0.000
Xenobiotics	Benzoate Metabolism	hippurate	1.36	3.515E-01	0.216
		3-hydroxyhippurate	1.53	2.627E-01	0.173
		benzoate	0.70	1.609E-01	0.117
		catechol sulfate	1.60	1.350E-01	0.102
		guaiacol sulfate	**1.57**	3.800E-02	0.037
		4-methylcatechol sulfate	1.33	1.559E-01	0.114
		p-cresol sulfate	**1.68**	1.000E-04	0.000
	Food Component/Plant	3-formylindole	**1.44**	4.230E-02	0.040
		gluconate	0.59	3.388E-01	0.210
		beta-guanidinopropanoate	**0.53**	1.400E-03	0.002
		ergothioneine	**0.61**	1.040E-02	0.012

Table 2 Continued

		erythritol	**0.82**	6.600E-03	0.008
		homostachydrine*	**0.50**	7.727E-07	0.000
		mannonate*	**0.42**	1.754E-06	0.000
		stachydrine	**0.47**	6.798E-07	0.000
		methyl glucopyranoside (alpha + beta)	**3.31**	1.933E-06	0.000
		ethyl beta-glucopyranoside	0.35	4.159E-01	0.246
		2-aminophenol sulfate	**0.46**	8.000E-04	0.001
	Drug - Antibiotic	penicillin G	1.15	5.355E-01	0.299
	Chemical	sulfate*	0.84	7.547E-01	0.381
		O-sulfo-L-tyrosine	1.10	2.825E-01	0.183
		2,4-di-tert-butylphenol	0.79	9.538E-01	0.441
		phenol red	1.17	3.055E-01	0.195
		thioproline	1.01	9.527E-01	0.441
		4-chlorobenzoic acid	0.97	8.919E-01	0.427
Partially Characterized Molecules	Partially Characterized Molecules	branched-chain, straight-chain, or cyclopropyl 12:1 fatty acid*	1.04	9.218E-01	0.433

Table 3 Metabolomics dataset for VEM treated A375 cells.

Super Pathway	Sub Pathway	Biochemical Name	Fold Change	p-value	q-value
Amino Acid	Glycine, Serine and Threonine Metabolism	glycine	0.57	0.000	0.000
		sarcosine	0.06	0.000	0.000
		dimethylglycine	0.73	0.005	0.003
		betaine	0.66	0.000	0.000
		serine	1.10	0.237	0.085
		N-acetylserine	0.24	0.000	0.000
		threonine	0.86	0.174	0.064
		N-acetylthreonine	0.37	0.000	0.000
	Alanine and Aspartate Metabolism	alanine	0.87	0.160	0.060
		N-acetylalanine	0.35	0.000	0.000
		aspartate	1.77	0.000	0.000
		N-acetylaspartate (NAA)	0.62	0.000	0.000
		asparagine	1.17	0.080	0.032
		N-acetylasparagine	0.83	0.169	0.063
		hydroxyasparagine**	0.39	0.001	0.000
	Glutamate Metabolism	glutamate	1.03	0.589	0.187
		glutamine	0.61	0.003	0.002
		alpha-ketoglutaramate*	0.34	0.004	0.003
		N-acetylglutamate	0.24	0.000	0.000
		N-acetylglutamine	0.36	0.000	0.000
		4-hydroxyglutamate	0.24	0.000	0.000
		glutamate, gamma-methyl ester	0.34	0.000	0.000
		pyroglutamine*	0.30	0.000	0.000
		N-acetyl-aspartyl-glutamate (NAAG)	0.77	0.022	0.010
		beta-citrylglutamate	1.11	0.183	0.067
		carboxyethyl-GABA	9.71	0.000	0.000
		S-1-pyrroline-5-carboxylate	0.53	0.090	0.036
	Histidine Metabolism	histidine	1.34	0.007	0.004
		1-methylhistidine	1.15	0.267	0.094
		3-methylhistidine	0.40	0.000	0.000
		N-acetylhistidine	8.13	0.000	0.000
		N-acetyl-3-methylhistidine*	8.46	0.000	0.000
		N-acetyl-1-methylhistidine*	0.76	0.270	0.095
		trans-urocanate	1.32	0.193	0.071
		imidazole propionate	0.05	0.000	0.000
		formiminoglutamate	1.57	0.048	0.021
		imidazole lactate	0.06	0.000	0.000
		carnosine	1.49	0.001	0.001
		1-methyl-4-imidazoleacetate	0.75	0.011	0.006
		1-methyl-5-imidazoleacetate	0.09	0.000	0.000
		1-ribosyl-imidazoleacetate*	0.41	0.000	0.000

Table 3 Continued

		4-imidazoleacetate	**0.27**	0.000	0.000
		histidine methyl ester	0.91	0.338	0.116
	Lysine Metabolism	lysine	**1.83**	0.000	0.000
		N2-acetyllysine	**6.64**	0.000	0.000
		N6-acetyllysine	0.94	0.568	0.182
		N6-methyllysine	**1.63**	0.000	0.000
		N6,N6-dimethyllysine	0.95	0.450	0.148
		N6,N6,N6-trimethyllysine	0.96	0.667	0.208
		hydroxy-N6,N6,N6-trimethyllysine*	0.93	0.500	0.163
		5-hydroxylysine	**2.34**	0.000	0.000
		5-(galactosylhydroxy)-L-lysine	**4.20**	0.000	0.000
		fructosyllysine	1.41	0.288	0.100
		saccharopine	**3.50**	0.000	0.000
		2-aminoadipate	**2.29**	0.002	0.002
		glutarylcarnitine (C5-DC)	**9.63**	0.000	0.000
		pipecolate	**0.62**	0.000	0.000
		6-oxopiperidine-2-carboxylate	**0.70**	0.004	0.002
		cadaverine	**0.87**	0.006	0.004
		N-acetyl-cadaverine	**0.24**	0.007	0.004
		5-aminovalerate	**0.39**	0.000	0.000
		N,N,N-trimethyl-5-aminovalerate	0.99	0.896	0.270
	Phenylalanine Metabolism	phenylalanine	**1.21**	0.021	0.010
		N-acetylphenylalanine	**0.50**	0.000	0.000
		1-carboxyethylphenylalanine	**0.23**	0.000	0.000
		phenylpyruvate	1.37	0.395	0.132
		phenyllactate (PLA)	**0.40**	0.000	0.000
		phenethylamine	**5.48**	0.000	0.000
	Tyrosine Metabolism	tyrosine	**1.32**	0.016	0.008
		N-acetyltyrosine	**1.53**	0.000	0.000
		1-carboxyethyltyrosine	**0.09**	0.000	0.000
		4-hydroxyphenylpyruvate	**2.24**	0.000	0.000
		3-(4-hydroxyphenyl)lactate	**0.29**	0.000	0.000
		phenol sulfate	**1.48**	0.038	0.017
		3-methoxytyrosine	**0.69**	0.063	0.026
		o-Tyrosine	1.57	0.345	0.117
		O-methyltyrosine	**0.78**	0.009	0.005
	Tryptophan Metabolism	tryptophan	1.00	0.902	0.271
		N-acetyltryptophan	1.00	1.000	0.291
		C-glycosyltryptophan	**4.42**	0.000	0.000
		tryptophan betaine	**0.25**	0.000	0.000
		kynurenine	**0.81**	0.051	0.022
		kynurenate	**4.88**	0.000	0.000
		serotonin	**3.44**	0.000	0.000

Table 3 Continued

		tryptamine	1.39	0.244	0.087
		indolelactate	**0.61**	0.033	0.015
		indoleacetate	**1.92**	0.006	0.003
	Leucine, Isoleucine and Valine Metabolism	leucine	**1.28**	0.004	0.002
		N-acetylleucine	**0.48**	0.000	0.000
		1-carboxyethylleucine	**0.41**	0.000	0.000
		4-methyl-2-oxopentanoate	**0.47**	0.000	0.000
		alpha-hydroxyisocaproate	**0.45**	0.000	0.000
		isovalerylglycine	1.19	0.762	0.234
		isovalerylcarnitine (C5)	**1.56**	0.018	0.008
		beta-hydroxyisovalerate	**0.32**	0.000	0.000
		beta-hydroxyisovaleroylcarnitine	**2.84**	0.000	0.000
		3-methylglutaconate	1.08	0.391	0.131
		isoleucine	**1.26**	0.004	0.003
		N-acetylisoleucine	**0.46**	0.005	0.003
		1-carboxyethylisoleucine	**0.14**	0.000	0.000
		3-methyl-2-oxovalerate	**0.41**	0.006	0.003
		2-hydroxy-3-methylvalerate	**0.38**	0.000	0.000
		2-methylbutyrylcarnitine (C5)	**1.54**	0.008	0.004
		2-methylbutyrylglycine	0.75	0.114	0.044
		tiglylcarnitine (C5:1-DC)	**2.65**	0.000	0.000
		3-hydroxy-2-ethylpropionate	0.99	0.976	0.290
		ethylmalonate	**0.13**	0.000	0.000
		methylsuccinate	**0.77**	0.048	0.021
		valine	1.04	0.573	0.183
		N-acetylvaline	**0.60**	0.000	0.000
		1-carboxyethylvaline	**0.14**	0.000	0.000
		3-methyl-2-oxobutyrate	**0.45**	0.005	0.003
		alpha-hydroxyisovalerate	**0.23**	0.000	0.000
		isobutyrylcarnitine (C4)	**1.99**	0.000	0.000
		3-hydroxyisobutyrate	0.96	0.822	0.251
		2,3-dihydroxy-2-methylbutyrate	**0.35**	0.000	0.000
	Methionine, Cysteine, SAM and Taurine Metabolism	methionine	**1.26**	0.007	0.004
		N-acetylmethionine	**1.72**	0.001	0.001
		N-formylmethionine	1.03	0.759	0.233
		S-methylmethionine	1.23	0.370	0.125
		methionine sulfone	**0.41**	0.000	0.000
		methionine sulfoxide	**1.71**	0.002	0.001
		N-acetylmethionine sulfoxide	**5.35**	0.000	0.000
		S-adenosylmethionine (SAM)	**0.82**	0.037	0.016
		S-adenosylhomocysteine (SAH)	**0.66**	0.000	0.000
		2,3-dihydroxy-5-methylthio-4-pentenoate (DMTPA)*	**0.61**	0.000	0.000

Table 3 Continued

		homocysteine	**0.64**	0.023	0.011
		cystathionine	**0.15**	0.000	0.000
		cysteine	1.06	0.591	0.188
		N-acetylcysteine	**1.69**	0.010	0.005
		S-methylcysteine sulfoxide	**0.61**	0.041	0.018
		S-carboxyethylcysteine	**1.63**	0.001	0.001
		hypotaurine	0.93	0.437	0.145
		taurine	1.20	0.441	0.145
		N-acetyltaurine	**0.34**	0.000	0.000
	Urea cycle; Arginine and Proline Metabolism	arginine	**1.97**	0.000	0.000
		argininosuccinate	**0.66**	0.081	0.033
		ornithine	**1.75**	0.017	0.008
		3-amino-2-piperidone	**4.08**	0.000	0.000
		2-oxoarginine*	**1.25**	0.096	0.038
		citrulline	**0.78**	0.012	0.006
		proline	**0.52**	0.000	0.000
		dimethylarginine (SDMA + ADMA)	**1.58**	0.004	0.002
		N-acetylarginine	**1.31**	0.002	0.001
		N-delta-acetylornithine	**0.54**	0.000	0.000
		trans-4-hydroxyproline	0.88	0.243	0.087
		pro-hydroxy-pro	**0.37**	0.001	0.000
		N-methylproline	**0.73**	0.047	0.020
		N,N,N-trimethyl-alanylproline betaine (TMAP)	**5.00**	0.000	0.000
		N-monomethylarginine	**3.09**	0.000	0.000
	Creatine Metabolism	creatine	**1.22**	0.006	0.004
		creatinine	**1.29**	0.010	0.005
		creatine phosphate	**0.72**	0.010	0.005
	Polyamine Metabolism	putrescine	**0.07**	0.000	0.000
		N-acetylputrescine	**0.31**	0.007	0.004
		N-acetyl-isoputreanine	**4.13**	0.000	0.000
		spermidine	**0.48**	0.000	0.000
		N('1)-acetylspermidine	**0.12**	0.000	0.000
		diacetylspermidine*	1.00	1.000	0.291
		spermine	**1.95**	0.077	0.031
		N(1)-acetylspermine	0.82	0.155	0.058
		N1,N12-diacetylspermine	1.00	1.000	0.291
		5-methylthioadenosine (MTA)	**0.83**	0.021	0.010
		4-acetamidobutanoate	**1.45**	0.012	0.006
	Guanidino and Acetamido Metabolism	1-methylguanidine	1.00	0.985	0.291
		4-guanidinobutanoate	**0.27**	0.000	0.000
	Glutathione Metabolism	glutathione, reduced (GSH)	**1.22**	0.048	0.021
		glutathione, oxidized (GSSG)	1.07	0.440	0.145

Table 3 Continued

		cyclic dGSH	**0.84**	0.060	0.025
		cysteine-glutathione disulfide	1.48	0.124	0.048
		S-methylglutathione	**0.38**	0.000	0.000
		cysteinylglycine	**0.64**	0.000	0.000
		5-oxoproline	**0.84**	0.025	0.012
		2-hydroxybutyrate/2-hydroxyisobutyrate	**0.73**	0.000	0.000
		ophthalmate	**9.86**	0.000	0.000
		S-(1,2-dicarboxyethyl)glutathione	**0.37**	0.000	0.000
		4-hydroxy-nonenal-glutathione	**2.11**	0.000	0.000
		CoA-glutathione*	**2.53**	0.000	0.000
Peptide	**Gamma-glutamyl Amino Acid**	gamma-glutamylcysteine	**0.72**	0.010	0.005
		gamma-glutamylglutamate	**1.39**	0.019	0.009
		gamma-glutamylglutamine	**5.98**	0.000	0.000
		gamma-glutamylhistidine	**1.69**	0.064	0.027
		gamma-glutamylisoleucine*	**3.02**	0.000	0.000
		gamma-glutamylleucine	**4.72**	0.000	0.000
		gamma-glutamylmethionine	**2.55**	0.000	0.000
		gamma-glutamylphenylalanine	0.83	0.100	0.039
		gamma-glutamylthreonine	**10.50**	0.000	0.000
		gamma-glutamyltryptophan	1.00	1.000	0.291
		gamma-glutamyltyrosine	0.77	0.209	0.076
		gamma-glutamylvaline	**4.97**	0.000	0.000
	Dipeptide	alanylleucine	1.29	0.291	0.101
		glycylisoleucine	0.64	0.131	0.050
		glycylleucine	**1.44**	0.085	0.034
		glycylvaline	1.20	0.343	0.117
		isoleucylglycine	**2.98**	0.001	0.000
		leucylglycine	**2.67**	0.006	0.003
		phenylalanylalanine	**2.96**	0.001	0.001
		phenylalanylglycine	**3.01**	0.000	0.000
		prolylglycine	**0.73**	0.034	0.015
		threonylphenylalanine	1.00	1.000	0.291
		tryptophylglycine	**1.51**	0.085	0.034
		tyrosylglycine	**2.00**	0.010	0.005
		valylglutamine	1.13	0.472	0.155
		valylglycine	**3.04**	0.002	0.001
		valylleucine	**1.85**	0.096	0.038
		leucylglutamine*	**2.15**	0.004	0.002
	Acetylated Peptides	phenylacetylglycine	0.83	0.401	0.133
Carbohydrate	**Glycolysis, Gluconeogenesis, and Pyruvate Metabolism**	glucose	**51.27**	0.011	0.006
		glucose 6-phosphate	**30.81**	0.000	0.000
		fructose 1,6-diphosphate/glucose 1,6-diphosphate/myo-inositol diphosphates	**11.39**	0.000	0.000

Table 3 Continued

		dihydroxyacetone phosphate (DHAP)	2.35	0.866	0.263
		3-phosphoglycerate	0.91	0.592	0.188
		phosphoenolpyruvate (PEP)	16.43	0.000	0.000
		pyruvate	0.17	0.000	0.000
		lactate	1.06	0.520	0.169
		glycerate	5.03	0.000	0.000
	Pentose Phosphate Pathway	6-phosphogluconate	24.28	0.000	0.000
		sedoheptulose-7-phosphate	5.77	0.000	0.000
	Pentose Metabolism	ribose	2.49	0.001	0.001
		ribitol	0.15	0.000	0.000
		ribonate	0.23	0.000	0.000
		ribulose/xylulose	0.60	0.002	0.002
		arabinose	3.10	0.000	0.000
		arabitol/xylitol	0.94	0.504	0.164
		arabonate/xylonate	1.62	0.100	0.039
		ribulonate/xylulonate/lyxonate*	2.16	0.003	0.002
	Disaccharides and Oligosaccharides	lactose	9.93	0.000	0.000
	Fructose, Mannose and Galactose Metabolism	fructose	18.60	0.000	0.000
		mannitol/sorbitol	0.57	0.002	0.001
		mannose	9.42	0.262	0.093
		galactitol (dulcitol)	3.06	0.000	0.000
		galactonate	0.24	0.000	0.000
	Nucleotide Sugar	adenosine-5'-diphosphoglucose	7.34	0.000	0.000
		UDP-glucose	0.39	0.000	0.000
		UDP-galactose	0.81	0.092	0.036
		UDP-glucuronate	1.53	0.000	0.000
		guanosine 5'-diphospho-fucose	1.49	0.001	0.000
		UDP-N-acetylglucosamine/galactosamine	1.79	0.001	0.001
		cytidine 5'-monophospho-N-acetylneuraminic acid	0.71	0.003	0.002
	Aminosugar Metabolism	glucosamine-6-phosphate	118.21	0.000	0.000
		glucuronate	1.17	0.265	0.094
		N-acetylglucosamine 6-phosphate	7.44	0.000	0.000
		N-acetyl-glucosamine 1-phosphate	0.47	0.000	0.000
		N-acetylneuraminate	0.10	0.000	0.000
		N-acetylglucosaminylasparagine	0.89	0.078	0.032
		erythronate*	0.19	0.000	0.000
		N-acetylglucosamine/N-acetylgalactosamine	5.26	0.000	0.000
		N-glycolylneuraminate	0.09	0.000	0.000
	Advanced Glycation End-product	N6-carboxymethyllysine	0.99	0.611	0.193
Energy	**TCA Cycle**	citrate	2.29	0.000	0.000
		aconitate [cis or trans]	3.80	0.000	0.000

Table 3 Continued

		isocitrate	13.41	0.000	0.000
		alpha-ketoglutarate	0.38	0.000	0.000
		succinylcarnitine (C4-DC)	2.59	0.000	0.000
		succinate	0.68	0.000	0.000
		fumarate	0.91	0.383	0.129
		malate	1.12	0.187	0.069
		oxaloacetate	0.84	0.534	0.173
		2-methylcitrate/homocitrate	2.66	0.000	0.000
	Oxidative Phosphorylation	acetylphosphate	10.20	0.066	0.027
		phosphate	1.39	0.001	0.000
Lipid	**Fatty Acid Synthesis**	malonylcarnitine	6.35	0.000	0.000
	Fatty Acid Metabolism	acetyl CoA	3.62	0.001	0.001
		oleoyl CoA	1.85	0.014	0.007
		arachidonoyl CoA	2.47	0.002	0.001
	Short Chain Fatty Acid	butyrate/isobutyrate (4:0)	2.83	0.082	0.033
	Medium Chain Fatty Acid	heptanoate (7:0)	1.80	0.000	0.000
		(2 or 3)-decenoate (10:1n7 or n8)	1.43	0.181	0.067
		5-dodecenoate (12:1n7)	0.64	0.118	0.046
	Long Chain Saturated Fatty Acid	myristate (14:0)	1.72	0.341	0.117
		pentadecanoate (15:0)	3.53	0.035	0.015
		palmitate (16:0)	3.06	0.017	0.008
		margarate (17:0)	6.14	0.014	0.007
		stearate (18:0)	4.17	0.006	0.004
		nonadecanoate (19:0)	4.98	0.031	0.014
		arachidate (20:0)	2.57	0.144	0.054
	Long Chain Monounsaturated Fatty Acid	myristoleate (14:1n5)	1.14	0.676	0.211
		palmitoleate (16:1n7)	3.07	0.120	0.046
		10-heptadecenoate (17:1n7)	8.44	0.015	0.007
		oleate/vaccenate (18:1)	6.40	0.013	0.006
		10-nonadecenoate (19:1n9)	8.64	0.011	0.006
		eicosenoate (20:1)	4.16	0.057	0.024
		erucate (22:1n9)	2.63	0.139	0.053
	Long Chain Polyunsaturated Fatty Acid (n3 and n6)	eicosapentaenoate (EPA; 20:5n3)	34.92	0.003	0.002
		heneicosapentaenoate (21:5n3)	21.96	0.001	0.001
		docosapentaenoate (n3 DPA; 22:5n3)	35.48	0.002	0.001
		docosahexaenoate (DHA; 22:6n3)	13.02	0.009	0.005
		docosatrienoate (22:3n3)	7.69	0.030	0.014
		nisinate (24:6n3)	2.90	0.161	0.060
		hexadecadienoate (16:2n6)	6.56	0.006	0.003
		linoleate (18:2n6)	10.78	0.007	0.004
		linolenate [alpha or gamma; (18:3n3 or 6)]	2.75	0.099	0.039
		dihomo-linoleate (20:2n6)	16.02	0.003	0.002

Table 3 Continued

Table 3 Continued

		dihomo-linolenate (20:3n3 or n6)	**23.01**	0.001	0.001
		arachidonate (20:4n6)	**50.75**	0.001	0.001
		docosatrienoate (22:3n6)*	**11.09**	0.006	0.004
		docosapentaenoate (n6 DPA; 22:5n6)	**17.59**	0.002	0.001
		docosadienoate (22:2n6)	2.86	0.121	0.047
		mead acid (20:3n9)	**20.09**	0.002	0.001
	Fatty Acid, Branched	(12 or 13)-methylmyristate (a15:0 or i15:0)	2.24	0.107	0.042
		(14 or 15)-methylpalmitate (a17:0 or i17:0)	**4.69**	0.025	0.012
		(16 or 17)-methylstearate (a19:0 or i19:0)	**4.11**	0.050	0.021
	Fatty Acid, Dicarboxylate	dimethylmalonic acid	1.26	0.615	0.194
		glutarate (C5-DC)	0.96	0.540	0.175
		2-hydroxyglutarate	**0.55**	0.001	0.001
		2-hydroxyadipate	0.65	0.316	0.109
		3-hydroxyadipate*	1.28	0.137	0.052
		maleate	0.84	0.198	0.072
		dodecadienoate (12:2)*	**2.22**	0.011	0.005
	Fatty Acid Metabolism (also BCAA Metabolism)	butyrylcarnitine (C4)	**0.61**	0.001	0.001
		propionylcarnitine (C3)	0.94	0.479	0.157
		methylmalonate (MMA)	**2.20**	0.001	0.001
	Fatty Acid Metabolism (Acyl Glycine)	N-palmitoylglycine	**0.18**	0.035	0.015
	Fatty Acid Metabolism (Acyl Carnitine, Short Chain)	acetylcarnitine (C2)	1.05	0.940	0.281
	Fatty Acid Metabolism (Acyl Carnitine, Medium Chain)	hexanoylcarnitine (C6)	1.23	0.195	0.072
		octanoylcarnitine (C8)	1.37	0.221	0.080
		decanoylcarnitine (C10)	0.63	0.149	0.056
		laurylcarnitine (C12)	**0.41**	0.002	0.001
	Fatty Acid Metabolism (Acyl Carnitine, Long Chain Saturated)	myristoylcarnitine (C14)	**0.26**	0.000	0.000
		pentadecanoylcarnitine (C15)*	0.69	0.112	0.044
		palmitoylcarnitine (C16)	**0.40**	0.001	0.001
		margaroylcarnitine (C17)*	0.94	0.880	0.266
		stearoylcarnitine (C18)	0.86	0.611	0.193
		arachidoylcarnitine (C20)*	0.70	0.312	0.108
	Fatty Acid Metabolism (Acyl Carnitine, Monounsaturated)	cis-4-decenoylcarnitine (C10:1)	1.17	0.895	0.270
		5-dodecenoylcarnitine (C12:1)	0.70	0.157	0.059
		myristoleoylcarnitine (C14:1)*	0.94	0.916	0.275
		palmitoleoylcarnitine (C16:1)*	**0.50**	0.018	0.009
		oleoylcarnitine (C18:1)	0.69	0.165	0.062
		eicosenoylcarnitine (C20:1)*	**0.50**	0.031	0.014
		erucoylcarnitine (C22:1)*	0.80	0.316	0.109
	Fatty Acid Metabolism (Acyl Carnitine, Polyunsaturated)	linoleoylcarnitine (C18:2)*	1.56	0.147	0.056
		linolenoylcarnitine (C18:3)*	**0.47**	0.006	0.003
		dihomo-linoleoylcarnitine (C20:2)*	0.91	0.723	0.224

Table 3 Continued

		arachidonoylcarnitine (C20:4)	1.25	0.552	0.178
		dihomo-linolenoylcarnitine (C20:3n3 or 6)*	1.40	0.327	0.113
		adrenoylcarnitine (C22:4)*	1.33	0.550	0.177
		docosapentaenoylcarnitine (C22:5n3)*	1.20	0.747	0.231
		docosahexaenoylcarnitine (C22:6)*	**0.35**	0.045	0.020
	Fatty Acid Metabolism (Acyl Carnitine, Hydroxy)	(R)-3-hydroxybutyrylcarnitine	**1.68**	0.000	0.000
		(S)-3-hydroxybutyrylcarnitine	0.87	0.229	0.082
		3-hydroxyhexanoylcarnitine (1)	**3.41**	0.000	0.000
		3-hydroxydecanoylcarnitine	**1.75**	0.029	0.013
		3-hydroxypalmitoylcarnitine	**0.61**	0.054	0.023
		3-hydroxyoleoylcarnitine	1.30	0.339	0.116
	Carnitine Metabolism	deoxycarnitine	0.92	0.332	0.114
		carnitine	**1.72**	0.002	0.001
	Ketone Bodies	3-hydroxybutyrate (BHBA)	**1.58**	0.004	0.002
	Fatty Acid Metabolism (Acyl Choline)	palmitoylcholine	**3.00**	0.008	0.004
		oleoylcholine	**4.46**	0.000	0.000
		palmitoloelycholine	**3.24**	0.002	0.001
		linoleoylcholine*	**2.64**	0.002	0.002
		docosahexaenoylcholine	**7.30**	0.000	0.000
		arachidonoylcholine	1.00	1.000	0.291
	Fatty Acid, Monohydroxy	4-hydroxybutyrate (GHB)	0.84	0.216	0.078
		2-hydroxypalmitate	**2.86**	0.093	0.037
		2-hydroxystearate	**3.27**	0.067	0.028
		3-hydroxyhexanoate	1.01	0.902	0.271
		3-hydroxyoctanoate	1.01	0.937	0.281
		3-hydroxydecanoate	1.21	0.445	0.146
		3-hydroxytridecanoate	**2.61**	0.009	0.005
		3-hydroxylaurate	1.11	0.648	0.203
		3-hydroxymyristate	1.51	0.357	0.121
		3-hydroxypalmitate	2.20	0.236	0.085
		3-hydroxystearate	1.99	0.222	0.080
		3-hydroxyoleate*	**4.11**	0.077	0.031
		9-hydroxystearate	0.50	0.433	0.144
	Fatty Acid, Dihydroxy	2S,3R-dihydroxybutyrate	0.57	0.202	0.074
		2R,3R-dihydroxybutyrate	**0.61**	0.010	0.005
		2,4-dihydroxybutyrate	**0.39**	0.000	0.000
	Endocannabinoid	oleoyl ethanolamide	**3.55**	0.000	0.000
		palmitoyl ethanolamide	**1.69**	0.007	0.004
		stearoyl ethanolamide	**1.60**	0.023	0.011
		arachidonoyl ethanolamide	**3.13**	0.022	0.010
		N-myristoyltaurine*	**2.91**	0.036	0.016
		N-arachidonoyltaurine	**5.96**	0.053	0.022

Table 3 Continued

		N-oleoyltaurine	11.58	0.007	0.004
		N-stearoyltaurine	8.88	0.013	0.006
		N-palmitoyltaurine	9.83	0.013	0.006
		N-linoleoyltaurine*	7.98	0.026	0.012
		linoleoyl ethanolamide	4.89	0.068	0.028
		palmitoleoyl ethanolamide*	1.43	0.379	0.127
		N-oleoylserine	0.74	0.794	0.243
	Inositol Metabolism	myo-inositol	1.09	0.268	0.094
		inositol 1-phosphate (I1P)	6.60	0.000	0.000
	Phospholipid Metabolism	choline	2.03	0.000	0.000
		choline phosphate	1.04	0.637	0.200
		cytidine 5'-diphosphocholine	2.00	0.000	0.000
		glycerophosphorylcholine (GPC)	6.62	0.000	0.000
		phosphoethanolamine	37.36	0.000	0.000
		cytidine-5'-diphosphoethanolamine	2.98	0.000	0.000
		glycerophosphoethanolamine	3.64	0.000	0.000
		glycerophosphoserine*	0.42	0.000	0.000
		glycerophosphoinositol*	1.77	0.000	0.000
		trimethylamine N-oxide	0.55	0.000	0.000
	Phosphatidylcholine (PC)	1-myristoyl-2-palmitoyl-GPC (14:0/16:0)	1.51	0.004	0.003
		1-myristoyl-2-arachidonoyl-GPC (14:0/20:4)*	4.62	0.000	0.000
		1,2-dipalmitoyl-GPC (16:0/16:0)	1.84	0.001	0.000
		1-palmitoyl-2-palmitoleoyl-GPC (16:0/16:1)*	1.45	0.009	0.005
		1-palmitoyl-2-stearoyl-GPC (16:0/18:0)	1.31	0.153	0.058
		1-palmitoyl-2-oleoyl-GPC (16:0/18:1)	1.82	0.000	0.000
		1-palmitoyl-2-arachidonoyl-GPC (16:0/20:4n6)	5.92	0.000	0.000
		1-palmitoyl-2-docosahexaenoyl-GPC (16:0/22:6)	2.98	0.000	0.000
		1-palmitoleoyl-2-linolenoyl-GPC (16:1/18:3)*	0.18	0.000	0.000
		1-stearoyl-2-oleoyl-GPC (18:0/18:1)	2.19	0.000	0.000
		1-stearoyl-2-linoleoyl-GPC (18:0/18:2)*	2.17	0.000	0.000
		1-stearoyl-2-arachidonoyl-GPC (18:0/20:4)	11.00	0.000	0.000
		1-stearoyl-2-docosahexaenoyl-GPC (18:0/22:6)	5.43	0.000	0.000
		1,2-dioleoyl-GPC (18:1/18:1)	1.68	0.004	0.002
		1-oleoyl-2-docosahexaenoyl-GPC (18:1/22:6)*	2.91	0.000	0.000
		1,2-dilinoleoyl-GPC (18:2/18:2)	1.78	0.015	0.007
	Phosphatidylethanolamine (PE)	1,2-dipalmitoyl-GPE (16:0/16:0)*	1.52	0.023	0.011
		1-palmitoyl-2-oleoyl-GPE (16:0/18:1)	1.03	0.987	0.291
		1-palmitoyl-2-arachidonoyl-GPE (16:0/20:4)*	2.00	0.001	0.001

Table 3 Continued

		1-palmitoyl-2-docosahexaenoyl-GPE (16:0/22:6)*	3.73	0.000	0.000
		1-stearoyl-2-oleoyl-GPE (18:0/18:1)	2.03	0.000	0.000
		1-stearoyl-2-arachidonoyl-GPE (18:0/20:4)	3.33	0.000	0.000
		1-oleoyl-2-linoleoyl-GPE (18:1/18:2)*	1.31	0.051	0.022
		1-oleoyl-2-arachidonoyl-GPE (18:1/20:4)*	3.78	0.000	0.000
		1-oleoyl-2-docosahexaenoyl-GPE (18:1/22:6)*	5.98	0.000	0.000
	Phosphatidylserine (PS)	1-palmitoyl-2-oleoyl-GPS (16:0/18:1)	0.86	0.221	0.080
		1-stearoyl-2-oleoyl-GPS (18:0/18:1)	2.20	0.000	0.000
		1-stearoyl-2-arachidonoyl-GPS (18:0/20:4)	3.00	0.000	0.000
	Phosphatidylglycerol (PG)	1-palmitoyl-2-oleoyl-GPG (16:0/18:1)	2.31	0.011	0.005
	Phosphatidylinositol (PI)	1-palmitoyl-2-oleoyl-GPI (16:0/18:1)*	1.54	0.004	0.002
		1-palmitoyl-2-arachidonoyl-GPI (16:0/20:4)*	1.87	0.037	0.016
		1-stearoyl-2-oleoyl-GPI (18:0/18:1)*	1.68	0.547	0.177
		1-stearoyl-2-arachidonoyl-GPI (18:0/20:4)	3.79	0.001	0.001
		1-oleoyl-2-arachidonoyl-GPI (18:1/20:4)*	3.18	0.000	0.000
	Lysophospholipid	1-palmitoyl-GPC (16:0)	1.38	0.057	0.024
		2-palmitoyl-GPC (16:0)*	2.18	0.204	0.074
		1-palmitoleoyl-GPC (16:1)*	1.07	0.585	0.186
		2-palmitoleoyl-GPC (16:1)*	0.90	0.378	0.127
		1-stearoyl-GPC (18:0)	3.82	0.000	0.000
		1-oleoyl-GPC (18:1)	1.58	0.019	0.009
		1-lignoceroyl-GPC (24:0)	1.13	0.738	0.228
		1-palmitoyl-GPE (16:0)	1.81	0.033	0.015
		1-stearoyl-GPE (18:0)	3.50	0.000	0.000
		2-stearoyl-GPE (18:0)*	3.40	0.063	0.026
		1-oleoyl-GPE (18:1)	2.54	0.000	0.000
		1-linoleoyl-GPE (18:2)*	1.61	0.001	0.000
		1-arachidonoyl-GPE (20:4n6)*	3.38	0.000	0.000
		1-palmitoyl-GPS (16:0)*	0.40	0.376	0.127
		1-stearoyl-GPS (18:0)*	1.88	0.028	0.013
		1-oleoyl-GPS (18:1)	3.90	0.053	0.022
		1-palmitoyl-GPG (16:0)*	1.15	0.737	0.228
		1-stearoyl-GPG (18:0)	0.66	0.573	0.183
		1-oleoyl-GPG (18:1)*	1.23	0.144	0.054
		1-palmitoyl-GPI (16:0)	12.57	0.004	0.002
		1-stearoyl-GPI (18:0)	6.07	0.026	0.012
		1-oleoyl-GPI (18:1)	9.62	0.000	0.000
		1-arachidonoyl-GPI (20:4)*	47.22	0.000	0.000
	Plasmalogen	1-(1-enyl-palmitoyl)-2-oleoyl-GPE (P-16:0/18:1)*	1.97	0.000	0.000

Table 3 Continued

		1-(1-enyl-palmitoyl)-2-linoleoyl-GPE (P-16:0/18:2)*	1.56	0.004	0.002
		1-(1-enyl-palmitoyl)-2-palmitoyl-GPC (P-16:0/16:0)*	2.55	0.000	0.000
		1-(1-enyl-palmitoyl)-2-palmitoleoyl-GPC (P-16:0/16:1)*	1.67	0.005	0.003
		1-(1-enyl-palmitoyl)-2-arachidonoyl-GPE (P-16:0/20:4)*	2.79	0.000	0.000
		1-(1-enyl-palmitoyl)-2-oleoyl-GPC (P-16:0/18:1)*	1.60	0.011	0.006
		1-(1-enyl-stearoyl)-2-oleoyl-GPE (P-18:0/18:1)	2.07	0.006	0.004
		1-(1-enyl-palmitoyl)-2-arachidonoyl-GPC (P-16:0/20:4)*	11.29	0.000	0.000
		1-(1-enyl-palmitoyl)-2-linoleoyl-GPC (P-16:0/18:2)*	1.16	0.642	0.201
		1-(1-enyl-stearoyl)-2-arachidonoyl-GPE (P-18:0/20:4)*	4.54	0.000	0.000
	Lysoplasmalogen	1-(1-enyl-palmitoyl)-GPC (P-16:0)*	2.11	0.001	0.001
		1-(1-enyl-palmitoyl)-GPE (P-16:0)*	4.81	0.000	0.000
		1-(1-enyl-oleoyl)-GPE (P-18:1)*	6.81	0.000	0.000
		1-(1-enyl-stearoyl)-GPE (P-18:0)*	5.38	0.000	0.000
	Glycerolipid Metabolism	glycerol	0.81	0.033	0.015
		glycerol 3-phosphate	5.10	0.000	0.000
		glycerophosphoglycerol	0.96	0.714	0.222
	Monoacylglycerol	1-myristoylglycerol (14:0)	4.70	0.013	0.006
		1-pentadecanoylglycerol (15:0)	4.81	0.004	0.002
		1-palmitoylglycerol (16:0)	3.16	0.052	0.022
		1-palmitoleoylglycerol (16:1)*	4.74	0.044	0.019
		1-margaroylglycerol (17:0)	4.54	0.011	0.006
		1-oleoylglycerol (18:1)	6.97	0.016	0.008
		1-linoleoylglycerol (18:2)	11.77	0.002	0.002
		1-dihomo-linolenylglycerol (20:3)	26.02	0.002	0.001
		1-arachidonylglycerol (20:4)	48.16	0.000	0.000
		1-docosahexaenoylglycerol (22:6)	21.85	0.002	0.002
		2-myristoylglycerol (14:0)	4.22	0.028	0.013
		2-palmitoylglycerol (16:0)	3.66	0.486	0.159
		2-palmitoleoylglycerol (16:1)*	5.12	0.035	0.015
		2-oleoylglycerol (18:1)	6.46	0.020	0.009
		2-linoleoylglycerol (18:2)	14.44	0.005	0.003
		2-arachidonoylglycerol (20:4)	35.09	0.001	0.001
		2-docosahexaenoylglycerol (22:6)*	17.97	0.003	0.002
		1-heptadecenoylglycerol (17:1)*	6.26	0.021	0.010
		2-heptadecenoylglycerol (17:1)*	7.95	0.010	0.005
	Diacylglycerol	palmitoyl-oleoyl-glycerol (16:0/18:1) [2]*	0.21	0.000	0.000
		oleoyl-arachidonoyl-glycerol (18:1/20:4) [2]*	4.97	0.088	0.035

Table 3 Continued

	Galactosyl Glycerolipids	galactosylglycerol	**0.12**	0.000	0.000
	Sphingolipid Synthesis	3-ketosphinganine	0.93	0.438	0.145
		sphinganine	0.93	0.773	0.237
		sphingadienine	**6.26**	0.000	0.000
		phytosphingosine	0.74	0.102	0.040
	Dihydroceramides	N-palmitoyl-sphinganine (d18:0/16:0)	0.72	0.297	0.103
		N-stearoyl-sphinganine (d18:0/18:0)*	1.12	0.944	0.282
	Ceramides	N-palmitoyl-sphingosine (d18:1/16:0)	1.21	0.569	0.183
		N-stearoyl-sphingosine (d18:1/18:0)*	**2.69**	0.002	0.001
		N-palmitoyl-sphingadienine (d18:2/16:0)*	1.07	0.930	0.279
		ceramide (d18:1/14:0, d16:1/16:0)*	0.85	0.280	0.098
		ceramide (d18:1/17:0, d17:1/18:0)*	**2.10**	0.083	0.034
		ceramide (d16:1/24:1, d18:1/22:1)*	0.66	0.168	0.063
		ceramide (d18:2/24:1, d18:1/24:2)*	1.43	0.281	0.098
	Hexosylceramides (HCER)	glycosyl-N-stearoyl-sphinganine (d18:0/18:0)*	**4.95**	0.016	0.008
		glycosyl-N-palmitoyl-sphingosine (d18:1/16:0)	1.05	0.847	0.258
		glycosyl-N-stearoyl-sphingosine (d18:1/18:0)	**3.32**	0.001	0.001
		glycosyl-N-behenoyl-sphingadienine (d18:2/22:0)*	**1.79**	0.077	0.031
		glycosyl ceramide (d18:1/20:0, d16:1/22:0)*	**7.63**	0.000	0.000
		glycosyl ceramide (d16:1/24:1, d18:1/22:1)*	1.77	0.112	0.044
		glycosyl ceramide (d18:1/23:1, d17:1/24:1)*	**1.87**	0.091	0.036
		glycosyl ceramide (d18:2/24:1, d18:1/24:2)*	**1.82**	0.030	0.014
	Lactosylceramides (LCER)	lactosyl-N-palmitoyl-sphingosine (d18:1/16:0)	**1.93**	0.000	0.000
		lactosyl-N-stearoyl-sphingosine (d18:1/18:0)*	**4.49**	0.000	0.000
		lactosyl-N-behenoyl-sphingosine (d18:1/22:0)*	**3.90**	0.000	0.000
		lactosyl-N-nervonoyl-sphingosine (d18:1/24:1)*	**3.33**	0.000	0.000
	Dihydrosphingomyelins	myristoyl dihydrosphingomyelin (d18:0/14:0)*	**1.49**	0.092	0.036
		palmitoyl dihydrosphingomyelin (d18:0/16:0)*	**2.16**	0.005	0.003
		behenoyl dihydrosphingomyelin (d18:0/22:0)*	**2.09**	0.063	0.026
		sphingomyelin (d18:0/18:0, d19:0/17:0)*	**3.82**	0.001	0.001
		sphingomyelin (d18:0/20:0, d16:0/22:0)*	**2.29**	0.009	0.005
	Sphingomyelins	palmitoyl sphingomyelin (d18:1/16:0)	**2.26**	0.000	0.000
		stearoyl sphingomyelin (d18:1/18:0)	**4.80**	0.000	0.000
		behenoyl sphingomyelin (d18:1/22:0)*	**2.29**	0.015	0.008
		tricosanoyl sphingomyelin (d18:1/23:0)*	**1.97**	0.021	0.010

Table 3 Continued

		lignoceroyl sphingomyelin (d18:1/24:0)	2.51	0.007	0.004
		sphingomyelin (d18:2/23:1)*	2.03	0.007	0.004
		sphingomyelin (d18:2/24:2)*	1.56	0.069	0.028
		sphingomyelin (d17:1/14:0, d16:1/15:0)*	0.45	0.001	0.000
		sphingomyelin (d18:1/14:0, d16:1/16:0)*	1.09	0.763	0.234
		sphingomyelin (d18:2/14:0, d18:1/14:1)*	0.48	0.001	0.000
		sphingomyelin (d17:1/16:0, d18:1/15:0, d16:1/17:0)*	1.20	0.433	0.144
		sphingomyelin (d17:2/16:0, d18:2/15:0)*	1.05	0.859	0.261
		sphingomyelin (d18:2/16:0, d18:1/16:1)*	1.10	0.719	0.223
		sphingomyelin (d18:1/17:0, d17:1/18:0, d19:1/16:0)	3.91	0.000	0.000
		sphingomyelin (d18:1/18:1, d18:2/18:0)	2.97	0.000	0.000
		sphingomyelin (d18:1/20:0, d16:1/22:0)*	5.36	0.000	0.000
		sphingomyelin (d18:1/21:0, d17:1/22:0, d16:1/23:0)*	2.23	0.015	0.007
		sphingomyelin (d18:1/22:1, d18:2/22:0, d16:1/24:1)*	1.89	0.007	0.004
		sphingomyelin (d18:1/22:2, d18:2/22:1, d16:1/24:2)*	1.84	0.135	0.052
		sphingomyelin (d18:2/23:0, d18:1/23:1, d17:1/24:1)*	2.26	0.008	0.004
		sphingomyelin (d18:1/24:1, d18:2/24:0)*	2.57	0.002	0.001
		sphingomyelin (d18:2/24:1, d18:1/24:2)*	2.15	0.001	0.001
	Sphingosines	sphingosine	2.72	0.002	0.001
		sphingosine 1-phosphate	1.07	0.749	0.231
		hexadecasphingosine (d16:1)*	2.57	0.010	0.005
		heptadecasphingosine (d17:1)	2.40	0.009	0.005
		eicosanoylsphingosine (d20:1)*	1.37	0.362	0.123
	Mevalonate Metabolism	3-hydroxy-3-methylglutarate	0.22	0.000	0.000
	Sterol	cholesterol	1.16	0.138	0.053
		7-dehydrocholesterol	3.86	0.000	0.000
		4-cholesten-3-one	1.65	0.341	0.117
		beta-sitosterol	1.00	1.000	0.291
		campesterol	0.94	0.826	0.252
		7-hydroxycholesterol (alpha or beta)	1.99	0.003	0.002
	Primary Bile Acid Metabolism	glycochenodeoxycholate	1.00	1.000	0.291
		taurochenodeoxycholate	1.00	1.000	0.291
	Secondary Bile Acid Metabolism	glycodeoxycholate	1.00	1.000	0.291
Nucleotide	**Purine Metabolism, (Hypo)Xanthine/Inosine containing**	AICA ribonucleotide	0.19	0.000	0.000
		inosine 5'-monophosphate (IMP)	1.95	0.025	0.012
		inosine	1.57	0.016	0.008
		hypoxanthine	0.97	0.984	0.291
		xanthine	1.00	0.874	0.265

Table 3 Continued

		xanthosine	2.07	0.008	0.004
		N1-methylinosine	13.48	0.000	0.000
		2'-deoxyinosine	0.19	0.000	0.000
		urate	1.21	0.365	0.124
		allantoin	0.94	0.394	0.132
	Purine Metabolism, Adenine containing	adenosine 5'-triphosphate (ATP)	11.90	0.000	0.000
		adenosine 5'-diphosphate (ADP)	2.21	0.004	0.002
		adenosine 5'-monophosphate (AMP)	0.61	0.003	0.002
		adenosine 3',5'-cyclic monophosphate (cAMP)	0.38	0.000	0.000
		adenylosuccinate	0.19	0.000	0.000
		adenosine	0.86	0.626	0.197
		adenine	0.50	0.000	0.000
		N1-methyladenosine	4.12	0.000	0.000
		N6-methyladenosine	1.29	0.560	0.180
		N6-carbamoylthreonyladenosine	1.54	0.000	0.000
		2'-deoxyadenosine 5'-diphosphate	0.58	0.008	0.004
		2'-deoxyadenosine 5'-monophosphate	0.03	0.000	0.000
		2'-deoxyadenosine	0.47	0.005	0.003
		diadenosine triphosphate	1.08	0.600	0.190
		N6-succinyladenosine	0.93	0.621	0.195
	Purine Metabolism, Guanine containing	guanosine 5'- diphosphate (GDP)	9.15	0.000	0.000
		guanosine 5'- monophosphate (5'-GMP)	0.73	0.017	0.008
		guanosine	2.12	0.001	0.000
		guanine	1.19	0.250	0.089
		7-methylguanine	1.09	0.317	0.110
		N2-methylguanosine	2.41	0.000	0.000
		N2,N2-dimethylguanosine	1.93	0.000	0.000
		2'-deoxyguanosine	0.48	0.002	0.002
	Pyrimidine Metabolism, Orotate containing	dihydroorotate	0.16	0.003	0.002
		orotate	0.03	0.000	0.000
		orotidine	0.04	0.000	0.000
	Pyrimidine Metabolism, Uracil containing	uridine 5'-triphosphate (UTP)	12.44	0.000	0.000
		uridine 5'-diphosphate (UDP)	3.30	0.001	0.001
		uridine 5'-monophosphate (UMP)	0.73	0.076	0.031
		uridine 3'-monophosphate (3'-UMP)	3.89	0.001	0.001
		uridine	1.20	0.113	0.044
		uracil	0.40	0.003	0.002
		pseudouridine	1.97	0.000	0.000
		5,6-dihydrouridine	2.52	0.000	0.000
		2'-O-methyluridine	1.94	0.000	0.000
		5-methyluridine (ribothymidine)	0.47	0.002	0.002
		2'-deoxyuridine	7.77	0.000	0.000

Table 3 Continued

		3-ureidopropionate	**0.49**	0.000	0.000
		beta-alanine	**0.19**	0.000	0.000
		3-(3-amino-3-carboxypropyl)uridine*	**0.78**	0.004	0.003
	Pyrimidine Metabolism, Cytidine containing	cytidine triphosphate	**20.20**	0.000	0.000
		cytidine diphosphate	**4.18**	0.000	0.000
		cytidine 5'-monophosphate (5'-CMP)	**0.61**	0.000	0.000
		cytidine	**2.26**	0.000	0.000
		cytosine	**5.58**	0.000	0.000
		3-methylcytidine	**4.62**	0.000	0.000
		5-methylcytidine	1.12	0.154	0.058
		2'-deoxycytidine 5'-monophosphate	**0.19**	0.000	0.000
		2'-deoxycytidine	**0.24**	0.000	0.000
		2'-O-methylcytidine	**6.39**	0.000	0.000
	Pyrimidine Metabolism, Thymine containing	thymidine 5'-monophosphate	**0.09**	0.000	0.000
		thymidine	1.03	0.972	0.289
		thymine	**0.55**	0.008	0.004
		5,6-dihydrothymine	**0.91**	0.006	0.004
		3-aminoisobutyrate	**2.31**	0.000	0.000
	Purine and Pyrimidine Metabolism	methylphosphate	**1.50**	0.041	0.018
Cofactors and Vitamins	**Nicotinate and Nicotinamide Metabolism**	quinolinate	0.79	0.506	0.165
		nicotinamide	**2.00**	0.000	0.000
		nicotinamide ribonucleotide (NMN)	**1.61**	0.022	0.010
		nicotinamide riboside	**2.32**	0.000	0.000
		nicotinamide adenine dinucleotide (NAD+)	**0.84**	0.036	0.016
		nicotinamide adenine dinucleotide reduced (NADH)	**0.42**	0.001	0.001
		nicotinamide adenine dinucleotide phosphate reduced (NADPH)	**5.37**	0.001	0.001
		1-methylnicotinamide	**1.98**	0.000	0.000
		trigonelline (N'-methylnicotinate)	0.87	0.248	0.088
		adenosine 5'-diphosphoribose (ADP-ribose)	**9.84**	0.000	0.000
	Riboflavin Metabolism	riboflavin (Vitamin B2)	**1.14**	0.071	0.029
		flavin adenine dinucleotide (FAD)	**1.40**	0.002	0.001
		flavin mononucleotide (FMN)	0.89	0.275	0.096
	Pantothenate and CoA Metabolism	pantoate	**1.50**	0.008	0.005
		pantothenate	**1.38**	0.003	0.002
		pantetheine	**3.29**	0.000	0.000
		phosphopantetheine	1.21	0.226	0.082
		3'-dephosphocoenzyme A	**1.94**	0.017	0.008
		coenzyme A	1.22	0.198	0.072
	Ascorbate and Aldarate Metabolism	2-O-methylascorbic acid	**1.87**	0.000	0.000
		threonate	**1.37**	0.012	0.006
		gulonate*	**0.07**	0.000	0.000

Table 3 Continued

	Tocopherol Metabolism	alpha-tocopherol	0.95	0.580	0.185
	Biotin Metabolism	biotin	0.73	0.268	0.094
	Folate Metabolism	folate	1.00	1.000	0.291
		5-methyltetrahydrofolate (5MeTHF)	**0.35**	0.000	0.000
	Pterin Metabolism	pterin	**2.01**	0.023	0.011
	Hemoglobin and Porphyrin Metabolism	bilirubin (Z,Z)	**0.52**	0.007	0.004
	Thiamine Metabolism	thiamin (Vitamin B1)	**3.69**	0.000	0.000
		thiamin monophosphate	**20.97**	0.000	0.000
		thiamin diphosphate	**1.84**	0.052	0.022
		5-(2-Hydroxyethyl)-4-methylthiazole	**3.55**	0.000	0.000
	Vitamin A Metabolism	retinol (Vitamin A)	**7.71**	0.000	0.000
	Vitamin B6 Metabolism	pyridoxine (Vitamin B6)	**1.30**	0.030	0.014
		pyridoxamine	**1.80**	0.002	0.001
		pyridoxamine phosphate	**1.93**	0.000	0.000
		pyridoxal phosphate	1.01	0.980	0.291
		pyridoxal	**1.52**	0.001	0.001
		pyridoxate	**5.33**	0.000	0.000
Xenobiotics	**Benzoate Metabolism**	hippurate	**3.92**	0.000	0.000
		3-hydroxyhippurate	**3.72**	0.005	0.003
		benzoate	1.38	0.244	0.087
		catechol sulfate	**3.05**	0.001	0.001
		guaiacol sulfate	1.44	0.113	0.044
		4-methylcatechol sulfate	**3.24**	0.000	0.000
		p-cresol sulfate	**3.65**	0.000	0.000
	Food Component/Plant	3-formylindole	**1.61**	0.013	0.006
		gluconate	**5.99**	0.000	0.000
		beta-guanidinopropanoate	**0.57**	0.003	0.002
		ergothioneine	0.80	0.140	0.053
		erythritol	**0.55**	0.000	0.000
		homostachydrine*	**0.46**	0.000	0.000
		mannonate*	**0.74**	0.008	0.004
		stachydrine	**0.57**	0.000	0.000
		methyl glucopyranoside (alpha + beta)	**6.36**	0.000	0.000
		ethyl beta-glucopyranoside	1.00	0.942	0.281
		2-aminophenol sulfate	**0.28**	0.000	0.000
	Drug - Antibiotic	penicillin G	**3.43**	0.000	0.000
	Chemical	sulfate*	**6.30**	0.000	0.000
		O-sulfo-L-tyrosine	**0.65**	0.000	0.000
		2,4-di-tert-butylphenol	1.29	0.394	0.132
		phenol red	**2.69**	0.000	0.000
		thioproline	**1.63**	0.000	0.000
		4-chlorobenzoic acid	**2.19**	0.020	0.009

Table 3 Continued

Partially Characterized Molecules	**Partially Characterized Molecules**	branched-chain, straight-chain, or cyclopropyl 12:1 fatty acid*	1.35	0.318	0.110

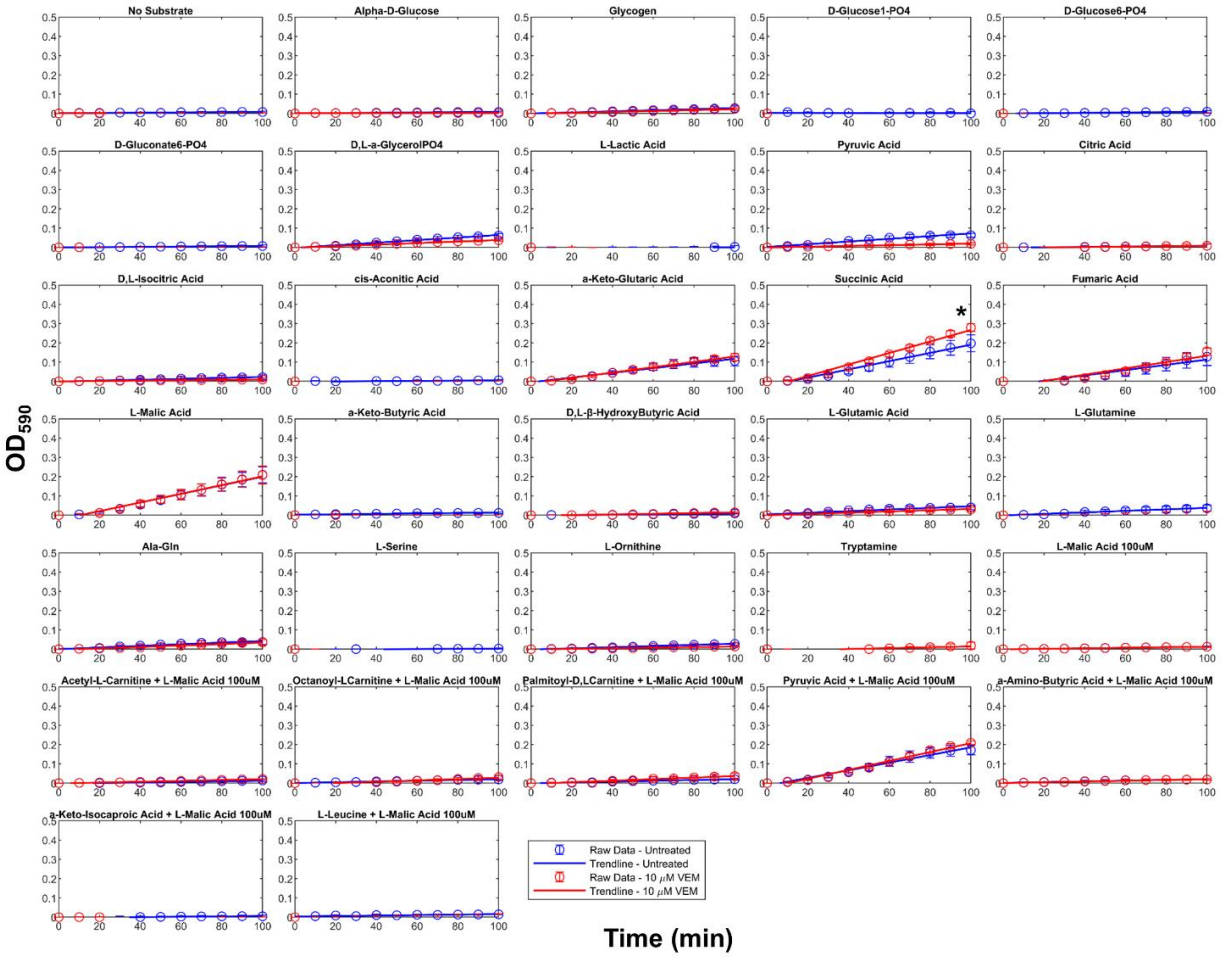

Figure 5.1 Mitoplate assays to assess the mitochondrial activities of VEM persister cells. The consumption rates of substrates were monitored by measuring the OD590 at the indicated time points. Statistical analysis was performed using a linear regression analysis (F-Statistics, *P<0.001). N = 4.

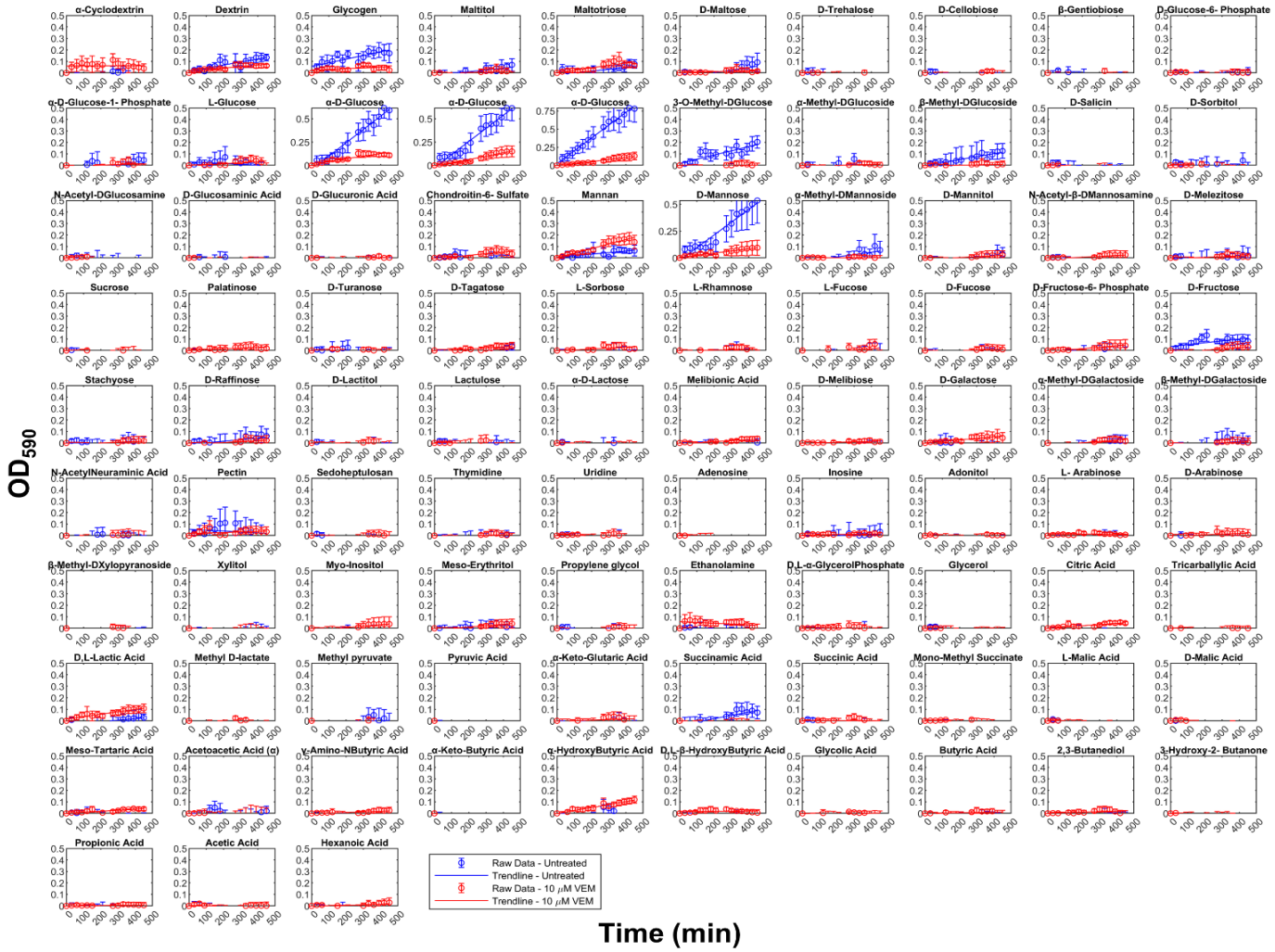

Figure 5.2 Phenotype microarray (PM-M1) assays to assess the metabolism of VEM persister cells.

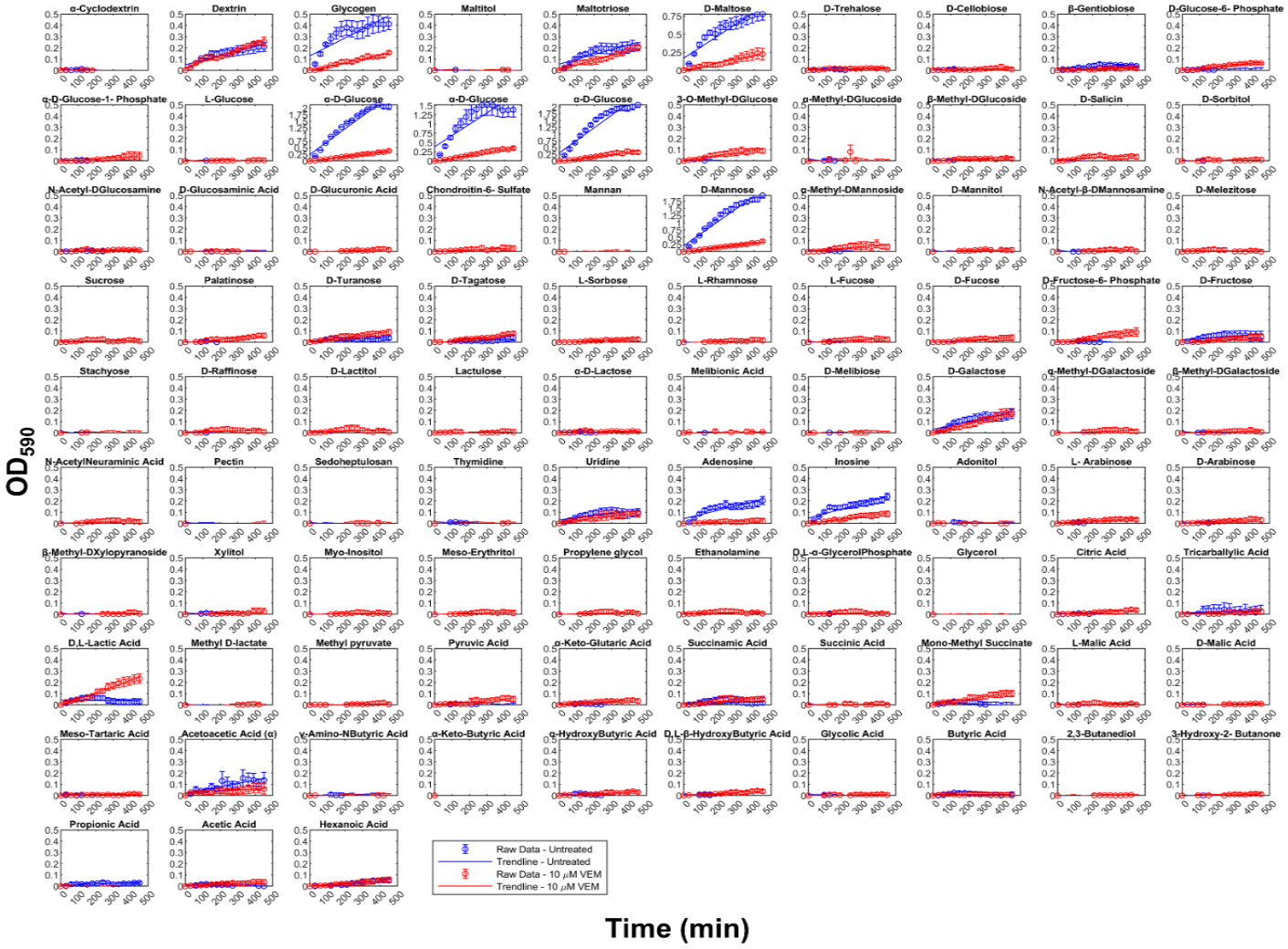

Figure 5.3 Phenotype microarray (PM-M1) assays (24h incubation) to assess the metabolism of VEM persister cells.

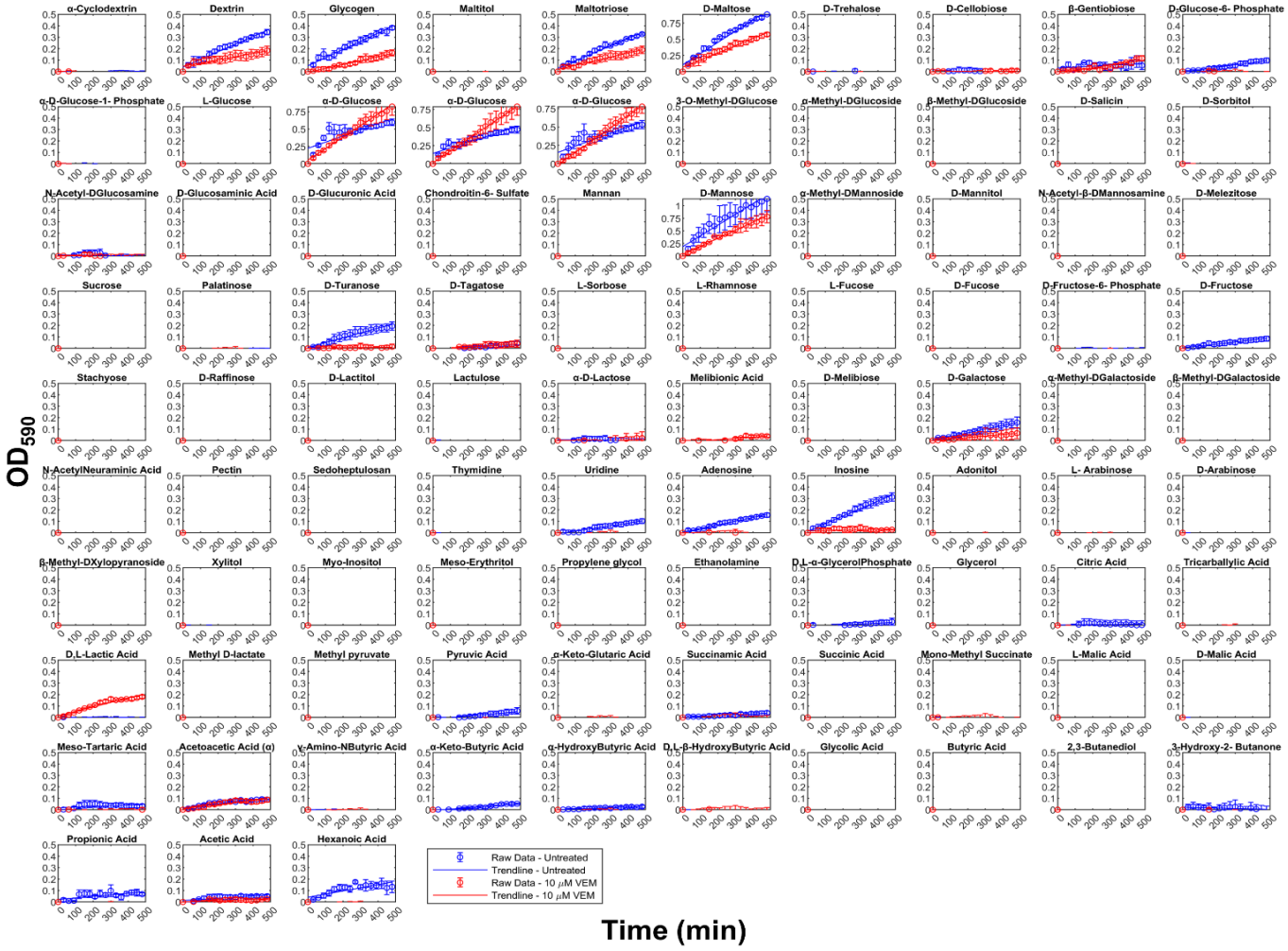

Figure 5.4 Phenotype microarray (PM-M1) assays (48h incubation) to assess the metabolism of VEM persister cells

References

(1) Siegel, R. L.; Miller, K. D.; Fuchs, H. E.; Jemal, A. Cancer Statistics, 2021. *CA. Cancer J. Clin.* **2021**, *71* (1), 7–33. https://doi.org/10.3322/caac.21654.

(2) Hassanpour, S. H.; Dehghani, M. Review of Cancer from Perspective of Molecular. *J. Cancer Res. Pract.* **2017**, *4* (4), 127–129. https://doi.org/10.1016/J.JCRPR.2017.07.001.

(3) Antwi, S. O.; Eckert, E. C.; Sabaque, C. V.; Leof, E. R.; Hawthorne, K. M.; Bamlet, W. R.; Chaffee, K. G.; Oberg, A. L.; Petersen, G. M. Exposure to Environmental Chemicals and Heavy Metals, and Risk of Pancreatic Cancer. *Cancer Causes Control* **2015**, *26* (11), 1583–1591. https://doi.org/10.1007/s10552-015-0652-y.

(4) Trafialek, J.; Kolanowski, W. Dietary Exposure to Meat-Related Carcinogenic Substances: Is There a Way to Estimate the Risk? *International Journal of Food Sciences and Nutrition*. Taylor & Francis 2014, pp 774–780. https://doi.org/10.3109/09637486.2014.917146.

(5) Aizawa, K.; Liu, C.; Tang, S.; Veeramachaneni, S.; Hu, K. Q.; Smith, D. E.; Wang, X. D. Tobacco Carcinogen Induces Both Lung Cancer and Non-Alcoholic Steatohepatitis and Hepatocellular Carcinomas in Ferrets Which Can Be Attenuated by Lycopene Supplementation. *Int. J. Cancer* **2016**, *139* (5), 1171–1181. https://doi.org/10.1002/ijc.30161.

(6) Domingues, B.; Lopes, J.; Soares, P.; Populo, H. Melanoma Treatment in Review. *ImmunoTargets Ther.* **2018**, *Volume 7*, 35–49. https://doi.org/10.2147/itt.s134842.

(7) Jemal, A.; Siegel, R.; Miller, K. D. Home | American Cancer Society - Cancer Facts & Statistics https://cancerstatisticscenter.cancer.org/?_ga=2.242081546.925338221.1599614578-

1606375298.1599614578#!/ (accessed Sep 8, 2020).

(8) SEER. Melanoma of the Skin - Cancer Stat Facts https://seer.cancer.gov/statfacts/html/melan.html (accessed Jul 26, 2021).

(9) Feigelson, H. S.; Powers, J. D.; Kumar, M.; Carroll, N. M.; Pathy, A.; Ritzwoller, D. P. Melanoma Incidence, Recurrence, and Mortality in an Integrated Healthcare System: A Retrospective Cohort Study. *Cancer Med.* **2019**, *8* (9), 4508–4516. https://doi.org/10.1002/cam4.2252.

(10) Davies, H.; Bignell, G. R.; Cox, C.; Stephens, P.; Edkins, S.; Clegg, S.; Teague, J.; Woffendin, H.; Garnett, M. J.; Bottomley, W.; Davis, N.; Dicks, E.; Ewing, R.; Floyd, Y.; Gray, K.; Hall, S.; Hawes, R.; Hughes, J.; Kosmidou, V.; Menzies, A.; Mould, C.; Parker, A.; Stevens, C.; Watt, S.; Hooper, S.; Jayatilake, H.; Gusterson, B. A.; Cooper, C.; Shipley, J.; Hargrave, D.; Pritchard-Jones, K.; Maitland, N.; Chenevix-Trench, G.; Riggins, G. J.; Bigner, D. D.; Palmieri, G.; Cossu, A.; Flanagan, A.; Nicholson, A.; Ho, J. W. C.; Leung, S. Y.; Yuen, S. T.; Weber, B. L.; Seigler, H. F.; Darrow, T. L.; Paterson, H.; Wooster, R.; Stratton, M. R.; Futreal, P. A. Mutations of the BRAF Gene in Human Cancer. *Nature* **2002**, *417* (6892), 949–954. https://doi.org/10.1038/nature00766.

(11) Roberts, R. The Extracellular Signal-Regulated Kinase (ERK) Pathway: A Potential Therapeutic Target in Hypertension. *J. Exp. Pharmacol.* **2012**, *4*, 77. https://doi.org/10.2147/jep.s28907.

(12) Batus, M.; Waheed, S.; Ruby, C.; Petersen, L.; Bines, S. D.; Kaufman, H. L. Optimal Management of Metastatic Melanoma: Current Strategies and Future Directions. *American Journal of Clinical Dermatology*. NIH Public Access June 2013, pp 179–194. https://doi.org/10.1007/s40257-013-0025-9.

(13) van Zeijl, M. C. T.; van den Eertwegh, A. J.; Haanen, J. B.; Wouters, M. W. J. M.

(Neo)Adjuvant Systemic Therapy for Melanoma. *European Journal of Surgical Oncology*. Eur J Surg Oncol March 1, 2017, pp 534–543. https://doi.org/10.1016/j.ejso.2016.07.001.

(14) Wilson, M. A.; Schuchter, L. M. Chemotherapy for Melanoma. In *Cancer Treatment and Research*; Springer, Cham, 2016; Vol. 167, pp 209–229. https://doi.org/10.1007/978-3-319-22539-5_8.

(15) Nygren, P. What Is Cancer Chemotherapy? *Acta Oncologica*. Taylor & Francis 2001, pp 166–174. https://doi.org/10.1080/02841860151116204.

(16) Nakamura, H.; Maeda, H. Cancer Chemotherapy. In *Fundamentals of Pharmaceutical Nanoscience*; StatPearls Publishing, 2013; pp 401–427. https://doi.org/10.1007/978-1-4614-9164-4_15.

(17) Kim, C.; Lee, C. W.; Kovacic, L.; Shah, A.; Klasa, R.; Savage, K. J. Long-Term Survival in Patients with Metastatic Melanoma Treated with DTIC or Temozolomide. *Oncologist* **2010**, *15* (7), 765–771. https://doi.org/10.1634/theoncologist.2009-0237.

(18) Middleton, M. R.; Grob, J. J.; Aaronson, N.; Fierlbeck, G.; Tilgen, W.; Seiter, S.; Gore, M.; Aamdal, S.; Cebon, J.; Coates, A.; Dreno, B.; Henz, M.; Schadendorf, D.; Kapp, A.; Weiss, J.; Fraass, U.; Statkevich, P.; Muller, M.; Thatcher, N. Randomized Phase III Study of Temozolomide versus Dacarbazine in the Treatment of Patients with Advanced Metastatic Malignant Melanoma. *J. Clin. Oncol.* **2000**, *18* (1), 158–166. https://doi.org/10.1200/jco.2000.18.1.158.

(19) Carter, S. K.; Friedman, M. A. 5-(3,3-Dimethyl-1-Triazeno)-Imidazole-4-Carboxamide (DTIC, DIC, NSC-45388)-A New Antitumor Agent with Activity against Malignant Melanoma. *Eur. J. Cancer* **1972**, *8* (1), 85–92. https://doi.org/10.1016/0014-2964(72)90087-4.

(20) Nathanson, L.; Wolter, J.; Horton, J.; Colsky, J.; Shnider, B. I.; Schilling, A. Characteristics of Prognosis and Response to an Imidazole Carboxamide in Malignant Melanoma. *Clin. Pharmacol. Ther.* **1971**, *12* (6), 955–962. https://doi.org/10.1002/cpt1971126955.

(21) Eggermont, A. M. M.; Kirkwood, J. M. Re-Evaluating the Role of Dacarbazine in Metastatic Melanoma: What Have We Learned in 30 Years? *Eur. J. Cancer* **2004**, *40* (12), 1825–1836. https://doi.org/10.1016/j.ejca.2004.04.030.

(22) Vasan, N.; Baselga, J.; Hyman, D. M. A View on Drug Resistance in Cancer. *Nature*. Nature Publishing Group November 13, 2019, pp 299–309. https://doi.org/10.1038/s41586-019-1730-1.

(23) Bosl, G. J.; Gluckman, R.; Geller, N. L.; Golbey, R. B.; Whitmore, W. F.; Herr, H.; Sogani, P.; Morse, M.; Martini, N.; Bains, M. VAB-6: An Effective Chemotherapy Regimen for Patients with Germ-Cell Tumors. *J. Clin. Oncol.* **1986**, *4* (10), 1493–1499. https://doi.org/10.1200/JCO.1986.4.10.1493.

(24) Bonadonna, G.; Brusamolino, E.; Valagussa, P.; Rossi, A.; Brugnatelli, L.; Brambilla, C.; De Lena, M.; Tancini, G.; Bajetta, E.; Musumeci, R.; Veronesi, U. Combination Chemotherapy as an Adjuvant Treatment in Operable Breast Cancer. *N. Engl. J. Med.* **1976**, *294* (8), 405–410. https://doi.org/10.1056/nejm197602192940801.

(25) DeVita, V. T.; Simon, R. M.; Hubbard, S. M. Curability of Advanced Hodgkin's Disease with Chemotherapy. Long-Term Follow-up of MOPP-Treated Patients at the National Cancer Institute. *Ann. Intern. Med.* **1980**, *92* (5), 587–595. https://doi.org/10.7326/0003-4819-92-5-587.

(26) Phi, L. T. H.; Sari, I. N.; Yang, Y. G.; Lee, S. H.; Jun, N.; Kim, K. S.; Lee, Y. K.; Kwon, H. Y. Cancer Stem Cells (CSCs) in Drug Resistance and Their Therapeutic Implications in

Cancer Treatment. *Stem Cells Int.* **2018**, *2018*. https://doi.org/10.1155/2018/5416923.

(27) Alexandrov, L. B.; Nik-Zainal, S.; Wedge, D. C.; Aparicio, S. A. J. R.; Behjati, S.; Biankin, A. V.; Bignell, G. R.; Bolli, N.; Borg, A.; Børresen-Dale, A. L.; Boyault, S.; Burkhardt, B.; Butler, A. P.; Caldas, C.; Davies, H. R.; Desmedt, C.; Eils, R.; Eyfjörd, J. E.; Foekens, J. A.; Greaves, M.; Hosoda, F.; Hutter, B.; Ilicic, T.; Imbeaud, S.; Imielinsk, M.; Jäger, N.; Jones, D. T. W.; Jonas, D.; Knappskog, S.; Koo, M.; Lakhani, S. R.; López-Otín, C.; Martin, S.; Munshi, N. C.; Nakamura, H.; Northcott, P. A.; Pajic, M.; Papaemmanuil, E.; Paradiso, A.; Pearson, J. V.; Puente, X. S.; Raine, K.; Ramakrishna, M.; Richardson, A. L.; Richter, J.; Rosenstiel, P.; Schlesner, M.; Schumacher, T. N.; Span, P. N.; Teague, J. W.; Totoki, Y.; Tutt, A. N. J.; Valdés-Mas, R.; Van Buuren, M. M.; Van 'T Veer, L.; Vincent-Salomon, A.; Waddell, N.; Yates, L. R.; Zucman-Rossi, J.; Andrew Futreal, P.; McDermott, U.; Lichter, P.; Meyerson, M.; Grimmond, S. M.; Siebert, R.; Campo, E.; Shibata, T.; Pfister, S. M.; Campbell, P. J.; Stratton, M. R. Signatures of Mutational Processes in Human Cancer. *Nature* **2013**, *500* (7463), 415–421. https://doi.org/10.1038/nature12477.

(28) Junttila, M. R.; De Sauvage, F. J. Influence of Tumour Micro-Environment Heterogeneity on Therapeutic Response. *Nature*. 2013, pp 346–354. https://doi.org/10.1038/nature12626.

(29) Dong, N.; Shi, L.; Wang, D. C.; Chen, C.; Wang, X. Role of Epigenetics in Lung Cancer Heterogeneity and Clinical Implication. *Seminars in Cell and Developmental Biology*. Academic Press April 1, 2017, pp 18–25. https://doi.org/10.1016/j.semcdb.2016.08.029.

(30) Rich, J. N. Cancer Stem Cells: Understanding Tumor Hierarchy and Heterogeneity. *Medicine (United States)*. Wolters Kluwer Health 2016, pp S2–S7. https://doi.org/10.1097/MD.0000000000004764.

(31) Sharma, S. V.; Lee, D. Y.; Li, B.; Quinlan, M. P.; Takahashi, F.; Maheswaran, S.;

McDermott, U.; Azizian, N.; Zou, L.; Fischbach, M. A.; Wong, K. K.; Brandstetter, K.; Wittner, B.; Ramaswamy, S.; Classon, M.; Settleman, J. A Chromatin-Mediated Reversible Drug-Tolerant State in Cancer Cell Subpopulations. *Cell* **2010**, *141* (1), 69–80. https://doi.org/10.1016/j.cell.2010.02.027.

(32) Hangauer, M. J.; Viswanathan, V. S.; Ryan, M. J.; Bole, D.; Eaton, J. K.; Matov, A.; Galeas, J.; Dhruv, H. D.; Berens, M. E.; Schreiber, S. L.; McCormick, F.; McManus, M. T. Drug-Tolerant Persister Cancer Cells Are Vulnerable to GPX4 Inhibition. *Nature* **2017**, *551* (7679), 247–250. https://doi.org/10.1038/nature24297.

(33) Roesch, A.; Fukunaga-Kalabis, M.; Schmidt, E. C.; Zabierowski, S. E.; Brafford, P. A.; Vultur, A.; Basu, D.; Gimotty, P.; Vogt, T.; Herlyn, M. A Temporarily Distinct Subpopulation of Slow-Cycling Melanoma Cells Is Required for Continuous Tumor Growth. *Cell* **2010**, *141* (4), 583–594. https://doi.org/10.1016/j.cell.2010.04.020.

(34) Karki, P.; Angardi, V.; Mier, J. C.; Orman, M. A. A Transient Metabolic State In Melanoma Persister Cells Mediated By Chemotherapeutic Treatments. *bioRxiv* **2021**, 2021.02.21.432154. https://doi.org/10.1101/2021.02.21.432154.

(35) Rehman, S.; Haynes, J.; Collignon, E.; Cell, K. B.-; 2021, U. Colorectal Cancer Cells Enter a Diapause-like DTP State to Survive Chemotherapy | Elsevier Enhanced Reader https://www.sciencedirect.com/science/article/pii/S009286742031535X (accessed Apr 11, 2022).

(36) Dhimolea, E.; Simoes, R. de M.; Cell, D. K.-C.; 2021, U. An Embryonic Diapause-like Adaptation with Suppressed Myc Activity Enables Tumor Treatment Persistence. *Elsevier*.

(37) Shaffer, S. M.; Dunagin, M. C.; Torborg, S. R.; Torre, E. A.; Emert, B.; Krepler, C.; Beqiri, M.; Sproesser, K.; Brafford, P. A.; Xiao, M.; Eggan, E.; Anastopoulos, I. N.;

Vargas-Garcia, C. A.; Singh, A.; Nathanson, K. L.; Herlyn, M.; Raj, A. Rare Cell Variability and Drug-Induced Reprogramming as a Mode of Cancer Drug Resistance. *Nature* **2017**, *546* (7658), 431–435. https://doi.org/10.1038/nature22794.

(38) Echeverria, G. V.; Ge, Z.; Seth, S.; Zhang, X.; Jeter-Jones, S.; Zhou, X.; Cai, S.; Tu, Y.; McCoy, A.; Peoples, M.; Sun, Y.; Qiu, H.; Chang, Q.; Bristow, C.; Carugo, A.; Shao, J.; Ma, X.; Harris, A.; Mundi, P.; Lau, R.; Ramamoorthy, V.; Wu, Y.; Alvarez, M. J.; Califano, A.; Moulder, S. L.; Symmans, W. F.; Marszalek, J. R.; Heffernan, T. P.; Chang, J. T.; Piwnica-Worms, H. Resistance to Neoadjuvant Chemotherapy in Triple-Negative Breast Cancer Mediated by a Reversible Drug-Tolerant State. *Sci. Transl. Med.* **2019**, *11* (488), 936. https://doi.org/10.1126/scitranslmed.aav0936.

(39) Mikubo, M.; Inoue, Y.; Liu, G.; Tsao, M. S. Mechanism of Drug Tolerant Persister Cancer Cells: The Landscape and Clinical Implication for Therapy. *Journal of Thoracic Oncology*. Elsevier August 3, 2021. https://doi.org/10.1016/j.jtho.2021.07.017.

(40) Raha, D.; Wilson, T. R.; Peng, J.; Peterson, D.; Yue, P.; Evangelista, M.; Wilson, C.; Merchant, M.; Settleman, J. The Cancer Stem Cell Marker Aldehyde Dehydrogenase Is Required to Maintain a Drug-Tolerant Tumor Cell Subpopulation. *Cancer Res.* **2014**, *74* (13), 3579–3590. https://doi.org/10.1158/0008-5472.CAN-13-3456.

(41) Roesch, A.; Vultur, A.; Bogeski, I.; Wang, H.; Zimmermann, K. M.; Speicher, D.; Körbel, C.; Laschke, M. W.; Gimotty, P. A.; Philipp, S. E.; Krause, E.; Pätzold, S.; Villanueva, J.; Krepler, C.; Fukunaga-Kalabis, M.; Hoth, M.; Bastian, B. C.; Vogt, T.; Herlyn, M. Overcoming Intrinsic Multidrug Resistance in Melanoma by Blocking the Mitochondrial Respiratory Chain of Slow-Cycling JARID1Bhigh Cells. *Cancer Cell* **2013**, *23* (6), 811–825. https://doi.org/10.1016/j.ccr.2013.05.003.

(42) Liau, B. B.; Sievers, C.; Donohue, L. K.; Gillespie, S. M.; Flavahan, W. A.; Miller, T. E.;

Venteicher, A. S.; Hebert, C. H.; Carey, C. D.; Rodig, S. J.; Shareef, S. J.; Najm, F. J.; van Galen, P.; Wakimoto, H.; Cahill, D. P.; Rich, J. N.; Aster, J. C.; Suvà, M. L.; Patel, A. P.; Bernstein, B. E. Adaptive Chromatin Remodeling Drives Glioblastoma Stem Cell Plasticity and Drug Tolerance. *Cell Stem Cell* **2017**, *20* (2), 233-246.e7. https://doi.org/10.1016/j.stem.2016.11.003.

(43) Menon, D. R.; Das, S.; Krepler, C.; Vultur, A.; Rinner, B.; Schauer, S.; Kashofer, K.; Wagner, K.; Zhang, G.; Bonyadi Rad, E.; Haass, N. K.; Soyer, H. P.; Gabrielli, B.; Somasundaram, R.; Hoefler, G.; Herlyn, M.; Schaider, H. A Stress-Induced Early Innate Response Causes Multidrug Tolerance in Melanoma. *Oncogene* **2015**, *34* (34), 4448–4459. https://doi.org/10.1038/onc.2014.372.

(44) Kurppa, K. J.; Liu, Y.; Long, H. W.; Gray, N. S.; J€ Anne Correspondence, P. A.; To, C.; Zhang, T.; Fan, M.; Vajdi, A.; Knelson, E. H.; Xie, Y.; Lim, K.; Cejas, P.; Portell, A.; Lizotte, P. H.; Ficarro, S. B.; Li, S.; Chen, T.; Haikala, H. M.; Wang, H.; Bahcall, M.; Gao, Y.; Shalhout, S.; Boettcher, S.; Shin, B. H.; Thai, T.; Wilkens, M. K.; Tillgren, M. L.; Mushajiang, M.; Xu, M.; Choi, J. Treatment-Induced Tumor Dormancy through YAP-Mediated Transcriptional Reprogramming of the Apoptotic Pathway Article Treatment-Induced Tumor Dormancy through YAP-Mediated Transcriptional Reprogramming of the Apoptotic Pathway. *Cancer Cell* **2019**, *37*, 104–122.

(45) Braeken, K.; Moris, M.; Daniels, R.; Vanderleyden, J.; Michiels, J. New Horizons for (p)PpGpp in Bacterial and Plant Physiology. *Trends in Microbiology*. January 2006, pp 45–54. https://doi.org/10.1016/j.tim.2005.11.006.

(46) Klose, R. J.; Yan, Q.; Tothova, Z.; Yamane, K.; Erdjument-Bromage, H.; Tempst, P.; Gilliland, D. G.; Zhang, Y.; Kaelin, W. G. The Retinoblastoma Binding Protein RBP2 Is an H3K4 Demethylase. *Cell* **2007**, *128* (5), 889–900.

https://doi.org/10.1016/j.cell.2007.02.013.

(47) Aloia, A.; Müllhaupt, D.; Chabbert, C. D.; Eberhart, T.; Flückiger-Mangual, S.; Vukolic, A.; Eichhoff, O.; Irmisch, A.; Alexander, L. T.; Scibona, E.; Frederick, D. T.; Miao, B.; Tian, T.; Cheng, C.; Kwong, L. N.; Wei, Z.; Sullivan, R. J.; Boland, G. M.; Herlyn, M.; Flaherty, K. T.; Zamboni, N.; Dummer, R.; Zhang, G.; Levesque, M. P.; Krek, W.; Kovacs, W. J. A Fatty Acid Oxidation-Dependent Metabolic Shift Regulates the Adaptation of BRAF-Mutated Melanoma to MAPK Inhibitors. *Clin. Cancer Res.* **2019**, *25* (22), 6852–6867. https://doi.org/10.1158/1078-0432.CCR-19-0253.

(48) American Cancer Society https://www.cancer.org/cancer/melanoma-skin-cancer/treating/by-stage.html (accessed Apr 2, 2021). https://doi.org/10.2310/6650.2001.33798.

(49) Woods, D.; Turchi, J. J. Chemotherapy Induced DNA Damage Response. *Cancer Biol. Ther.* **2013**, *14* (5), 379–389. https://doi.org/10.4161/cbt.23761.

(50) Liu, J.; Zhang, C.; Hu, W.; Feng, Z. Tumor Suppressor P53 and Metabolism. *Journal of Molecular Cell Biology*. Oxford University Press April 1, 2019, pp 284–292. https://doi.org/10.1093/jmcb/mjy070.

(51) He, G.; Siddik, Z. H.; Huang, Z.; Wang, R.; Koomen, J.; Kobayashi, R.; Khokhar, A. R.; Kuang, J. Induction of P21 by P53 Following DNA Damage Inhibits Both Cdk4 and Cdk2 Activities. *Oncogene* **2005**, *24* (18), 2929–2943. https://doi.org/10.1038/sj.onc.1208474.

(52) Reinhardt, H. C.; Aslanian, A. S.; Lees, J. A.; Yaffe, M. B. P53-Deficient Cells Rely on ATM- and ATR-Mediated Checkpoint Signaling through the P38MAPK/MK2 Pathway for Survival after DNA Damage. *Cancer Cell* **2007**, *11* (2), 175–189. https://doi.org/10.1016/j.ccr.2006.11.024.

(53) Hanahan, D.; Weinberg, R. A. Hallmarks of Cancer: The next Generation. *Cell*. Cell March 4, 2011, pp 646–674. https://doi.org/10.1016/j.cell.2011.02.013.

(54) Warburg, O. The Metabolism of Carcinoma Cells 1. *J. Cancer Res.* **1925**, *9* (1), 148–163. https://doi.org/10.1158/jcr.1925.148.

(55) Liberti, M. V.; Locasale, J. W. The Warburg Effect: How Does It Benefit Cancer Cells? *Trends in Biochemical Sciences*. Elsevier Ltd March 1, 2016, pp 211–218. https://doi.org/10.1016/j.tibs.2015.12.001.

(56) Warburg, O. Tests on Surviving Carcinoma Cultures. *Biochem. Z.* **1923**, *142*, 317–333.

(57) Shen, S.; Faouzi, S.; Souquere, S.; Roy, S.; Routier, E.; Libenciuc, C.; André, F.; Pierron, G.; Scoazec, J. Y.; Robert, C. Melanoma Persister Cells Are Tolerant to BRAF/MEK Inhibitors via ACOX1-Mediated Fatty Acid Oxidation. *Cell Rep.* **2020**, *33* (8). https://doi.org/10.1016/j.celrep.2020.108421.

(58) Viale, A.; Pettazzoni, P.; Lyssiotis, C. A.; Ying, H.; Sánchez, N.; Marchesini, M.; Carugo, A.; Green, T.; Seth, S.; Giuliani, V.; Kost-Alimova, M.; Muller, F.; Colla, S.; Nezi, L.; Genovese, G.; Deem, A. K.; Kapoor, A.; Yao, W.; Brunetto, E.; Kang, Y.; Yuan, M.; Asara, J. M.; Wang, Y. A.; Heffernan, T. P.; Kimmelman, A. C.; Wang, H.; Fleming, J. B.; Cantley, L. C.; DePinho, R. A.; Draetta, G. F. Oncogene Ablation-Resistant Pancreatic Cancer Cells Depend on Mitochondrial Function. *Nature* **2014**, *514* (7524), 628–632. https://doi.org/10.1038/nature13611.

(59) Wang, L.; Yang, Q.; Peng, S.; Liu, X. The Combination of the Glycolysis Inhibitor 2-DG and Sorafenib Can Be Effective against Sorafenib-Tolerant Persister Cancer Cells. *Onco. Targets. Ther.* **2019**, *12*, 5359–5373. https://doi.org/10.2147/OTT.S212465.

(60) Shen, S.; Faouzi, S.; Bastide, A.; Martineau, S.; Malka-Mahieu, H.; Fu, Y.; Sun, X.;

Mateus, C.; Routier, E.; Roy, S.; Desaubry, L.; André, F.; Eggermont, A.; David, A.; Scoazec, J. Y.; Vagner, S.; Robert, C. An Epitranscriptomic Mechanism Underlies Selective MRNA Translation Remodelling in Melanoma Persister Cells. *Nat. Commun.* **2019**, *10* (1). https://doi.org/10.1038/s41467-019-13360-6.

(61) Louis, K. S.; Siegel, A. C. Cell Viability Analysis Using Trypan Blue: Manual and Automated Methods. *Methods Mol. Biol.* **2011**, *740*, 7–12. https://doi.org/10.1007/978-1-61779-108-6_2.

(62) Van Engeland, M.; Nieland, L. J. W.; Ramaekers, F. C. S.; Schutte, B.; Reutelingsperger, C. P. M. Annexin V-Affinity Assay: A Review on an Apoptosis Detection System Based on Phosphatidylserine Exposure. *Cytometry*. 1998, pp 1–9. https://doi.org/10.1002/(SICI)1097-0320(19980101)31:1<1::AID-CYTO1>3.0.CO;2-R.

(63) Wlodkowic, D.; Skommer, J.; Darzynkiewicz, Z. Flow Cytometry-Based Apoptosis Detection. *Methods Mol. Biol.* **2009**, *559*, 19–32. https://doi.org/10.1007/978-1-60327-017-5_2.

(64) Vincelette, N. D.; Yun, S. Assessing the Mechanism of Cytarabine-Induced Killing in Acute Leukemia. *Blood* **2014**, *124* (21), 5210–5210. https://doi.org/10.1182/blood.v124.21.5210.5210.

(65) Evans, A. M.; DeHaven, C. D.; Barrett, T.; Mitchell, M.; Milgram, E. Integrated, Nontargeted Ultrahigh Performance Liquid Chromatography/ Electrospray Ionization Tandem Mass Spectrometry Platform for the Identification and Relative Quantification of the Small-Molecule Complement of Biological Systems. *Anal. Chem.* **2009**, *81* (16), 6656–6667. https://doi.org/10.1021/ac901536h.

(66) Lyons, A. B.; Parish, C. R. Determination of Lymphocyte Division by Flow Cytometry. *J. Immunol. Methods* **1994**, *171* (1), 131–137. https://doi.org/10.1016/0022-1759(94)90236-

4.

(67) Riss, T. L.; Moravec, R. A.; Niles, A. L.; Duellman, S.; Benink, H. A.; Worzella, T. J.; Minor, L. *Cell Viability Assays*; Eli Lilly & Company and the National Center for Advancing Translational Sciences, 2004.

(68) Noble, S.; Goa, K. L. Gemcitabine. A Review of Its Pharmacology and Clinical Potential in Non-Small Cell Lung Cancer and Pancreatic Cancer. *Drugs*. Springer International Publishing October 27, 1997, pp 447–472. https://doi.org/10.2165/00003495-199754030-00009.

(69) Iorio, F.; Knijnenburg, T. A.; Vis, D. J.; Bignell, G. R.; Menden, M. P.; Schubert, M.; Aben, N.; Gonçalves, E.; Barthorpe, S.; Lightfoot, H.; Cokelaer, T.; Greninger, P.; van Dyk, E.; Chang, H.; de Silva, H.; Heyn, H.; Deng, X.; Egan, R. K.; Liu, Q.; Mironenko, T.; Mitropoulos, X.; Richardson, L.; Wang, J.; Zhang, T.; Moran, S.; Sayols, S.; Soleimani, M.; Tamborero, D.; Lopez-Bigas, N.; Ross-Macdonald, P.; Esteller, M.; Gray, N. S.; Haber, D. A.; Stratton, M. R.; Benes, C. H.; Wessels, L. F. A.; Saez-Rodriguez, J.; McDermott, U.; Garnett, M. J. A Landscape of Pharmacogenomic Interactions in Cancer. *Cell* **2016**, *166* (3), 740–754. https://doi.org/10.1016/j.cell.2016.06.017.

(70) Yang, W.; Soares, J.; Greninger, P.; Edelman, E. J.; Lightfoot, H.; Forbes, S.; Bindal, N.; Beare, D.; Smith, J. A.; Thompson, I. R.; Ramaswamy, S.; Futreal, P. A.; Haber, D. A.; Stratton, M. R.; Benes, C.; McDermott, U.; Garnett, M. J. Genomics of Drug Sensitivity in Cancer (GDSC): A Resource for Therapeutic Biomarker Discovery in Cancer Cells. *Nucleic Acids Res.* **2013**, *41* (D1). https://doi.org/10.1093/nar/gks1111.

(71) Keener, A. B. Shapeshifters in Cancer: How Some Tumor Cells Change Phenotype to Evade Therapy. *Nature Medicine*. Nat Med November 8, 2016, pp 1194–1196. https://doi.org/10.1038/nm1116-1194.

(72) Rambow, F.; Marine, J. C.; Goding, C. R. Melanoma Plasticity and Phenotypic Diversity: Therapeutic Barriers and Opportunities. *Genes and Development*. Genes Dev October 1, 2019, pp 1295–1318. https://doi.org/10.1101/gad.329771.119.

(73) Paulis, Y. W. J.; Huijbers, E. J. M.; van der Schaft, D. W. J.; Soetekouw, P. M. M. B.; Pauwels, P.; Tjan-Heijnen, V. C. G.; Griffioen, A. W. CD44 Enhances Tumor Aggressiveness by Promoting Tumor Cell Plasticity. *Oncotarget* **2015**, *6* (23), 19634–19646. https://doi.org/10.18632/oncotarget.3839.

(74) Luo, Y.; Dallaglio, K.; Chen, Y.; Robinson, W. A.; Robinson, S. E.; McCarter, M. D.; Wang, J.; Gonzalez, R.; Thompson, D. C.; Norris, D. A.; Roop, D. R.; Vasiliou, V.; Fujita, M. ALDH1A Isozymes Are Markers of Human Melanoma Stem Cells and Potential Therapeutic Targets. *Stem Cells* **2012**, *30* (10), 2100–2113. https://doi.org/10.1002/stem.1193.

(75) Sciacovelli, M.; Gaude, E.; Hilvo, M.; Frezza, C. The Metabolic Alterations of Cancer Cells. In *Methods in Enzymology*; Academic Press Inc., 2014; Vol. 542, pp 1–23. https://doi.org/10.1016/B978-0-12-416618-9.00001-7.

(76) Islam, S. R.; Manna, S. K. Lipidomic Analysis of Cancer Cell and Tumor Tissues. In *Methods in Molecular Biology*; Humana Press Inc., 2019; Vol. 1928, pp 175–204. https://doi.org/10.1007/978-1-4939-9027-6_11.

(77) Kopecka, J.; Trouillas, P.; Gašparović, A. Č.; Gazzano, E.; Assaraf, Y. G.; Riganti, C. Phospholipids and Cholesterol: Inducers of Cancer Multidrug Resistance and Therapeutic Targets. *Drug Resistance Updates*. Churchill Livingstone March 1, 2020. https://doi.org/10.1016/j.drup.2019.100670.

(78) Ponnusamy, S.; Meyers-Needham, M.; Senkal, C. E.; Saddoughi, S. A.; Sentelle, D.; Selvam, S. P.; Salas, A.; Ogretmen, B. Sphingolipids and Cancer: Ceramide and

Sphingosine-1-Phosphate in the Regulation of Cell Death and Drug Resistance. *Future Oncology*. Future Oncol October 2010, pp 1603–1624. https://doi.org/10.2217/fon.10.116.

(79) Newman, A. C.; Maddocks, O. D. K. One-Carbon Metabolism in Cancer. *British Journal of Cancer*. Nature Publishing Group June 6, 2017, pp 1499–1504. https://doi.org/10.1038/bjc.2017.118.

(80) Shimomura, Y.; Kitaura, Y. Physiological and Pathological Roles of Branched-Chain Amino Acids in the Regulation of Protein and Energy Metabolism and Neurological Functions. *Pharmacological Research*. Academic Press July 1, 2018, pp 215–217. https://doi.org/10.1016/j.phrs.2018.05.014.

(81) Stincone, A.; Prigione, A.; Cramer, T.; Wamelink, M. M. C.; Campbell, K.; Cheung, E.; Olin-Sandoval, V.; Grüning, N.; Krüger, A.; Tauqeer Alam, M.; Keller, M. A.; Breitenbach, M.; Brindle, K. M.; Rabinowitz, J. D.; Ralser, M. The Return of Metabolism: Biochemistry and Physiology of the Pentose Phosphate Pathway. *Biol. Rev.* **2015**, *90* (3), 927–963. https://doi.org/10.1111/brv.12140.

(82) Li, N.; Ragheb, K.; Lawler, G.; Sturgis, J.; Rajwa, B.; Melendez, J. A.; Robinson, J. P. Mitochondrial Complex I Inhibitor Rotenone Induces Apoptosis through Enhancing Mitochondrial Reactive Oxygen Species Production. *J. Biol. Chem.* **2003**, *278* (10), 8516–8525. https://doi.org/10.1074/jbc.M210432200.

(83) Huang, L. S.; Cobessi, D.; Tung, E. Y.; Berry, E. A. Binding of the Respiratory Chain Inhibitor Antimycin to the Mitochondrial Bc1 Complex: A New Crystal Structure Reveals an Altered Intramolecular Hydrogen-Bonding Pattern. *J. Mol. Biol.* **2005**, *351* (3), 573–597. https://doi.org/10.1016/j.jmb.2005.05.053.

(84) Wishart, D. S.; Knox, C.; Guo, A. C.; Shrivastava, S.; Hassanali, M.; Stothard, P.; Chang, Z.; Woolsey, J. DrugBank: A Comprehensive Resource for in Silico Drug Discovery and

Exploration. *Nucleic Acids Res.* **2006**, *34* (Database issue). https://doi.org/10.1093/nar/gkj067.

(85) Arinbasarova, A. Y.; Medentsev, A. G.; Krupyanko, V. I. Gossypol Inhibits Electron Transport and Stimulates ROS Generation in Yarrowia Lipolytica Mitochondria. *Open Biochem. J.* **2012**, *6*, 11–15. https://doi.org/10.2174/1874091x01206010011.

(86) Chen, G.; Zhang, X.; Zhao, M.; Wang, Y.; Cheng, X.; Wang, D.; Xu, Y.; Du, Z.; Yu, X. Celastrol Targets Mitochondrial Respiratory Chain Complex I to Induce Reactive Oxygen Species-Dependent Cytotoxicity in Tumor Cells. *BMC Cancer* **2011**, *11*, 170–170. https://doi.org/10.1186/1471-2407-11-170.

(87) Motohashi, N.; Kawase, M.; Satoh, K.; Sakagami, H. Cytotoxic Potential of Phenothiazines. *Curr. Drug Targets* **2006**, *7* (9), 1055–1066. https://doi.org/10.2174/138945006778226624.

(88) Spengler, G.; Csonka, Á.; Molnár, J.; Amaral, L. The Anticancer Activity of the Old Neuroleptic Phenothiazine-Type Drug Thioridazine. *Anticancer Res.* **2016**, *36* (11), 5701–5706. https://doi.org/10.21873/anticanres.11153.

(89) Qian, K.; Sun, L.; Zhou, G.; Ge, H.; Meng, Y.; Li, J.; Li, X.; Fang, X. Trifluoperazine as an Alternative Strategy for the Inhibition of Tumor Growth of Colorectal Cancer. *J. Cell. Biochem.* **2019**, *120* (9), 15756–15765. https://doi.org/10.1002/jcb.28845.

(90) Recasens, A.; Munoz, L. Targeting Cancer Cell Dormancy. *Trends in Pharmacological Sciences*. Elsevier Ltd February 1, 2019, pp 128–141. https://doi.org/10.1016/j.tips.2018.12.004.

(91) Vallette, F. M.; Olivier, C.; Lézot, F.; Oliver, L.; Cochonneau, D.; Lalier, L.; Cartron, P. F.; Heymann, D. Dormant, Quiescent, Tolerant and Persister Cells: Four Synonyms for the

Same Target in Cancer. *Biochemical Pharmacology*. Elsevier Inc. April 1, 2019, pp 169–176. https://doi.org/10.1016/j.bcp.2018.11.004.

(92) Raha, D.; Wilson, T. R.; Peng, J.; Peterson, D.; Yue, P.; Evangelista, M.; Wilson, C.; Merchant, M.; Settleman, J. The Cancer Stem Cell Marker Aldehyde Dehydrogenase Is Required to Maintain a Drug-Tolerant Tumor Cell Subpopulation. *Cancer Res.* **2014**, *74* (13), 3579–3590. https://doi.org/10.1158/0008-5472.CAN-13-3456.

(93) Cotte, A. K.; Aires, V.; Fredon, M.; Limagne, E.; Derangère, V.; Thibaudin, M.; Humblin, E.; Scagliarini, A.; De Barros, J. P. P.; Hillon, P.; Ghiringhelli, F.; Delmas, D. Lysophosphatidylcholine Acyltransferase 2-Mediated Lipid Droplet Production Supports Colorectal Cancer Chemoresistance. *Nat. Commun.* **2018**, *9* (1), 1–16. https://doi.org/10.1038/s41467-017-02732-5.

(94) Brachtendorf, S.; El-Hindi, K.; Grösch, S. Ceramide Synthases in Cancer Therapy and Chemoresistance. *Progress in Lipid Research*. Elsevier Ltd April 1, 2019, pp 160–185. https://doi.org/10.1016/j.plipres.2019.04.002.

(95) Ananieva, E. A.; Wilkinson, A. C. Branched-Chain Amino Acid Metabolism in Cancer. *Current Opinion in Clinical Nutrition and Metabolic Care*. Lippincott Williams and Wilkins January 1, 2018, pp 64–70. https://doi.org/10.1097/MCO.0000000000000430.

(96) Zheng, Y. H.; Hu, W. J.; Chen, B. C.; Grahn, T. H. M.; Zhao, Y. R.; Bao, H. L.; Zhu, Y. F.; Zhang, Q. Y. BCAT1, a Key Prognostic Predictor of Hepatocellular Carcinoma, Promotes Cell Proliferation and Induces Chemoresistance to Cisplatin. *Liver Int.* **2016**, *36* (12), 1836–1847. https://doi.org/10.1111/liv.13178.

(97) Zhang, L.; Han, J. Branched-Chain Amino Acid Transaminase 1 (BCAT1) Promotes the Growth of Breast Cancer Cells through Improving MTOR-Mediated Mitochondrial Biogenesis and Function. *Biochem. Biophys. Res. Commun.* **2017**, *486* (2), 224–231.

https://doi.org/10.1016/j.bbrc.2017.02.101.

(98) Wang, Y.; Zhang, J.; Ren, S.; Sun, D.; Huang, H. Y.; Wang, H.; Jin, Y.; Li, F.; Zheng, C.; Yang, L.; Deng, L.; Jiang, Z.; Jiang, T.; Han, X.; Hou, S.; Guo, C.; Li, F.; Gao, D.; Qin, J.; Gao, D.; Chen, L.; Lin, S. H.; Wong, K. K.; Li, C.; Hu, L.; Zhou, C.; Ji, H. Branched-Chain Amino Acid Metabolic Reprogramming Orchestrates Drug Resistance to EGFR Tyrosine Kinase Inhibitors. *Cell Rep.* **2019**, *28* (2), 512-525.e6. https://doi.org/10.1016/j.celrep.2019.06.026.

(99) Patra, K. C.; Hay, N. The Pentose Phosphate Pathway and Cancer. *Trends in Biochemical Sciences*. Elsevier Ltd August 1, 2014, pp 347–354. https://doi.org/10.1016/j.tibs.2014.06.005.

(100) Lemons, J. M. S.; Coller, H. A.; Feng, X. J.; Bennett, B. D.; Legesse-Miller, A.; Johnson, E. L.; Raitman, I.; Pollina, E. A.; Rabitz, H. A.; Rabinowitz, J. D. Quiescent Fibroblasts Exhibit High Metabolic Activity. *PLoS Biol.* **2010**, *8* (10). https://doi.org/10.1371/journal.pbio.1000514.

(101) Debeb, B. G.; Lacerda, L.; Larson, R.; Wolfe, A. R.; Krishnamurthy, S.; Reuben, J. M.; Ueno, N. T.; Gilcrease, M.; Woodward, W. A. Histone Deacetylase Inhibitor-Induced Cancer Stem Cells Exhibit High Pentose Phosphate Pathway Metabolism. *Oncotarget* **2016**, *7* (19), 28329–28339. https://doi.org/10.18632/oncotarget.8631.

(102) Jensena, R. B.; Rothenberg, E. Preserving Genome Integrity in Human Cells via DNA Double-Strand Break Repair. *Molecular Biology of the Cell*. Mol Biol Cell April 15, 2020, pp 859–865. https://doi.org/10.1091/MBC.E18-10-0668.

(103) Minchom, A.; Aversa, C.; Lopez, J. Dancing with the DNA Damage Response: Next-Generation Anti-Cancer Therapeutic Strategies. *Therapeutic Advances in Medical Oncology*. Ther Adv Med Oncol January 1, 2018.

https://doi.org/10.1177/1758835918786658.

(104) Cosentino, C.; Grieco, D.; Costanzo, V. ATM Activates the Pentose Phosphate Pathway Promoting Anti-Oxidant Defence and DNA Repair. *EMBO J.* **2011**, *30* (3), 546–555. https://doi.org/10.1038/emboj.2010.330.

(105) Suzuki, S.; Tanaka, T.; Poyurovsky, M. V.; Nagano, H.; Mayama, T.; Ohkubo, S.; Lokshin, M.; Hosokawa, H.; Nakayama, T.; Suzuki, Y.; Sugano, S.; Sato, E.; Nagao, T.; Yokote, K.; Tatsuno, I.; Prives, C. Phosphate-Activated Glutaminase (GLS2), a P53-Inducible Regulator of Glutamine Metabolism and Reactive Oxygen Species. *Proc. Natl. Acad. Sci. U. S. A.* **2010**, *107* (16), 7461–7466. https://doi.org/10.1073/pnas.1002459107.

(106) Wanka, C.; Brucker, D. P.; Bähr, O.; Ronellenfitsch, M.; Weller, M.; Steinbach, J. P.; Rieger, J. Synthesis of Cytochrome c Oxidase 2: A P53-Dependent Metabolic Regulator That Promotes Respiratory Function and Protects Glioma and Colon Cancer Cells from Hypoxia-Induced Cell Death. *Oncogene* **2012**, *31* (33), 3764–3776. https://doi.org/10.1038/onc.2011.530.

(107) Matoba, S.; Kang, J. G.; Patino, W. D.; Wragg, A.; Boehm, M.; Gavrilova, O.; Hurley, P. J.; Bunz, F.; Hwang, P. M. P53 Regulates Mitochondrial Respiration. *Science (80-.).* **2006**, *312* (5780), 1650–1653. https://doi.org/10.1126/science.1126863.

(108) Lee, K. min; Giltnane, J. M.; Balko, J. M.; Schwarz, L. J.; Guerrero-Zotano, A. L.; Hutchinson, K. E.; Nixon, M. J.; Estrada, M. V.; Sánchez, V.; Sanders, M. E.; Lee, T.; Gómez, H.; Lluch, A.; Pérez-Fidalgo, J. A.; Wolf, M. M.; Andrejeva, G.; Rathmell, J. C.; Fesik, S. W.; Arteaga, C. L. MYC and MCL1 Cooperatively Promote Chemotherapy-Resistant Breast Cancer Stem Cells via Regulation of Mitochondrial Oxidative Phosphorylation. *Cell Metab.* **2017**, *26* (4), 633-647.e7. https://doi.org/10.1016/j.cmet.2017.09.009.

(109) Wilson, T.; Johnston, P.; Longley, D. Anti-Apoptotic Mechanisms of Drug Resistance in Cancer. *Curr. Cancer Drug Targets* **2009**, *9* (3), 307–319. https://doi.org/10.2174/156800909788166547.

(110) Johnstone, R. W.; Ruefli, A. A.; Lowe, S. W. Apoptosis: A Link between Cancer Genetics and Chemotherapy. *Cell*. Cell January 25, 2002, pp 153–164. https://doi.org/10.1016/S0092-8674(02)00625-6.

(111) Schmitt, C. A.; Lowe, S. W. Bcl-2 Mediates Chemoresistance in Matched Pairs of Primary Eμ-Myc Lymphomas in Vivo. *Blood Cells, Mol. Dis.* **2001**, *27* (1), 206–216. https://doi.org/10.1006/bcmd.2000.0372.

(112) Ramirez, M.; Rajaram, S.; Steininger, R. J.; Osipchuk, D.; Roth, M. A.; Morinishi, L. S.; Evans, L.; Ji, W.; Hsu, C. H.; Thurley, K.; Wei, S.; Zhou, A.; Koduru, P. R.; Posner, B. A.; Wu, L. F.; Altschuler, S. J. Diverse Drug-Resistance Mechanisms Can Emerge from Drug-Tolerant Cancer Persister Cells. *Nat. Commun.* **2016**, *7*. https://doi.org/10.1038/ncomms10690.

(113) Chong, J.; Wishart, D. S.; Xia, J. Using MetaboAnalyst 4.0 for Comprehensive and Integrative Metabolomics Data Analysis. *Curr. Protoc. Bioinforma.* **2019**, *68* (1), e86. https://doi.org/10.1002/cpbi.86.

(114) Xia, J.; Wishart, D. S. Web-Based Inference of Biological Patterns, Functions and Pathways from Metabolomic Data Using MetaboAnalyst. *Nat. Protoc.* **2011**, *6* (6), 743–760. https://doi.org/10.1038/nprot.2011.319.

(115) Bochner, B. R.; Siri, M.; Huang, R. H.; Noble, S.; Lei, X. H.; Clemons, P. A.; Wagner, B. K. Assay of the Multiple Energy-Producing Pathways of Mammalian Cells. *PLoS One* **2011**, *6* (3). https://doi.org/10.1371/journal.pone.0018147.

(116) Sharma, A.; Shah, S. R.; Illum, H.; Dowell, J. Vemurafenib: Targeted Inhibition of Mutated BRAF for Treatment of Advanced Melanoma and Its Potential in Other Malignancies. *Drugs*. Drugs 2012, pp 2207–2222. https://doi.org/10.2165/11640870-000000000-00000.

(117) Lyons, A. B.; Blake, S. J.; Doherty, K. V. Flow Cytometric Analysis of Cell Division by Dilution of CFSE and Related Dyes. *Curr. Protoc. Cytom.* **2013**, *64* (1), 9.11.1-9.11.12. https://doi.org/10.1002/0471142956.cy0911s64.

(118) Parmiani, G. Melanoma Cancer Stem Cells: Markers and Functions. *Cancers*. Multidisciplinary Digital Publishing Institute (MDPI) March 11, 2016. https://doi.org/10.3390/cancers8030034.

(119) Rambow, F.; Rogiers, A.; Marin-Bejar, O.; Aibar, S.; Femel, J.; Dewaele, M.; Karras, P.; Brown, D.; Chang, Y. H.; Debiec-Rychter, M.; Adriaens, C.; Radaelli, E.; Wolter, P.; Bechter, O.; Dummer, R.; Levesque, M.; Piris, A.; Frederick, D. T.; Boland, G.; Flaherty, K. T.; van den Oord, J.; Voet, T.; Aerts, S.; Lund, A. W.; Marine, J. C. Toward Minimal Residual Disease-Directed Therapy in Melanoma. *Cell* **2018**, *174* (4), 843-855.e19. https://doi.org/10.1016/j.cell.2018.06.025.

(120) Restivo, G.; Diener, J.; Cheng, P. F.; Kiowski, G.; Bonalli, M.; Biedermann, T.; Reichmann, E.; Levesque, M. P.; Dummer, R.; Sommer, L. Low Neurotrophin Receptor CD271 Regulates Phenotype Switching in Melanoma. *Nat. Commun.* **2017**, *8* (1), 1–16. https://doi.org/10.1038/s41467-017-01573-6.

(121) Merighi, S.; Mirandola, P.; Milani, D.; Varani, K.; Gessi, S.; Klotz, K. N.; Leung, E.; Baraldi, P. G.; Borea, P. A. Adenosine Receptors as Mediators of Both Cell Proliferation and Cell Death of Cultured Human Melanoma Cells. *J. Invest. Dermatol.* **2002**, *119* (4), 923–933. https://doi.org/10.1046/j.1523-1747.2002.00111.x.

(122) Schrimpe-Rutledge, A. C.; Codreanu, S. G.; Sherrod, S. D.; McLean, J. A. Untargeted Metabolomics Strategies—Challenges and Emerging Directions. *J. Am. Soc. Mass Spectrom.* **2016**, *27* (12), 1897–1905. https://doi.org/10.1007/s13361-016-1469-y.

(123) Zhang, J.; Zhang, Q. Using Seahorse Machine to Measure OCR and ECAR in Cancer Cells. In *Methods in Molecular Biology*; Humana Press, New York, NY, 2019; Vol. 1928, pp 353–363. https://doi.org/10.1007/978-1-4939-9027-6_18.

(124) de la Cruz-López, K. G.; Castro-Muñoz, L. J.; Reyes-Hernández, D. O.; García-Carrancá, A.; Manzo-Merino, J. Lactate in the Regulation of Tumor Microenvironment and Therapeutic Approaches. *Frontiers in Oncology*. Frontiers November 1, 2019, p 1143. https://doi.org/10.3389/fonc.2019.01143.

(125) Chen, Y. J.; Mahieu, N. G.; Huang, X.; Singh, M.; Crawford, P. A.; Johnson, S. L.; Gross, R. W.; Schaefer, J.; Patti, G. J. Lactate Metabolism Is Associated with Mammalian Mitochondria. *Nat. Chem. Biol*. **2016**, *12* (11), 937–943. https://doi.org/10.1038/nchembio.2172.

(126) Germain, N.; Dhayer, M.; Boileau, M.; Fovez, Q.; Kluza, J.; Marchetti, P. Lipid Metabolism and Resistance to Anticancer Treatment. *Biology*. Multidisciplinary Digital Publishing Institute December 16, 2020, pp 1–23. https://doi.org/10.3390/biology9120474.

(127) Pellerin, L.; Carrié, L.; Dufau, C.; Nieto, L.; Ségui, B.; Levade, T.; Riond, J.; Andrieu-Abadie, N. Lipid Metabolic Reprogramming: Role in Melanoma Progression and Therapeutic Perspectives. *Cancers*. Cancers (Basel) November 1, 2020, pp 1–33. https://doi.org/10.3390/cancers12113147.

(128) Delgado-Goñi, T.; Galobart, T. C.; Wantuch, S.; Normantaite, D.; Leach, M. O.; Whittaker, S. R.; Beloueche-Babari, M. Increased Inflammatory Lipid Metabolism and

Anaplerotic Mitochondrial Activation Follow Acquired Resistance to Vemurafenib in BRAF-Mutant Melanoma Cells. *Br. J. Cancer* **2020**, *122* (1), 72–81. https://doi.org/10.1038/s41416-019-0628-x.

(129) Mashima, T.; Seimiya, H.; Tsuruo, T. De Novo Fatty-Acid Synthesis and Related Pathways as Molecular Targets for Cancer Therapy. *British Journal of Cancer*. Nature Publishing Group April 7, 2009, pp 1369–1372. https://doi.org/10.1038/sj.bjc.6605007.

(130) Soares, A. S.; Costa, V. M.; Diniz, C.; Fresco, P. Inosine Strongly Enhances Proliferation of Human C32 Melanoma Cells through PLC-PKC-MEK1/2-ERK1/2 and PI3K Pathways. *Basic Clin. Pharmacol. Toxicol.* **2015**, *116* (1), 25–36. https://doi.org/10.1111/bcpt.12280.

(131) Shuvalov, O.; Petukhov, A.; Daks, A.; Fedorova, O.; Vasileva, E.; Barlev, N. A. One-Carbon Metabolism and Nucleotide Biosynthesis as Attractive Targets for Anticancer Therapy. *Oncotarget*. Impact Journals, LLC 2017, pp 23955–23977. https://doi.org/10.18632/oncotarget.15053.

(132) Sivanand, S.; Vander Heiden, M. G. Emerging Roles for Branched-Chain Amino Acid Metabolism in Cancer. *Cancer Cell*. Cell Press February 10, 2020, pp 147–156. https://doi.org/10.1016/j.ccell.2019.12.011.

(133) Xu, Y.; Yu, W.; Yang, T.; Zhang, M.; Liang, C.; Cai, X.; Shao, Q. Overexpression of BCAT1 Is a Prognostic Marker in Gastric Cancer. *Hum. Pathol.* **2018**, *75*, 41–46. https://doi.org/10.1016/j.humpath.2018.02.003.

(134) Parmenter, T. J.; Kleinschmidt, M.; Kinross, K. M.; Bond, S. T.; Li, J.; Kaadige, M. R.; Rao, A.; Sheppard, K. E.; Hugo, W.; Pupo, G. M.; Pearson, R. B.; McGee, S. L.; Long, G. V.; Scolyer, R. A.; Rizos, H.; Lo, R. S.; Cullinane, C.; Ayer, D. E.; Ribas, A.; Johnstone, R. W.; Hicks, R. J.; McArthur, G. A. Response of BRAF-Mutant Melanoma to BRAF Inhibition Is Mediated by a Network of Transcriptional Regulators of Glycolysis. *Cancer*

Discov. **2014**, *4* (4), 423–433. https://doi.org/10.1158/2159-8290.CD-13-0440.

(135) Asati, V.; Mahapatra, D. K.; Bharti, S. K. PI3K/Akt/MTOR and Ras/Raf/MEK/ERK Signaling Pathways Inhibitors as Anticancer Agents: Structural and Pharmacological Perspectives. *European Journal of Medicinal Chemistry*. Eur J Med Chem February 15, 2016, pp 314–341. https://doi.org/10.1016/j.ejmech.2016.01.012.

(136) Gough, D. J.; Koetz, L.; Levy, D. E. The MEK-ERK Pathway Is Necessary for Serine Phosphorylation of Mitochondrial STAT3 and Ras-Mediated Transformation. *PLoS One* **2013**, *8* (11). https://doi.org/10.1371/journal.pone.0083395.

(137) Ferber, E. C.; Peck, B.; Delpuech, O.; Bell, G. P.; East, P.; Schulze, A. FOXO3a Regulates Reactive Oxygen Metabolism by Inhibiting Mitochondrial Gene Expression. *Cell Death Differ.* **2012**, *19* (6), 968–979. https://doi.org/10.1038/cdd.2011.179.

(138) Kapitsinou, P. P.; Haase, V. H. The VHL Tumor Suppressor and HIF: Insights from Genetic Studies in Mice. *Cell Death and Differentiation*. Cell Death Differ April 2008, pp 650–659. https://doi.org/10.1038/sj.cdd.4402313.

(139) King, A.; Selak, M. A.; Gottlieb, E. Succinate Dehydrogenase and Fumarate Hydratase: Linking Mitochondrial Dysfunction and Cancer. *Oncogene*. Nature Publishing Group August 7, 2006, pp 4675–4682. https://doi.org/10.1038/sj.onc.1209594.

(140) Dang, C. V.; Kim, J. W.; Gao, P.; Yustein, J. The Interplay between MYC and HIF in Cancer. *Nature Reviews Cancer*. Nat Rev Cancer January 2008, pp 51–56. https://doi.org/10.1038/nrc2274.

(141) Coller, H. A.; Grandori, C.; Tamayo, P.; Colbert, T.; Lander, E. S.; Eisenman, R. N.; Golub, T. R. Expression Analysis with Oligonucleotide Microarrays Reveals That MYC Regulates Genes Involved in Growth, Cell Cycle, Signaling, and Adhesion. *Proc. Natl.*

Acad. Sci. U. S. A. **2000**, *97* (7), 3260–3265. https://doi.org/10.1073/pnas.97.7.3260.

(142) Corazao-Rozas, P.; Guerreschi, P.; André, F.; Gabert, P. E.; Lancel, S.; Dekiouk, S.; Fontaine, D.; Tardivel, M.; Savina, A.; Quesnel, B.; Mortier, L.; Marchetti, P.; Kluza, J. Mitochondrial Oxidative Phosphorylation Controls Cancer Cell's Life and Death Decisions upon Exposure to MAPK Inhibitors. *Oncotarget* **2016**, *7* (26), 39473–39485. https://doi.org/10.18632/oncotarget.7790.

(143) Hardeman, K. N.; Peng, C.; Paudel, B. B.; Meyer, C. T.; Luong, T.; Tyson, D. R.; Young, J. D.; Quaranta, V.; Fessel, J. P. Dependence on Glycolysis Sensitizes BRAF-Mutated Melanomas for Increased Response to Targeted BRAF Inhibition. *Sci. Rep.* **2017**, *7*. https://doi.org/10.1038/srep42604.

(144) Theodosakis, N.; Held, M. A.; Marzuka-Alcala, A.; Meeth, K. M.; Micevic, G.; Long, G. V.; Scolyer, R. A.; Stern, D. F.; Bosenberg, M. W. BRAF Inhibition Decreases Cellular Glucose Uptake in Melanoma in Association with Reduction in Cell Volume. *Mol. Cancer Ther.* **2015**, *14* (7), 1680–1692. https://doi.org/10.1158/1535-7163.MCT-15-0080.

(145) Delgado-Goni, T.; Miniotis, M. F.; Wantuch, S.; Parkes, H. G.; Marais, R.; Workman, P.; Leach, M. O.; Beloueche-Babari, M. The BRAF Inhibitor Vemurafenib Activates Mitochondrial Metabolism and Inhibits Hyperpolarized Pyruvate-Lactate Exchange in BRAF-Mutant Human Melanoma Cells. *Mol. Cancer Ther.* **2016**, *15* (12), 2987–2999. https://doi.org/10.1158/1535-7163.MCT-16-0068.

(146) Zhao, Y.; Li, M.; Yao, X.; Fei, Y.; Lin, Z.; Li, Z.; Cai, K.; Zhao, Y.; Luo, Z. HCAR1/MCT1 Regulates Tumor Ferroptosis through the Lactate-Mediated AMPK-SCD1 Activity and Its Therapeutic Implications. *Cell Rep.* **2020**, *33* (10). https://doi.org/10.1016/j.celrep.2020.108487.

(147) Sever, R.; Brugge, J. S. Signal Transduction in Cancer. *Cold Spring Harb. Perspect. Med.*

2015, *5* (4). https://doi.org/10.1101/cshperspect.a006098.

(148) Sanchez-Vega, F.; Mina, M.; Armenia, J.; Chatila, W. K.; Luna, A.; La, K. C.; Dimitriadoy, S.; Liu, D. L.; Kantheti, H. S.; Saghafinia, S.; Chakravarty, D.; Daian, F.; Gao, Q.; Bailey, M. H.; Liang, W. W.; Foltz, S. M.; Shmulevich, I.; Ding, L.; Heins, Z.; Ochoa, A.; Gross, B.; Gao, J.; Zhang, H.; Kundra, R.; Kandoth, C.; Bahceci, I.; Dervishi, L.; Dogrusoz, U.; Zhou, W.; Shen, H.; Laird, P. W.; Way, G. P.; Greene, C. S.; Liang, H.; Xiao, Y.; Wang, C.; Iavarone, A.; Berger, A. H.; Bivona, T. G.; Lazar, A. J.; Hammer, G. D.; Giordano, T.; Kwong, L. N.; McArthur, G.; Huang, C.; Tward, A. D.; Frederick, M. J.; McCormick, F.; Meyerson, M.; Caesar-Johnson, S. J.; Demchok, J. A.; Felau, I.; Kasapi, M.; Ferguson, M. L.; Hutter, C. M.; Sofia, H. J.; Tarnuzzer, R.; Wang, Z.; Yang, L.; Zenklusen, J. C.; Zhang, J. (Julia); Chudamani, S.; Liu, J.; Lolla, L.; Naresh, R.; Pihl, T.; Sun, Q.; Wan, Y.; Wu, Y.; Cho, J.; DeFreitas, T.; Frazer, S.; Gehlenborg, N.; Getz, G.; Heiman, D. I.; Kim, J.; Lawrence, M. S.; Lin, P.; Meier, S.; Noble, M. S.; Saksena, G.; Voet, D.; Zhang, H.; Bernard, B.; Chambwe, N.; Dhankani, V.; Knijnenburg, T.; Kramer, R.; Leinonen, K.; Liu, Y.; Miller, M.; Reynolds, S.; Shmulevich, I.; Thorsson, V.; Zhang, W.; Akbani, R.; Broom, B. M.; Hegde, A. M.; Ju, Z.; Kanchi, R. S.; Korkut, A.; Li, J.; Liang, H.; Ling, S.; Liu, W.; Lu, Y.; Mills, G. B.; Ng, K. S.; Rao, A.; Ryan, M.; Wang, J.; Weinstein, J. N.; Zhang, J.; Abeshouse, A.; Armenia, J.; Chakravarty, D.; Chatila, W. K.; de Bruijn, I.; Gross, B. E.; Heins, Z. J.; Kundra, R.; La, K.; Ladanyi, M.; Luna, A.; Nissan, M. G.; Ochoa, A.; Phillips, S. M.; Reznik, E.; Sanchez-Vega, F.; Sander, C.; Schultz, N.; Sheridan, R.; Sumer, S. O.; Sun, Y.; Taylor, B. S.; Wang, J.; Zhang, H.; Anur, P.; Peto, M.; Spellman, P.; Benz, C.; Stuart, J. M.; Wong, C. K.; Yau, C.; Hayes, D. N.; Parker, J. S.; Wilkerson, M. D.; Ally, A.; Balasundaram, M.; Bowlby, R.; Brooks, D.; Carlsen, R.; Chuah, E.; Dhalla, N.; Holt, R.; Jones, S. J. M.; Kasaian, K.; Lee, D.; Ma, Y.; Marra, M. A.; Mayo, M.; Moore, R. A.; Mungall, A. J.; Mungall, K.; Robertson, A. G.; Sadeghi, S.;

Schein, J. E.; Sipahimalani, P.; Tam, A.; Thiessen, N.; Tse, K.; Wong, T.; Berger, A. C.; Beroukhim, R.; Cherniack, A. D.; Cibulskis, C.; Gabriel, S. B.; Gao, G. F.; Ha, G.; Meyerson, M.; Schumacher, S. E.; Shih, J.; Kucherlapati, M. H.; Kucherlapati, R. S.; Baylin, S.; Cope, L.; Danilova, L.; Bootwalla, M. S.; Lai, P. H.; Maglinte, D. T.; Van Den Berg, D. J.; Weisenberger, D. J.; Auman, J. T.; Balu, S.; Bodenheimer, T.; Fan, C.; Hoadley, K. A.; Hoyle, A. P.; Jefferys, S. R.; Jones, C. D.; Meng, S.; Mieczkowski, P. A.; Mose, L. E.; Perou, A. H.; Perou, C. M.; Roach, J.; Shi, Y.; Simons, J. V.; Skelly, T.; Soloway, M. G.; Tan, D.; Veluvolu, U.; Fan, H.; Hinoue, T.; Laird, P. W.; Shen, H.; Zhou, W.; Bellair, M.; Chang, K.; Covington, K.; Creighton, C. J.; Dinh, H.; Doddapaneni, H. V.; Donehower, L. A.; Drummond, J.; Gibbs, R. A.; Glenn, R.; Hale, W.; Han, Y.; Hu, J.; Korchina, V.; Lee, S.; Lewis, L.; Li, W.; Liu, X.; Morgan, M.; Morton, D.; Muzny, D.; Santibanez, J.; Sheth, M.; Shinbrot, E.; Wang, L.; Wang, M.; Wheeler, D. A.; Xi, L.; Zhao, F.; Hess, J.; Appelbaum, E. L.; Bailey, M.; Cordes, M. G.; Ding, L.; Fronick, C. C.; Fulton, L. A.; Fulton, R. S.; Kandoth, C.; Mardis, E. R.; McLellan, M. D.; Miller, C. A.; Schmidt, H. K.; Wilson, R. K.; Crain, D.; Curley, E.; Gardner, J.; Lau, K.; Mallery, D.; Morris, S.; Paulauskis, J.; Penny, R.; Shelton, C.; Shelton, T.; Sherman, M.; Thompson, E.; Yena, P.; Bowen, J.; Gastier-Foster, J. M.; Gerken, M.; Leraas, K. M.; Lichtenberg, T. M.; Ramirez, N. C.; Wise, L.; Zmuda, E.; Corcoran, N.; Costello, T.; Hovens, C.; Carvalho, A. L.; de Carvalho, A. C.; Fregnani, J. H.; Longatto-Filho, A.; Reis, R. M.; Scapulatempo-Neto, C.; Silveira, H. C. S.; Vidal, D. O.; Burnette, A.; Eschbacher, J.; Hermes, B.; Noss, A.; Singh, R.; Anderson, M. L.; Castro, P. D.; Ittmann, M.; Huntsman, D.; Kohl, B.; Le, X.; Thorp, R.; Andry, C.; Duffy, E. R.; Lyadov, V.; Paklina, O.; Setdikova, G.; Shabunin, A.; Tavobilov, M.; McPherson, C.; Warnick, R.; Berkowitz, R.; Cramer, D.; Feltmate, C.; Horowitz, N.; Kibel, A.; Muto, M.; Raut, C. P.; Malykh, A.; Barnholtz-Sloan, J. S.; Barrett, W.; Devine, K.; Fulop, J.; Ostrom, Q. T.; Shimmel, K.; Wolinsky, Y.; Sloan, A. E.; De Rose, A.; Giuliante, F.; Goodman, M.; Karlan, B. Y.;

Hagedorn, C. H.; Eckman, J.; Harr, J.; Myers, J.; Tucker, K.; Zach, L. A.; Deyarmin, B.; Hu, H.; Kvecher, L.; Larson, C.; Mural, R. J.; Somiari, S.; Vicha, A.; Zelinka, T.; Bennett, J.; Iacocca, M.; Rabeno, B.; Swanson, P.; Latour, M.; Lacombe, L.; Têtu, B.; Bergeron, A.; McGraw, M.; Staugaitis, S. M.; Chabot, J.; Hibshoosh, H.; Sepulveda, A.; Su, T.; Wang, T.; Potapova, O.; Voronina, O.; Desjardins, L.; Mariani, O.; Roman-Roman, S.; Sastre, X.; Stern, M. H.; Cheng, F.; Signoretti, S.; Berchuck, A.; Bigner, D.; Lipp, E.; Marks, J.; McCall, S.; McLendon, R.; Secord, A.; Sharp, A.; Behera, M.; Brat, D. J.; Chen, A.; Delman, K.; Force, S.; Khuri, F.; Magliocca, K.; Maithel, S.; Olson, J. J.; Owonikoko, T.; Pickens, A.; Ramalingam, S.; Shin, D. M.; Sica, G.; Van Meir, E. G.; Zhang, H.; Eijckenboom, W.; Gillis, A.; Korpershoek, E.; Looijenga, L.; Oosterhuis, W.; Stoop, H.; van Kessel, K. E.; Zwarthoff, E. C.; Calatozzolo, C.; Cuppini, L.; Cuzzubbo, S.; DiMeco, F.; Finocchiaro, G.; Mattei, L.; Perin, A.; Pollo, B.; Chen, C.; Houck, J.; Lohavanichbutr, P.; Hartmann, A.; Stoehr, C.; Stoehr, R.; Taubert, H.; Wach, S.; Wullich, B.; Kycler, W.; Murawa, D.; Wiznerowicz, M.; Chung, K.; Edenfield, W. J.; Martin, J.; Baudin, E.; Bubley, G.; Bueno, R.; De Rienzo, A.; Richards, W. G.; Kalkanis, S.; Mikkelsen, T.; Noushmehr, H.; Scarpace, L.; Girard, N.; Aymerich, M.; Campo, E.; Giné, E.; Guillermo, A. L.; Van Bang, N.; Hanh, P. T.; Phu, B. D.; Tang, Y.; Colman, H.; Evason, K.; Dottino, P. R.; Martignetti, J. A.; Gabra, H.; Juhl, H.; Akeredolu, T.; Stepa, S.; Hoon, D.; Ahn, K.; Kang, K. J.; Beuschlein, F.; Breggia, A.; Birrer, M.; Bell, D.; Borad, M.; Bryce, A. H.; Castle, E.; Chandan, V.; Cheville, J.; Copland, J. A.; Farnell, M.; Flotte, T.; Giama, N.; Ho, T.; Kendrick, M.; Kocher, J. P.; Kopp, K.; Moser, C.; Nagorney, D.; O'Brien, D.; O'Neill, B. P.; Patel, T.; Petersen, G.; Que, F.; Rivera, M.; Roberts, L.; Smallridge, R.; Smyrk, T.; Stanton, M.; Thompson, R. H.; Torbenson, M.; Yang, J. D.; Zhang, L.; Brimo, F.; Ajani, J. A.; Gonzalez, A. M. A.; Behrens, C.; Bondaruk, J.; Broaddus, R.; Czerniak, B.; Esmaeli, B.; Fujimoto, J.; Gershenwald, J.; Guo, C.; Logothetis, C.; Meric-Bernstam, F.; Moran, C.; Ramondetta, L.; Rice, D.; Sood, A.;

Tamboli, P.; Thompson, T.; Troncoso, P.; Tsao, A.; Wistuba, I.; Carter, C.; Haydu, L.; Hersey, P.; Jakrot, V.; Kakavand, H.; Kefford, R.; Lee, K.; Long, G.; Mann, G.; Quinn, M.; Saw, R.; Scolyer, R.; Shannon, K.; Spillane, A.; Stretch, J.; Synott, M.; Thompson, J.; Wilmott, J.; Al-Ahmadie, H.; Chan, T. A.; Ghossein, R.; Gopalan, A.; Levine, D. A.; Reuter, V.; Singer, S.; Singh, B.; Tien, N. V.; Broudy, T.; Mirsaidi, C.; Nair, P.; Drwiega, P.; Miller, J.; Smith, J.; Zaren, H.; Park, J. W.; Hung, N. P.; Kebebew, E.; Linehan, W. M.; Metwalli, A. R.; Pacak, K.; Pinto, P. A.; Schiffman, M.; Schmidt, L. S.; Vocke, C. D.; Wentzensen, N.; Worrell, R.; Yang, H.; Moncrieff, M.; Goparaju, C.; Melamed, J.; Pass, H.; Botnariuc, N.; Caraman, I.; Cernat, M.; Chemencedji, I.; Clipca, A.; Doruc, S.; Gorincioi, G.; Mura, S.; Pirtac, M.; Stancul, I.; Tcaciuc, D.; Albert, M.; Alexopoulou, I.; Arnaout, A.; Bartlett, J.; Engel, J.; Gilbert, S.; Parfitt, J.; Sekhon, H.; Thomas, G.; Rassl, D. M.; Rintoul, R. C.; Bifulco, C.; Tamakawa, R.; Urba, W.; Hayward, N.; Timmers, H.; Antenucci, A.; Facciolo, F.; Grazi, G.; Marino, M.; Merola, R.; de Krijger, R.; Gimenez-Roqueplo, A. P.; Piché, A.; Chevalier, S.; McKercher, G.; Birsoy, K.; Barnett, G.; Brewer, C.; Farver, C.; Naska, T.; Pennell, N. A.; Raymond, D.; Schilero, C.; Smolenski, K.; Williams, F.; Morrison, C.; Borgia, J. A.; Liptay, M. J.; Pool, M.; Seder, C. W.; Junker, K.; Omberg, L.; Dinkin, M.; Manikhas, G.; Alvaro, D.; Bragazzi, M. C.; Cardinale, V.; Carpino, G.; Gaudio, E.; Chesla, D.; Cottingham, S.; Dubina, M.; Moiseenko, F.; Dhanasekaran, R.; Becker, K. F.; Janssen, K. P.; Slotta-Huspenina, J.; Abdel-Rahman, M. H.; Aziz, D.; Bell, S.; Cebulla, C. M.; Davis, A.; Duell, R.; Elder, J. B.; Hilty, J.; Kumar, B.; Lang, J.; Lehman, N. L.; Mandt, R.; Nguyen, P.; Pilarski, R.; Rai, K.; Schoenfield, L.; Senecal, K.; Wakely, P.; Hansen, P.; Lechan, R.; Powers, J.; Tischler, A.; Grizzle, W. E.; Sexton, K. C.; Kastl, A.; Henderson, J.; Porten, S.; Waldmann, J.; Fassnacht, M.; Asa, S. L.; Schadendorf, D.; Couce, M.; Graefen, M.; Huland, H.; Sauter, G.; Schlomm, T.; Simon, R.; Tennstedt, P.; Olabode, O.; Nelson, M.; Bathe, O.; Carroll, P. R.; Chan, J. M.; Disaia, P.; Glenn, P.; Kelley, R. K.; Landen, C. N.; Phillips, J.; Prados, M.; Simko, J.;

Smith-McCune, K.; VandenBerg, S.; Roggin, K.; Fehrenbach, A.; Kendler, A.; Sifri, S.; Steele, R.; Jimeno, A.; Carey, F.; Forgie, I.; Mannelli, M.; Carney, M.; Hernandez, B.; Campos, B.; Herold-Mende, C.; Jungk, C.; Unterberg, A.; von Deimling, A.; Bossler, A.; Galbraith, J.; Jacobus, L.; Knudson, M.; Knutson, T.; Ma, D.; Milhem, M.; Sigmund, R.; Godwin, A. K.; Madan, R.; Rosenthal, H. G.; Adebamowo, C.; Adebamowo, S. N.; Boussioutas, A.; Beer, D.; Giordano, T.; Mes-Masson, A. M.; Saad, F.; Bocklage, T.; Landrum, L.; Mannel, R.; Moore, K.; Moxley, K.; Postier, R.; Walker, J.; Zuna, R.; Feldman, M.; Valdivieso, F.; Dhir, R.; Luketich, J.; Pinero, E. M. M.; Quintero-Aguilo, M.; Carlotti, C. G.; Dos Santos, J. S.; Kemp, R.; Sankarankuty, A.; Tirapelli, D.; Catto, J.; Agnew, K.; Swisher, E.; Creaney, J.; Robinson, B.; Shelley, C. S.; Godwin, E. M.; Kendall, S.; Shipman, C.; Bradford, C.; Carey, T.; Haddad, A.; Moyer, J.; Peterson, L.; Prince, M.; Rozek, L.; Wolf, G.; Bowman, R.; Fong, K. M.; Yang, I.; Korst, R.; Rathmell, W. K.; Fantacone-Campbell, J. L.; Hooke, J. A.; Kovatich, A. J.; Shriver, C. D.; DiPersio, J.; Drake, B.; Govindan, R.; Heath, S.; Ley, T.; Van Tine, B.; Westervelt, P.; Rubin, M. A.; Lee, J. Il; Aredes, N. D.; Mariamidze, A.; Van Allen, E. M.; Cherniack, A. D.; Ciriello, G.; Sander, C.; Schultz, N. Oncogenic Signaling Pathways in The Cancer Genome Atlas. *Cell* **2018**, *173* (2), 321-337.e10. https://doi.org/10.1016/J.CELL.2018.03.035.

(149) Regad, T. Targeting RTK Signaling Pathways in Cancer. *Cancers*. 2015, pp 1758–1784. https://doi.org/10.3390/cancers7030860.

(150) Antonicelli, A.; Cafarotti, S.; Indini, A.; Galli, A.; Russo, A.; Cesario, A.; Lococo, F. M.; Russo, P.; Mainini, A. F.; Bonifati, L. G.; Nosotti, M.; Santambrogio, L.; Margaritora, S.; Granone, P. M.; Dutly, A. E. Egfr-Targeted Therapy for Non-Small Cell Lun Cancer: Focus on EGFR Oncogenic Mutation. *Int. J. Med. Sci.* **2013**, *10* (3), 320–330. https://doi.org/10.7150/ijms.4609.

(151) Li, X.; Wu, C.; Chen, N.; Gu, H.; Yen, A.; Cao, L.; Wang, E.; Wang, L. PI3K/Akt/MTOR Signaling Pathway and Targeted Therapy for Glioblastoma. *Oncotarget* **2016**, *7* (22), 33440–33450. https://doi.org/10.18632/oncotarget.7961.

(152) Menzer, C.; Menzies, A. M.; Carlino, M. S.; Reijers, I.; Groen, E. J.; Eigentler, T.; De Groot, J. W. B.; Van Der Veldt, A. A. M.; Johnson, D. B.; Meiss, F.; Schlaak, M.; Schilling, B.; Westgeest, H. M.; Gutzmer, R.; Pföhler, C.; Meier, F.; Zimmer, L.; Suijkerbuijk, K. P. M.; Haalck, T.; Thoms, K. M.; Herbschleb, K.; Leichsenring, J.; Menzer, A.; Kopp-Schneider, A.; Long, G. V.; Kefford, R.; Enk, A.; Blank, C. U.; Hassel, J. C. Targeted Therapy in Advanced Melanoma with Rare BRAF Mutations. In *Journal of Clinical Oncology*; American Society of Clinical Oncology, 2019; Vol. 37, pp 3142–3151. https://doi.org/10.1200/JCO.19.00489.

(153) Vanella, V.; Festino, L.; Trojaniello, C.; Vitale, M. G.; Sorrentino, A.; Paone, M.; Ascierto, P. A. The Role of BRAF-Targeted Therapy for Advanced Melanoma in the Immunotherapy Era. *Current Oncology Reports*. Current Medicine Group LLC 1 September 1, 2019, pp 1–11. https://doi.org/10.1007/s11912-019-0827-x.

(154) Lee, Y. T.; Tan, Y. J.; Oon, C. E. Molecular Targeted Therapy: Treating Cancer with Specificity. *European Journal of Pharmacology*. Elsevier September 5, 2018, pp 188–196. https://doi.org/10.1016/j.ejphar.2018.07.034.

(155) Zhang, T.; Inesta-Vaquera, F.; Niepel, M.; Zhang, J.; Ficarro, S. B.; MacHleidt, T.; Xie, T.; Marto, J. A.; Kim, N.; Sim, T.; Laughlin, J. D.; Park, H.; Lograsso, P. V.; Patricelli, M.; Nomanbhoy, T. K.; Sorger, P. K.; Alessi, D. R.; Gray, N. S. Discovery of Potent and Selective Covalent Inhibitors of JNK. *Chem. Biol.* **2012**, *19* (1), 140–154. https://doi.org/10.1016/j.chembiol.2011.11.010.

(156) Meng, Q.; Xia, Y. C-Jun, at the Crossroad of the Signaling Network. *Protein and Cell*.

Springer 2011, pp 889–898. https://doi.org/10.1007/s13238-011-1113-3.

(157) Eckert, R. L.; Adhikary, G.; Young, C. A.; Jans, R.; Crish, J. F.; Xu, W.; Rorke, E. A. AP1 Transcription Factors in Epidermal Differentiation and Skin Cancer. *J. Skin Cancer* **2013**, *2013*, 1–9. https://doi.org/10.1155/2013/537028.

(158) Müller, R.; Bravo, R.; Burckhardt, J.; Curran, T. Induction of C-Fos Gene and Protein by Growth Factors Precedes Activation of c-Myc. *Nature* **1984**, *312* (5996), 716–720. https://doi.org/10.1038/312716a0.

(159) Vierbuchen, T.; Ling, E.; Cowley, C. J.; Couch, C. H.; Wang, X.; Harmin, D. A.; Roberts, C. W. M.; Greenberg, M. E. AP-1 Transcription Factors and the BAF Complex Mediate Signal-Dependent Enhancer Selection. *Mol. Cell* **2017**, *68* (6), 1067-1082.e12. https://doi.org/10.1016/j.molcel.2017.11.026.

(160) Angel, P.; Karin, M. The Role of Jun, Fos and the AP-1 Complex in Cell-Proliferation and Transformation. *BBA - Reviews on Cancer*. 1991, pp 129–157. https://doi.org/10.1016/0304-419X(91)90011-9.

(161) Hai, T. W.; Liu, F.; Allegretto, E. A.; Karin, M.; Green, M. R. A Family of Immunologically Related Transcription Factors That Includes Multiple Forms of ATF and AP-1. *Genes Dev.* **1988**, *2* (10), 1216–1226. https://doi.org/10.1101/gad.2.10.1216.

(162) Ryder, K.; Nathans, D. Production of Protooncogene C-Jun by Serum Growth Factors. *Proc. Natl. Acad. Sci. U. S. A.* **1988**, *85* (22), 8464–8467. https://doi.org/10.1073/pnas.85.22.8464.

(163) Devary, Y.; Gottlieb, R. A.; Lau, L. F.; Karin, M. Rapid and Preferential Activation of the C-Jun Gene during the Mammalian UV Response. *Mol. Cell. Biol.* **1991**, *11* (5), 2804–2811. https://doi.org/10.1128/mcb.11.5.2804.

(164) Lee, W.; Mitchell, P.; Tjian, R. Purified Transcription Factor AP-1 Interacts with TPA-Inducible Enhancer Elements. *Cell* **1987**, *49* (6), 741–752. https://doi.org/10.1016/0092-8674(87)90612-X.

(165) Quantin, B.; Breathnach, R. Epidermal Growth Factor Stimulates Transcription of the C-Jun Proto-Oncogene in Rat Fibroblasts. *Nature* **1988**, *334* (6182), 538–539. https://doi.org/10.1038/334538a0.

(166) Baker, S. J.; Kerppola, T. K.; Luk, D.; Vandenberg, M. T.; Marshak, D. R.; Curran, T.; Abate, C. Jun Is Phosphorylated by Several Protein Kinases at the Same Sites That Are Modified in Serum-Stimulated Fibroblasts. *Mol. Cell. Biol.* **1992**, *12* (10), 4694–4705. https://doi.org/10.1128/mcb.12.10.4694.

(167) Boyle, W. J.; Smeal, T.; Defize, L. H. K.; Angel, P.; Woodgett, J. R.; Karin, M.; Hunter, T. Activation of Protein Kinase C Decreases Phosphorylation of C-Jun at Sites That Negatively Regulate Its DNA-Binding Activity. *Cell* **1991**, *64* (3), 573–584. https://doi.org/10.1016/0092-8674(91)90241-P.

(168) Black, E. J.; Street, A. J.; Gillespie, D. A. F. Protein Phosphatase 2A Reverses Phosphorylation of C-Jun Specified by the Delta Domain in Vitro: Correlation with Oncogenic Activation and Deregulated Transactivation Activity of v-Jun. *Oncogene* **1991**, *6* (11), 1949–1958.

(169) Franklin, C. C.; McCulloch, A. V.; Kraft, A. S. In Vitro Association between the Jun Protein Family and the General Transcription Factors, TBP and TFIIB. *Biochem. J.* **1995**, *305* (3), 967–974. https://doi.org/10.1042/bj3050967.

(170) Sabapathy, K.; Hochedlinger, K.; Nam, S. Y.; Bauer, A.; Karin, M.; Wagner, E. F. Distinct Roles for JNK1 and JNK2 in Regulating JNK Activity and C-Jun-Dependent Cell Proliferation. *Mol. Cell* **2004**, *15* (5), 713–725.

https://doi.org/10.1016/j.molcel.2004.08.028.

(171) Hui, L.; Bakiri, L.; Mairhorfer, A.; Schweifer, N.; Haslinger, C.; Kenner, L.; Komnenovic, V.; Scheuch, H.; Beug, H.; Wagner, E. F. P38α Suppresses Normal and Cancer Cell Proliferation by Antagonizing the JNK-c-Jun Pathway. *Nat. Genet.* **2007**, *39* (6), 741–749. https://doi.org/10.1038/ng2033.

(172) Wisdom, R.; Johnson, R. S.; Moore, C. C-Jun Regulates Cell Cycle Progression and Apoptosis by Distinct Mechanisms. *EMBO J.* **1999**, *18* (1), 188–197. https://doi.org/10.1093/emboj/18.1.188.

(173) Leppä, S.; Bohmann, D. Diverse Functions of JNK Signaling and C-Jun in Stress Response and Apoptosis. *Oncogene*. Nature Publishing Group November 4, 1999, pp 6158–6162. https://doi.org/10.1038/sj.onc.1203173.

(174) Szabo, E.; Riffe, M. E.; Steinberg, S. M.; Birrer, M. J.; Linnoila, R. I. Altered CJun Expression: An Early Event in Human Lung Carcinogenesis. *Cancer Res.* **1996**, *56* (2), 305–315. https://doi.org/10.1016/0169-5002(96)84172-9.

(175) Vleugel, M. M.; Greijer, A. E.; Bos, R.; van der Wall, E.; van Diest, P. J. C-Jun Activation Is Associated with Proliferation and Angiogenesis in Invasive Breast Cancer. *Hum. Pathol.* **2006**, *37* (6), 668–674. https://doi.org/10.1016/j.humpath.2006.01.022.

(176) Wang, H.; Birkenbach, M.; Hart, J. Expression of Jun Family Members in Human Colorectal Adenocarcinoma. *Carcinogenesis* **2000**, *21* (7), 1313–1317. https://doi.org/10.1093/carcin/21.5.313.

(177) Eferl, R.; Wagner, E. F. AP-1: A Double-Edged Sword in Tumorigenesis. *Nature Reviews Cancer*. Nat Rev Cancer 2003, pp 859–868. https://doi.org/10.1038/nrc1209.

(178) Ye, N.; Ding, Y.; Wild, C.; Shen, Q.; Zhou, J. Small Molecule Inhibitors Targeting

Activator Protein 1 (AP-1). *Journal of Medicinal Chemistry*. J Med Chem 2014, pp 6930–6948. https://doi.org/10.1021/jm5004733.

(179) Bakiri, L.; Lallemand, D.; Bossy-Wetzel, E.; Yaniv, M. Cell Cycle-Dependent Variations in c-Jun and JunB Phosphorylation: A Role in the Control of Cyclin D1 Expression. *EMBO J.* **2000**, *19* (9), 2056–2068. https://doi.org/10.1093/emboj/19.9.2056.

(180) Ivanov, V. N.; Bhoumik, A.; Krasilnikov, M.; Raz, R.; Owen-Schaub, L. B.; Levy, D.; Horvath, C. M.; Ronai, Z. Cooperation between STAT3 and C-Jun Suppresses Fas Transcription. *Mol. Cell* **2001**, *7* (3), 517–528. https://doi.org/10.1016/S1097-2765(01)00199-X.

(181) Toft, D. J.; Rosenberg, S. B.; Bergers, G.; Volpert, O.; Linzer, D. I. H. Reactivation of Proliferin Gene Expression Is Associated with Increased Angiogenesis in a Cell Culture Model of Fibrosarcoma Tumor Progression. *Proc. Natl. Acad. Sci. U. S. A.* **2001**, *98* (23), 13055–13059. https://doi.org/10.1073/pnas.231364798.

(182) Deng, T.; Karin, M. JunB Differs from C-Jun in Its DNA-Binding and Dimerization Domains, and Respresses c-Jun by Formation of Inactive Heterodimers. *Genes Dev.* **1993**, *7* (3), 479–490. https://doi.org/10.1101/gad.7.3.479.

(183) Ramsdale, R.; Jorissen, R. N.; Li, F. Z.; Al-Obaidi, S.; Ward, T.; Sheppard, K. E.; Bukczynska, P. E.; Young, R. J.; Boyle, S. E.; Shackleton, M.; Bollag, G.; Long, G. V.; Tulchinsky, E.; Rizos, H.; Pearson, R. B.; McArthur, G. A.; Dhillon, A. S.; Ferrao, P. T. The Transcription Cofactor C-JUN Mediates Phenotype Switching and BRAF Inhibitor Resistance in Melanoma. *Sci. Signal.* **2015**, *8* (390), ra82. https://doi.org/10.1126/SCISIGNAL.AAB1111/SUPPL_FILE/8_RA82_SM.PDF.

(184) Taniguchi, H.; Yamada, T.; Wang, R.; Tanimura, K.; Adachi, Y.; Nishiyama, A.; Tanimoto, A.; Takeuchi, S.; Araujo, L. H.; Boroni, M.; Yoshimura, A.; Shiotsu, S.;

Matsumoto, I.; Watanabe, S.; Kikuchi, T.; Miura, S.; Tanaka, H.; Kitazaki, T.; Yamaguchi, H.; Mukae, H.; Uchino, J.; Uehara, H.; Takayama, K.; Yano, S. AXL Confers Intrinsic Resistance to Osimertinib and Advances the Emergence of Tolerant Cells. *Nat. Commun.* **2019**, *10* (1). https://doi.org/10.1038/s41467-018-08074-0.

(185) Zhang, Z.; Lee, J. C.; Lin, L.; Olivas, V.; Au, V.; Laframboise, T.; Abdel-Rahman, M.; Wang, X.; Levine, A. D.; Rho, J. K.; Choi, Y. J.; Choi, C. M.; Kim, S. W.; Jang, S. J.; Park, Y. S.; Kim, W. S.; Lee, D. H.; Lee, J. S.; Miller, V. A.; Arcila, M.; Ladanyi, M.; Moonsamy, P.; Sawyers, C.; Boggon, T. J.; Ma, P. C.; Costa, C.; Taron, M.; Rosell, R.; Halmos, B.; Bivona, T. G. Activation of the AXL Kinase Causes Resistance to EGFR-Targeted Therapy in Lung Cancer. *Nat. Genet. 2012 448* **2012**, *44* (8), 852–860. https://doi.org/10.1038/ng.2330.

(186) Zhan, T.; Rindtorff, N.; Boutros, M. Wnt Signaling in Cancer. *Oncogene*. Nature Publishing Group September 12, 2017, pp 1461–1473. https://doi.org/10.1038/onc.2016.304.

(187) Arasada, R. R.; Shilo, K.; Yamada, T.; Zhang, J.; Yano, S.; Ghanem, R.; Wang, W.; Takeuchi, S.; Fukuda, K.; Katakami, N.; Tomii, K.; Ogushi, F.; Nishioka, Y.; Talabere, T.; Misra, S.; Duan, W.; Fadda, P.; Rahman, M. A.; Nana-Sinkam, P.; Evans, J.; Amann, J.; Tchekneva, E. E.; Dikov, M. M.; Carbone, D. P. Notch3-Dependent β-Catenin Signaling Mediates EGFR TKI Drug Persistence in EGFR Mutant NSCLC. *Nat. Commun.* **2018**, *9* (1). https://doi.org/10.1038/s41467-018-05626-2.

Disclosures

1. Chapter 2 has been published in Frontiers in molecular biosciences journal.

   Karki, P., Angardi, V., Mier, J. C. & Orman, M. A. A Transient Metabolic State in Melanoma Persister Cells Mediated by Chemotherapeutic Treatments. *Front. Mol. Biosci.* **8**, 1398 (2022).

2. Chapter 3 has been published in MDPI metabolites journal.

   Karki, P., Sensenbach, S., Angardi, V. & Orman, M. A. Braf-inhibitor-induced metabolic alterations in a375 melanoma cells. *Metabolites* **11**, (2021).